Title
Flexible supercapacitors based on micro/nanofibers

Author
Shen, Caiwei

Publication Date
2018

Flexible supercapacitors based on micro/nanofibers

By

Caiwei Shen

A dissertation submitted in partial satisfaction of the

requirements for the degree of

Doctor of Philosophy

in

Engineering - Mechanical Engineering

in the

Graduate Division

of the

University of California, Berkeley

Committee in charge:

Professor Liwei Lin, Chair
Professor Bryan McCloskey
Professor Van Carey

Summer 2018

Abstract

Flexible supercapacitors based on micro/nanofibers

by

Caiwei Shen

Doctor of Philosophy in Engineering – Mechanical Engineering

University of California, Berkeley

Professor Liwei Lin, Chair

Flexible energy storage components are indispensable in the field of flexible electronics. Supercapacitors featuring high power density, fast charge/discharge rate, long cycle life, and safe operation are desirable devices. Micro/nanofiber-based electrode materials, fabrication processes, and device configurations are investigated towards flexible supercapacitors applications.

Micro flexible supercapacitors (FSCs) prepared using direct-write nanofibers is demonstrated for flexible integrated microelectronics. The micro electrodes with porous network are fabricated by the near-field electrospinning process of polypyrrole (PPy) nanofibers on a patterned metal layer on flexible substrate. Such conductive nanofiber network with a pseudocapacitance effect greatly increases the capacitance and facilitates ion transport in the electrodes. The prototype micro FSCs are experimentally proved to be highly flexible with excellent electrochemical performance and cycling stability. The approach is simple, versatile, and compatible with different substrates for the direct integration of energy storage devices in flexible microsystems.

An ultra-thin micro coaxial fiber supercapacitor (μCFSC) with high energy and power densities, and excellent mechanical properties is demonstrated. The prototype with the smallest reported overall diameter of 13 μm is fabricated by successive coating of functional layers onto a single micro carbon fiber via a scalable process. Combining the simulation results via the electrochemical model, the high performance is attributed to the well-controlled thin coatings that make full use of the electrode materials and minimize the ion transport path between electrodes. Moreover, the μCFSC features high bending flexibility and large tensile strength (more than 1 GPa), which make it promising as a building block for various flexible energy storage applications.

Free-standing woven supercapacitor fabrics that can store high electrical energy and sustain large mechanical loads are demonstrated as flexible power sources. The prototype with reduced package weight/volume provides an impressive overall energy density of 2.58 mWh g^{-1} or 3.6 mWh cm^{-3}, high tensile strength of over 1000 MPa, and bearable

pressure of over 100 MPa. The nanoporous thread electrodes are prepared by the activation of commercial carbon fibers to have three-orders of magnitude increase in the specific surface area and 86% retention of the original mechanical strength. The novel device configuration woven by solid electrolyte-coated threads shows excellent flexibility and stability during repeated mechanical bending tests. Such scalable energy storage fabrics can be woven into daily graments as flexible power sources for a variety of wearable electronics.

Table of contents

List of figures

List of tables

Acknowledgments

I would like to first thank Professor Liwei Lin for his support to help me complete the PhD program. I am deeply grateful for the opportunity he gave me to enter the esteemed graduate school at UC Berkeley. He has not only guided me through the whole process, from course selection and preliminary preparation to qualifying exam and graduation, but also pushed me forward to do better on research. I appreciate both his criticism, which greatly improves the quality of my research, and his patience, which allows me to pass through all difficulties I have encountered.

Special thanks to Dr. Mohan Sanghadasa, who has been collaborating with me and supporting all my research projects for the past four years. He provided the initial motivation for me to work on flexible supercapacitors. He has been patiently meeting with me regularly, encouraging my new ideas, and understanding all my failures.

Many thanks to my collaborators who contributed to my research projects. Mr. Chun-Ping Wang from National Tsinghua University helped improve the results presented in Chapter 2. Dr. Yingxi Xie from South China University of Technology has contributed significant parts presented in Chapter 3. Ms. Bingquan Zhu from Tsinghua University collaborated with me on many experiments conducted in Chapter 4. Dr. Xining Zang, Dr. Guoxi Luo, Yuting Hsiao, Peter Wu, Guanya Shi, Tony Guo, Xuzhou Li, and other students visiting or pursuing degrees in Lin Lab have helped with my research presented in the dissertation. I would not be able to have conducted the research projects successfully without their effort and contribution.

I would also like to thank my family for the support and encouragement. Special thanks to my wife, Yuqian Han, for being by my side from the start of the graduate program through the end.

1 Introduction

1.1 Power sources for flexible electronics

Electronics have been continuously miniaturized and functionalized to be portable and wearable in the past decades. Flexible electronics have become a new trend of future wearable electronics in recent years, because they bring highly desirable features. For example, they can be easy to carry, integrated with daily garments, and comfortable to wear on human body. While matured commercial products such as smart wristbands, watches, and flexible displays have been developed, the concept of all-flexible devices has not been realized yet. As one of the key components of wearable electronics, the power source (usually a battery), which occupies a large portion of the volume/weight, is the bottleneck to develop flexible electronics.

Currently, wearable electronics use Lithium-ion batteries (LIBs) as the power sources because of their relatively high energy density and rechargeable feature[1]. However, unsatisfactory issues of LIBs can become more serious when researchers try to develop flexible forms of them. For example, LIBs are not always safe because they rely on flammable and explosive chemical reactions to store energy. Deformations such as bending of the LIB electrodes can increase the chance of safety issues to happen. On the other hand, LIB electrode materials are intrinsically rigid and researchers have to use ultrathin electrodes on much thicker flexible substrate/package materials to introduce flexible feature, which greatly lower the energy density of LIBs [2]–[4].

Other flexible power solutions, such as flexible energy harvesters, have been proposed and intensively studied recently. Most of the reported flexible energy harvesters for wearable applications are based on piezoelectric, electrostatic, and triboelectric effects to harvest mechanical energy from human body movement [5]–[10]. Such energy sources, similar to other sources from the environment, is unstable and intermittent. Moreover, the efficiencies of such energy harvesters are also low (<1 % [8]), and they only generates small power (<1 mW) that is not significant for current smart devices. As an example, AirPods [11], one of the smallest wearable electronics, is powered by a LIB with a capacity of 93 mWh, and it consumes a power of ~19 mW (5 hrs of battery life) when it is working. It is impossible for an energy harvester of 1 mW to power it directly. If the harvester is used as the additional power, it will take 93 hrs to charge the battery, which is also impractical.

Flexible supercapacitors (FSC), which are another type of electrochemical energy storage devices, have been investigated as a candidate to replace LIBs in flexible applications. While supercapacitors usually provide lower energy density than LIBs, they are much safer and more durable because of their working principles [12]–[19]. Moreover, supercapacitors have simpler configuration and various choices of flexible electrode materials. As a result, they can be promising devices to power future flexible electronics. The focus of this dissertation is to study flexible supercapacitors using micro/nano fiber-based electrode materials. The working principles, research status, and challenges of FSC will be discussed in the following sections of Chapter 1. The detailed structure of the dissertation will also be described.

1.2 Supercapacitors as the power sources

1.2.1 Working principles of supercapacitors

Supercapacitors differ from conventional capacitors by their charge storage mechanisms. Four types of capacitors, including parallel-plate capacitor, electrolytic capacitor, EDL capacitor, and pseudo capacitor are illustrated in figure 1-1. A parallel-plate capacitor (figure 1-1a) is composed of two metal plates on which static charges are stored with a dielectric layer which separates the charges. Capacitance C of such a capacitor can be calculated as:

$$C = \varepsilon A / d \tag{1.1}$$

where ε is the permittivity of the dielectric material, A is the area of the plates, and d is the separation distance between plates. An electrolytic capacitor (figure 1-1b) works similarly to the parallel-plate capacitor except it has an electrolyte layer attached to one metal plate working together as a cathode. The dielectric is an oxide layer of anode and can be as thin as nanometers. The electrolytic capacitor usually has a larger capacitance than the parallel-plate capacitor of the same size because its charge separation distance, d, is smaller.

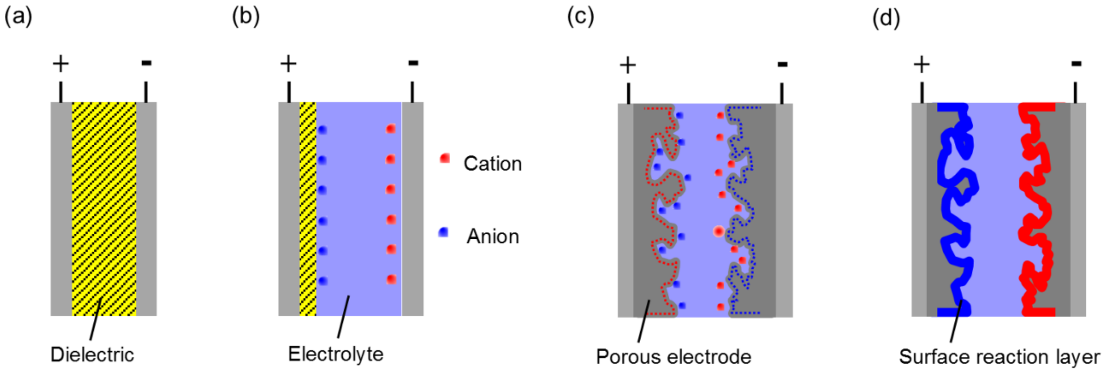

Figure 1-1. Schematics of the working principles of four types of capacitors: (a) parallel-plate capacitor, (b) electrolytic capacitor, (c) EDL capacitor, and (d) pseudo capacitor. EDL capacitor and pseudo capacitor are called supercapacitors because they have much larger capacitance than the other capacitors. [19]

An EDL capacitor (figure 1-1c) store charges by using the EDL at the electrode-electrolyte interface, in which charges (electrons in the electrode and ions in the electrolyte) are separated by a distance of less than 1 nm. Moreover, the area of the EDL is the interface area between the electrode and electrolyte, which can be as high as more than 3000 m^2/g for nanoporous carbon electrodes [20]. Therefore, EDL capacitor has much larger capacitance than the conventional ones of the same size, because of the large surface area and the small charge separation distance, according to equation (1). It is worth noting that, in an EDL capacitor, each electrode has an EDL and two electrodes are connected in series. Researchers have been reporting specific capacitance (capacitance divided by the mass or volume) of each electrode by testing it in a three-electrode system. The specific capacitance of a whole capacitor, however, is the serial capacitance of two electrodes divided by the total mass or volume, which can be a different (usually much smaller) value [21].

A pseudo capacitor (figure 1-1d) also stores energy at the electrode-electrolyte interface, except that fast redox reactions are involved [12], [13]. Compared with batteries which store energy by redox reactions in bulk materials, pseudo capacitors have reactions only near the surface of the electrode, and the potential of the electrode, V, is highly dependent on the extent of charge storage, q, which results in a derivative dq/dV equivalent to a capacitance. Pseudo capacitance is of great interest mainly because it shows much higher specific capacitance than that of EDL capacitance. However, unlike EDL capacitance that arises from surface charges stored electrostatically (i.e. non-Faradaically), pseudo capacitance involves the passage of charges across the electrode-electrolyte interface (i.e. Faradaic process), which reduces the power performance and cycle life.

EDL capacitors based on carbon electrodes usually exhibit 1-5% of pseudo capacitance due to Faradaic reactivity of surface oxygen functionalities, while pseudo capacitors always show some EDL capacitance proportional to the electrode-electrolyte interfacial area [12]. More balanced combinations of the two mechanisms results in hybrid supercapacitors [13]. For example, pseudo-capacitive materials can be deposited onto nanostructured carbon substrate to achieve high specific capacitance based on pseudo capacitors and high power density due to the effects of EDL capacitors [13], [22], [23].

1.2.2 Equivalent circuit models for supercapacitors

Equivalent circuit models for supercapacitors are significant tools to simulate and evaluate the working of the energy storage device in a whole electronic system. Besides, such models also help us understand and predict the performance of supercapacitors in different tests. An ideal capacitor can be modeled as a passive, linear element in electrical circuits, but a practical capacitor is always associated with an equivalent serial resistance (R_{ESR}) and an equivalent parallel resistance caused by leakage (R_{EPR}) as shown in figure 1-2a. Such a circuit can also be used to model supercapacitors to a first approximation, where C is the maximum total capacitance of the whole device, R_{ESR} is the equivalent resistance added up by the electrical resistances of the electrodes and the ionic resistance of the electrolyte, and R_{EPR} represents the total leakage of the supercapacitor through different mechanisms [24], [25].

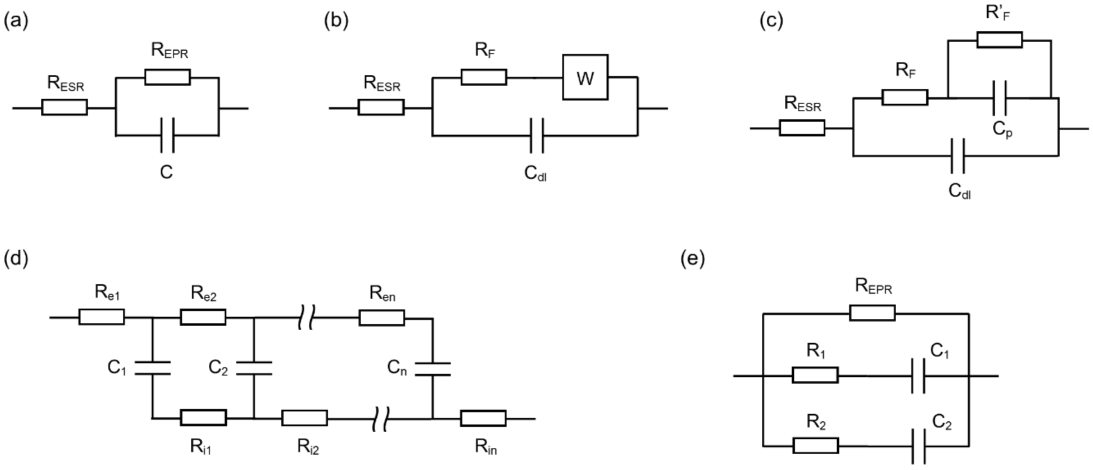

Figure 1-2. Equivalent circuit models of supercapacitors. (a) The simplest model including a capacitance, an equivalent serial resistance (R_{ESR}) and an equivalent parallel resistance (R_{EPR}). (b) The Randles circuit. (c) The equivalent circuit considering both EDL capacitance and pseudo capacitance. (d) The transmission line model that describes a porous electrode with both electronic resistance (R_e) and ionic resistance (R_i). (e) The two-branch model to simulate supercapacitor behaviors in two different time scales. [19]

More accurate models of supercapacitors can be established by considering the electrochemical processes in the device. For example, the charge transfer process in the electrolyte involves the diffusion of ions, which can be modeled as a Warburg impedance (W) [12]. A typical equivalent circuit taking W into account is the Randles circuit as shown in figure 1-2b [12]. Such a circuit can explain why a constant phase angle near 45^{o} is observed when testing the impedance of some supercapacitors in low frequency range.

When double-layer capacitance (C_{dl}) and pseudo capacitance (C_p) are considered separately, an equivalent circuit can be drawn as in figure 1-2c. Here, C_p is in series with a Faradaic charge transfer resistance (R_F) and in parallel with another resistance (R'_F) representing leakage through the Faradaic reactions.

The equivalent circuit can also become more complex when the structure of electrodes is considered. For example, a transmission line model (figure 1-2d) can be used to describe the bi-continuous nature of electron path (represented by R_e) and ion path (represented by R_i) in a porous electrode, and the capacitance (C) at the electrode-electrolyte interface.

In practical applications, a certain time scale may be of particular interest, and researchers can use multiple R-C branches to model supercapacitor's behavior in different time domains. For example, the two-branch model in figure 1-2e may describe the short-term behavior of the device with one branch, and the long-term behavior with the other one [26]–[28].

1.2.3 Calculation of energy and power

As an energy storage device, the most important features of a supercapacitor are the amount of energy it can store and power it can provide per unit weight or volume. Supercapacitors can store more energy than conventional capacitors because they have larger capacitance which can be as high as more than 1,000 F/g or 1,000 F/cm^3 [29]. But the energy E stored in a capacitor is not only proportional to the capacitance C, but also limited by the operational voltage V as:

$$E = 1/2CV^2 \tag{1.2}$$

Therefore, the maximum voltage of a supercapacitor should always be considered together with the capacitance.

The voltage limit of a supercapacitor is determined by the electrochemical and chemical stability of both electrode and electrolyte. For carbon based EDL electrodes, the electrolytes are usually more unstable and thus limit the voltage. For example, EDL capacitors using aqueous electrolytes have a voltage up to 1V since the electrolysis of water happens at 1.2V. But devices using organic solvent-based electrolytes or ion liquids can be charged to 2.5 – 3.5 V [30]. For pseudo capacitors, however, the reversible reactions that lead to capacitance effect only happen within certain voltage range. For example, one of the most studied pseudo capacitive material with very high specific capacitance, RuO_2, has three accessible oxidation states within 1.2 V. Another promising electrode material for pseudo supercapacitors, MnO_2, shows excellent capacitive behavior within less than 1 V [13].

It is worth noting that, although some pseudo capacitive material has extremely high capacitance, it may not store more energy than EDL capacitors because of low operation voltage. For example, a symmetric supercapacitor using MnO_2 with a capacitance of 1145 F/g for each electrode stores specific energy of ~25.4 Wh/kg at an operation voltage of 0.8 V [29], and the device using activated graphene with 166 F/g stores ~70 Wh/kg at 3.5 V [20].

To measure the capacitance and energy capacity of a supercapacitor, two electrochemical approaches are mostly adopted. One is cyclic voltammetry, which applies a linearly increasing/decreasing voltage and measures the charge/discharge current, the other is chronopotentiometry, which uses a constant current to charge/discharge the device and measures the voltage. The average capacitance over the measured voltage range can be calculated by definition as:

$$C_{avg} = \frac{\Delta Q}{\Delta V} = \frac{\int_0^{\Delta t} I\,dt}{\Delta V} \tag{1.3}$$

where ΔQ is the total charge transferred; ΔV is the voltage range measured; I is the current measured or applied; Δt is the total time of the measurement. The capacitance is usually not a constant over the operating voltage range, and equation (2) may not be accurate enough to calculate the energy for supercapacitors. Instead, more accurate calculation of energy by measurement is:

$$E = \int_0^{\Delta t} V \cdot I \, dt \tag{1.4}$$

where V and I are measured voltage and current over time. The power can be calculated at the same time:

$$P = \frac{E}{\Delta t} \tag{1.5}$$

It should be noted that measured energy densities are highly dependent on the test conditions, especially the charge/discharge rate of the device. Smaller value of energy density is always obtained when the device is working at higher power (i.e., under higher scan rate or larger charge/discharge current). The phenomenon is caused by the equivalent internal resistance, including electrical resistance and ionic resistance, of the device. By looking at the simplest equivalent circuit model in figure 1-2a, it is obvious that the equivalent serial resistance causes higher IR drop when a higher current goes through the circuit, and less charge/energy can be stored into or withdrawn from the capacitor. The input/output power of the supercapacitor will reach a maximum value before the IR drop exceeds the operation voltage.

A comprehensive approach to evaluate the performance of a supercapacitor device is to test over a wide range of various scan rates or charge/discharge currents, calculate the corresponding power and energy, and plot the results in a Ragone plot [12]. The Ragone plot provides the important information of how much energy can be stored into/withdrawn from an energy storage device when it’s working at a certain input/output power.

1.2.4 Performance metrics of supercapacitors

Researchers have been reporting the performances of supercapacitors normalized by weight or volume so that it’s easier to evaluate different electrode materials. Such values are of significance for evaluation of the potential energy capacity of a supercapacitor device. However, the volumetric/gravimetric capacitance of a certain material is usually not constant with different electrode thicknesses. Instead, it decreases when the electrode becomes thicker, especially for EDL electrodes with complex inner pore structure [31], or pseudo capacitive materials with inaccessible redox sites [32].

Another consideration is that, a practical supercapacitor device usually comprises of active electrode material, electrolyte, separator, current collector, and other package materials. The true energy/power density of a supercapacitor should include the volume/weight of the whole device [21]. The performance metrics used to evaluate a supercapacitor should also consider the application situation. For example, in an integrated micro systems with micro supercapacitors (MSC) as the power source, the weight of a MSC is negligible, and the substrate area and device volume are always limited. Therefore, the areal and volumetric performances of MSCs are of more significance than the gravimetric ones [19], [22]. In some wearable device such as a smart watch, the volume allocated for the power source is limited, and the volumetric energy/power density is the major concern.

Besides energy and power densities, other characteristics of supercapacitors can also be important for practical applications. Thanks to the working mechanisms of supercapacitors, they show shorter charge/discharge time, longer cycle life, and safer operation than LIBs. Table 1-1 compares some major characteristics of current commercial supercapacitors and LIBs. The major shortcoming of supercapacitors is their lower energy density (about 1 order lower) compared with LIBs. But supercapacitors outperform LIBs in power density (1 order higher), charge time (2 orders faster), and cycle life (3 orders longer). Moreover, LIBs rely on vigorous chemical reactions between cathode and anode, and are intrinsically explosive. The use of organic solvents and lithium ion electrolyte can also make them flammable and toxic. The charge/discharge of LIBs involves lithium ions insertion/de-insertion in both electrodes, which causes high stress and volume change and further increases the chance of unsafe issues. While some supercapacitors use toxic ions and flammable electrolytes, their operation can still be a lot safer than LIBs, because there is no mechanical stress or volume change when they are working. The working mechanisms of supercapacitors also allows more choices of electrode-electrolyte systems that are nontoxic and environmentally friendly.

Table 1-1. Comparison of current commercial supercapacitors and LIBs

	Current Commercial Devices	
	LIBs	Supercapacitors
Energy (Wh/kg)	10 - 200	1 - 20
Power (W/kg)	100 – 1,000	1,000 – 10,000
Charge time	Hours	Seconds/Minutes
Cycle life	~1,000	~1,000,000
Safety	Flammable, Explosive, Toxic	Safer (No violent reaction)

1.3 Flexible supercapacitors and research challenges

As safety and stability become more critical in flexible electronics, to replace LIBs with FSCs as the new flexible power sources is tempting. Although current commercial supercapacitors generally show 1 order lower energy density than LIBs with similar device configuration and package, the situation can be much better in flexible applications. Because Flexible LIBs have to sacrifice their overall energy density to be made flexible and safe enough with larger portion of additives, stabilizers, and package materials, while FSCs don't. Moreover, FSCs can use more space to store energy if they are flexible and safe enough. For example, a large piece of FSC can be integrated into a jacket and does not cause inconvenience, while a rigid LIB with the same weight/volume can be troublesome to carry.

Much attention has been drawn on FSCs in recent years due to their great potentials. Reported FSCs can be classified into either two-dimensional (2D) thin-film type or one-dimensional (1D) fiber type based on their overall configuration [16], [33]–[35]. The 2D type usually assembles active nanomaterials on a flexible substrate to construct FSCs, while the 1D type builds all functional components on thin and long fibers. Instead of electrode configurations, we may consider the potential applications of FSCs and divide them into two types, which are micro FSCs intended to be integrated with printed flexible electronics, and large-size wearable FSCs to be integrated with our daily wearables. Such classification is more useful to analyze and evaluate FSCs.

One research direction of FSCs is to study micro FSCs integrated with the electronics they are powering on the same flexible substrates. Potentially, such devices are supposed to be coupled with micro energy harvesters as power sources to realize self-powering systems for different wireless applications, such as wireless sensor networks (WSN), implantable medical devices, and active radio frequency identification (RFID) systems [19]. Small size, flexibility, and integrate-ability are all very important for certain device such as a medical sensor attached on human body. The coupling with energy harvesters may reduce the requirement of energy density of such FSCs, but the major challenge is to integrate them with other components in a cost-effective manner. As part of the dissertation, the direct writing of nanofibers on flexible substrate to construct micro FSCs that feature low cost and easy integration will be explored.

Another hot topic of FSCs is large-size wearable FSCs, which are potential power source for future wearable consumer electronics. As today's consumer electronics are usually multifunctional and consuming significant amount of power, considerable weight/volume will be needed for the power source. To integrate FSCs into our daily wearables is one of the most promising solutions. While researchers have developed various 1D and 2D FSCs [2], [18], [35], [36], the two major challenges remain: (1) The overall electrochemical performance (e.g. energy density) needs to be improved with substrate and package materials considered. (2) The mechanical property (e.g. flexibility, durability, strength) of the whole device should be comparable to wearables to be integrated with. The rest of the dissertation explores two solutions to consider both challenges for wearable FSCs. Both solutions are based on micro carbon fibers, including ultra-thin coaxial fiber supercapacitors and woven supercapacitor fabrics.

1.4 Structure of the dissertation

The dissertation aims to develop micro/nanofiber-based electrode materials, fabrication processes, and device configurations to improve properties of FSCs towards practical applications. While the motivation and research background have been introduced in Chapter 1, the content of the following chapters is briefly illustrated in Figure 1-3 and described below.

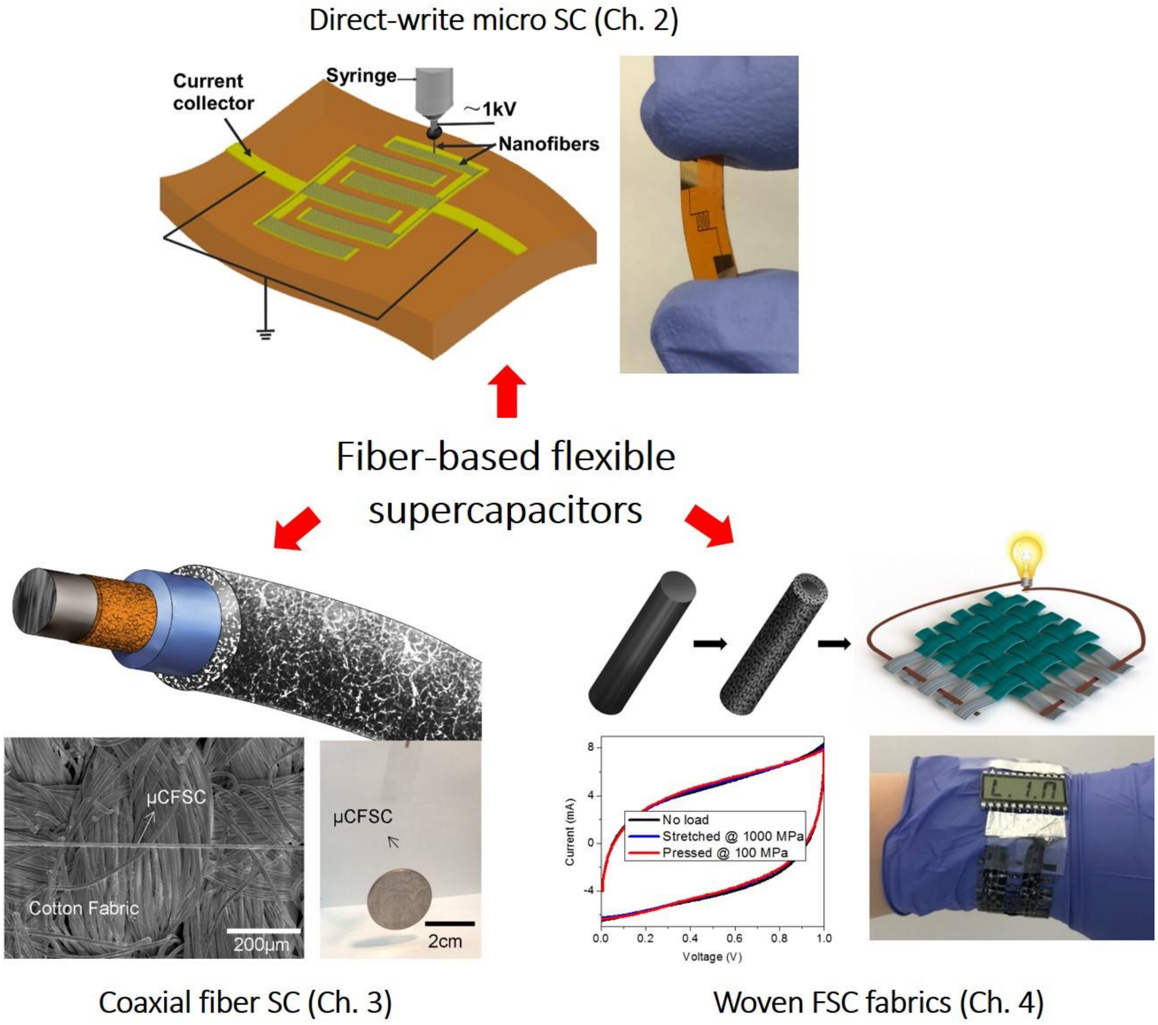

Figure 1-3. Summary of the micro/nanofiber based flexible supercapacitors developed in the dissertation.

In Chapter 2, micro FSCs prepared using direct-write nanofibers is demonstrated for flexible integrated microelectronics. The micro electrodes with porous network are fabricated by the near-field electrospinning of polypyrrole (PPy) nanofibers on a patterned metal layer deposited on flexible substrate. Such conductive nanofiber network with a pseudocapacitance effect greatly increases the capacitance and facilitates ion transport in the electrodes. The micro FSCs are experimentally proved to be highly flexible with excellent electrochemical performance and cycling stability. The approach is simple, versatile, and compatible with different substrates for the direct integration of energy storage devices in flexible microsystems. [37], [38] In Chapter 3, an ultra-thin micro coaxial fiber supercapacitor (μCFSC) with high energy and power densities, as well as excellent mechanical properties is demonstrated as functional fibers to be integrated into wearable fabrics. The prototype with the smallest reported overall diameter of 13 μm is fabricated by successive coating of functional layers onto a single micro carbon fiber via a scalable process. Combining the simulation results via the electrochemical model, the high performance is attributed to the well-controlled thin coatings that make full use of the electrode materials and minimize the ion transport path between electrodes. Moreover, the μCFSC features high bending flexibility and large tensile strength (more than 1 GPa), which make it promising as a building block for various flexible energy storage applications. [34], [39]

In Chapter 4, free-standing woven supercapacitor fabrics that can store high electrical energy and sustain large mechanical loads are proposed and demonstrated as readily scalable flexible power sources. The prototype with reduced package weight/volume provides an impressive overall energy density of 2.58 mWh g^{-1} or 3.6 mWh cm^{-3}, high tensile strength of over 1000 MPa, and bearable pressure of over 100 MPa. The nanoporous thread electrodes are prepared by the activation of commercial carbon fibers to have three-orders of magnitude increase in the specific surface area and 86% retention of the original strength. The novel device configuration woven by solid electrolyte-coated threads shows excellent flexibility and stability during repeated mechanical bending tests. Such scalable energy storage fabrics can be integrated into daily graments as flexible power sources for a variety of wearable electronics. [40]

Chapter 5 concludes the dissertation and suggests several future directions for the research.

2 Flexible micro supercapacitors based on direct-write nanofibers

2.1 Introduction

Miniaturized wearable electronics, implantable medical devices, and active radio frequency identification (RFID) have limited space for power sources inside them. Micro batteries are not sufficient to power such systems with high power consumption by wireless communications. The integration of micro energy harvesters with safe and durable energy storage elements, such as supercapacitors [8], [19], [41], is a better solution. To apply high-performance supercapacitor materials to energy storage devices in micro systems, considerations on both material synthesis and device fabrication are required. Desirable characteristics of such supercapacitors include: (1) small size compatible with other components; (2) low manufacturing cost with the possibility to directly integrate with the rest of the system; and (3) good flexibility to fit in with different form-factors, especially for the applications in flexible systems.

On-chip micro supercapacitors, especially carbon-based EDL capacitors, have been demonstrated by using various technologies to grow active materials, including chemical vapor deposition (CVD) used for the direct growth of CNTs [42]–[46], carbide derived carbon [31], [47], [48], silicon nanowires [49], silicon carbide nanowires [50]–[52], and carbonization used for the synthesis of patterned micro-sized carbon electrodes with nanopores [53], [54]. Some of these supercapacitor electrodes have been constructed on silicon wafers for possible integration with microelectronics. However, the typical high temperature process requirements in making these nanostructures prevent their direct integration with silicon-based devices. Electrophoresis has been used to assemble onion-like carbon particles to form interdigital electrodes with ultrahigh power [55], but it involves wet process which also limits the direct integration process when immersing the substrates in complex electrolytes. Similar issues are encountered when developing pseudo capacitors on a chip by evaporation [56], chemical growth [57], or electrochemical deposition [58], [59]. Printing of nanostructured carbon particles [60] and laser writing of graphene [61]–[63], on the other hand, have shown the good possibility of making micro supercapacitors on flexible substrates for EDL capacitors without the capability of making pseudo capacitors with higher capacitance.

In this chapter, the direct-write flexible micro supercapacitors by near-field electrospinning of polypyrrole nanofibers are proposed and demonstrated. The continuous nanofiber network with high surface area is ultra-flexible and makes full use of the active material for high pseudo capacitance. The direct-write process performed under room temperature does not involve wetting of the substrate. It is simple, low-cost, and applicable to arbitrary flexible surfaces for possible direct integrations with other devices and systems.

2.2 Materials and process design

Conducting polymers, such as polypyrrole, poly(3,4-ethylenedioxythiophene) and polyaniline, are a group of polymers that conduct electrons when they are doped [64]. They can work as pseudo capacitive materials to store energy by the doping/de-doping (charging/discharging) effect in ion-containing electrolytes. Conducting-polymer-based supercapacitors show much higher specific capacitances than EDL capacitors. Their power densities and cycling capabilities, on the other hand, can be improved by using proper nanostructures that reduce ion diffusion within the electrode material [23], [46], [64]. Electrodes with nanofiber network of such conducting polymers can offer not only high surface area and efficient ion transport path for improved energy and power density, but also high mechanical flexibility. The facile deposition of such nanostructured materials on arbitrary substrate can be a promising way to integrate high performance micro supercapacitors with other electronic components.

Electrospinning is a simple and versatile technique to generate continuous fibers with diameters from submicron down to nanometers [65], [66]. It uses electric force to draw charged threads of polymer solutions or polymer melts. Different kinds of functional fibers, most of which are made of chain polymers, can be produced by electrospinning as long as a uniform solution with proper viscosity and surface tension can be prepared. When a sufficiently high voltage is applied to such solution, the charges will accumulate at the surface and electrostatic repulsion counteracts the surface tension so that the surface is pulled and stretched. A stream of solution will erupt from the surface at a critical point, which is known as the Taylor cone. A charged liquid jet is formed without break as long as the molecular cohesion of the solution is high (viscous) enough. The jet dries in flight, and is then elongated and thinned by a whipping process caused by electrostatic repulsion initiated at small bends in the fiber, until it is finally deposited on the grounded collector, leading to the formation of uniform fibers with nanometer-scale diameters [67]. While traditional electrospinning is unstable in nature as it relies on the chaotic whipping of liquid jets to generate nanofibers, near-field electrospinning (NFES) [66], in which the electrode-to-collector distance is only 0.5-5 mm, utilizes the stable liquid jets region for controllable deposition [66], [68]. To deposit nanofiber network onto micro-patterned electrodes on flexible substrates, NFES of conducting polymer solution is proposed and demonstrated. The electrospun conducting polymer nanofibers can enhance the performance of supercapacitor electrodes, because the continuous nanoporous network provides a large surface area that ensures the full usage of active material and facilitates ion transport and diffusion in the electrode. Moreover, the micro energy storage device can be easily integrated with other flexible and miniaturized systems, since NFES can orderly deposit nanofibers onto micro-sized patterns on arbitrary surfaces, as illustrated in Figure 2-1a.

To demonstrate the feasibility of direct-write nanofiber network on patterned micro electrodes, the fabrication process of the micro supercapacitor prototype is designed as the cross-section illustration shown in Figure 2-1b to d. Photoresist is first spin-coated on the substrate and patterned by photolithography (Figure 1b). Then a layer of gold is thermally evaporated onto the substrate, and additional photoresist is removed by the lift-off process to construct interdigital electrodes (Figure 1c). The metal layer is much more conductive than the functional polypyrrole and it serves as the current collector to improve the overall performance of the device. Such a layer is also needed for electrical connection with other components in an integrated micro system, and it does not increase the complexity of the whole electronic system. NFES process is followed to deposit functional nanofibers onto the electrodes, during which the substrate is fixed on a computer-controlled X-Y motion stage. The solution containing conducting polymer is filled into a syringe equipped with a flat-end needle. The syringe is put above the gold pattern, and the needle is connected to a high voltage source with the gold electrode grounded. By tuning the output voltage, nanofibers can be pulled out of the tip from the viscous solution in the syringe by the electrostatic force and fall onto the grounded electrodes (Figure 1d). The motion stage is preprogrammed during the process to write the nanofibers on the interdigital patterns. [37]

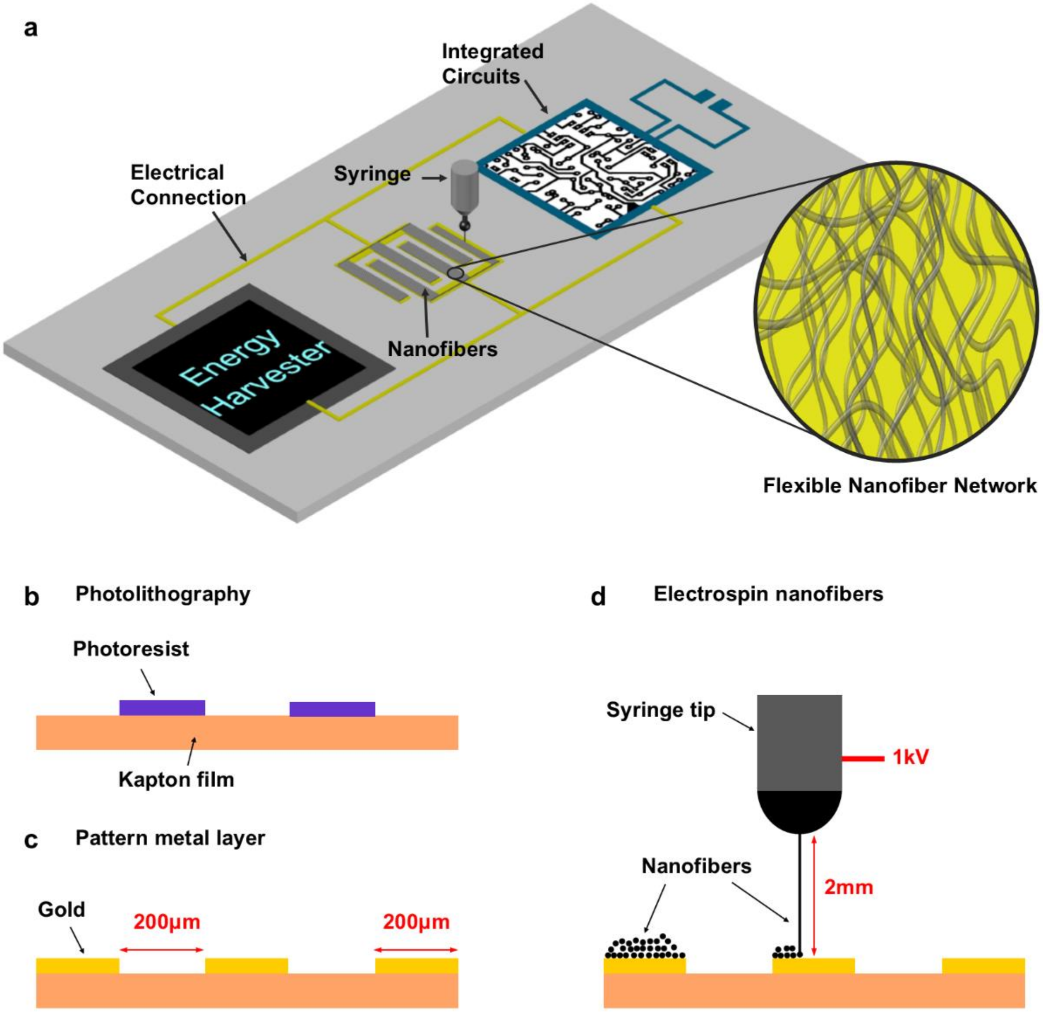

Figure 2-1. (a) Schematics of the direct writing of a nanofiber-based micro supercapacitor on an arbitrary substrate to integrate with an energy harvester and other circuits. Flexible nanofiber network is locally deposited on the metal electrodes with micro-sized patterns by using near-field electrospinning. (b)-(d) Cross-section schematics of the fabrication process. (b) Patterning of photoresist on the flexible substrate by photolithography. (c) Patterning of electrodes by the deposition of gold and the removal of the photoresist. (d) Writing of nanofibers onto electrodes by using NFES. [37]

2.3 Synthesis and electrospinning of conducting polymer

The key to process the nanostructure designed in section 2.2 is to prepare conducting polymer solution that is compatible with NFES. Here, Polypyrrole (PPy) is used as the active material for micro supercapacitors, because it has high theoretical capacitance and high conductivity when properly doped [64]. In fact, undoped PPy is not conductive and not soluble in water or organic solvents, which makes it difficult to process. In order to prepare uniform PPy solution for NFES, soluble doped PPy is first synthesized by using docusate sodium salt as the dopant [69]. Such a dopant contains both polar and non-polar chemical groups that help PPy dissolve in different kinds of organic solvents.

(1) Synthesis of soluble PPy:

In a typical process of this work, 8.05 g of pyrrole monomer is mixed with 26.67 g of docusate sodium salt in 180 mL of deionized water to make the solution A, while 4.01 g of ammonium persulfate is dissolved in 20 mL of deionized water to make the solution B. Both solutions are cooled down to 0 ^{o}C, and solution B is slowly added into solution A under stirring. The reaction is kept at 0 ^{o}C under continuous stirring for 24 h. The PPy becomes precipitate, and is then filtered, washed by methanol and water for several times. After drying under vacuum for 12 h, the PPy powder is collected and dissolved in dimethylformamide (DMF) to make up to 8 wt% solution for the following process (denoted as “lab-synthesized PPy”).

(2) Preparation of electrospinnable solution of lab-synthesized PPy:

Pure PPy solution shows low viscosity (low molecular cohesion) and high surface tension for NFES. To enhance the viscosity and reduce the surface tension of the solution, another polymer, polyethylene oxide (PEO), is added in the solution. The final deposited fiber contains both PPy and PEO, but only the PPy is functional as electrodes. Therefore, the minimum amount of PEO should be used. We applied a PEO product with very high molecule weight of ~5,000,000 so that small amount of PEO can significantly increase the viscosity of the composite solution. In a typical process, PEO is dissolved in a mixed solvent (DMF: Acetone=2:3) to make 2 wt% solution. The 8 wt% PPy solution is then mixed with the PEO solution so that the weight ratio of lab-synthesized PPy and PEO is controlled in the final solution.

(3) NFES of electrospinnable solutions:

The composition of polymer solution, the solution-to-substrate distance, and the applied voltage can all greatly affect the morphology of the electrospun nanofiber network. In the first step, the ratio of lab-synthesized PPy and PEO and the distance between the polymer solution and substrate are varied and experimented. We find that only certain combinations of conditions may result in nanofibers, as summarized in Table 2-1.

Table 2-1. Electrospinning results with different ratios of PPy and PEO and solution-to-substrate distances

Weight ratios (PPy:PEO)	Solution-to-substrate distance*			
	Far-field		Near-field	
	3cm	1cm	0.5cm	0.3cm
8:1	Nanofibers/droplets	N/A	N/A	N/A
5:1	Nanofibers/droplets	Droplets	N/A	N/A
4:1	Nanofibers	Nanofibers	N/A	N/A
3:1	Nanofibers	Nanofibers	N/A	N/A
1:1	N/A	Nanofibers (0.8-1.6kV)	Nanofibers (0.6-1kV)	Nanofibers (0.6-1kV)

*High voltage is applied between the polymer solution and substrate with fixed distance. The voltage is increased until spark (usually caused by the breakdown of the air) happens. N/A means no nanofibers are found on the substrate during the electrospinning.

The results from Table 2-1 show that, when the weight ratio of PPy and PEO is larger than 5:1, it is difficult to form continuous nanofibers by electrospinning, probably because the low viscosity of the solution makes the liquid jet easy to break during elongation. When the ratio is reduced to 4:1 and 3:1, it is possible to produce continuous fibers at far distance. But when the distance is reduced, the breakdown of air usually happens before the extrusion of polymer solution. The reason is that very high voltage is needed to overcome the surface tension of the solution. The solution with PPy:PEO=1:1, however, has sufficiently low surface tension and can be electrospun at near-field condition. Interestingly, such solution doesn’t work well for far-field electrospinning. The solution becomes dried long before falling onto the substrate and will float in the air (does not come down to the substrate).

With the optimized composition of the solution (PPy:PEO=1:1), PPy/PEO composite can be directly written and aligned on a substrate. Figure 2-2a shows the photo of the NFES setup including a syringe holding the polymer solution with metal tip connected to a high voltage source, and the substrate fixed on a motion stage. When the NFES starts, the motion stage moves with path controlled by a programmed controller so that the nanofibers will be written on the substrate. Figure 2-2b shows the result of writing parallel lines on a substrate with a gold layer. The parallel lines are programmed to be 10 μm apart. Such conductive, parallel fibers can also be used for sensing applications, as demonstrated in a paper by the author [70]. In fact, the motion stage has to move fast enough to write straight lines. If the motion stage moves slower than the nanofiber generation speed, the nanofibers will buckle on the substrate as shown in Figure 2-2c, and Figure 2-2d is the result when it moves even slower.

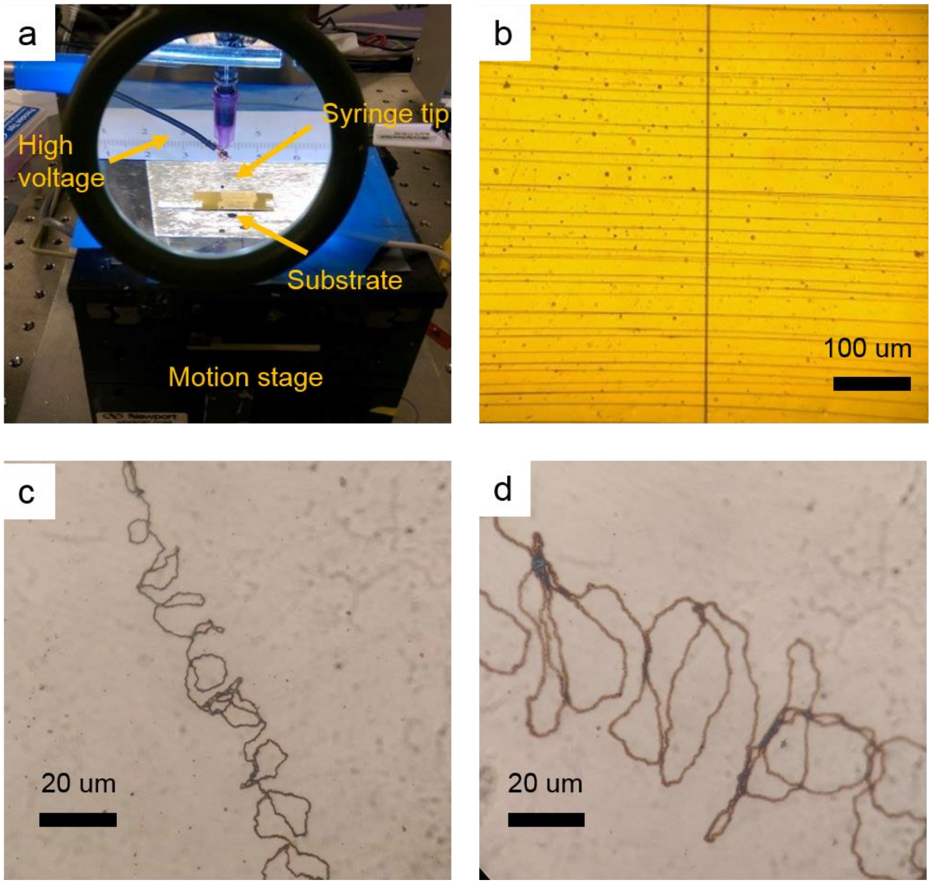

Figure 2-2. Near-field electrospinning (NFES) setup and results. (a) The setup of NFES including a syringe with metal tip connected to high voltage source and substrate fixed on a motion stage. (b) Horizontal, parallel nanofibers written on gold electrode deposited on a polymer substrate. (c) – (d) Buckling effect of direct-write nanofibers when the writing speed (speed of the motion stage) is smaller than the nanofiber generation speed.

(4) Preparation and electrospinning of commercial PPy as control:

Since the properties of conducting polymer vary a lot by using different synthetic processes, we also examine a commercially available PPy product (denoted as "commercial PPy") as a control in our experiments. The PPy dispersion (5 wt% in water) supplied from Sigma-Aldrich is mixed with PEO (Mw~300,000) and Triton X-100 in this case. The Triton X-100 acts as a surfactant that can greatly reduce the surface tension of the solution so that the NFES process can be easier to conduct. Typically, 0.5 g of PEO is dissolved in 2 g of de-ionized water and stirred for 3 h. Then 5 g of PPy suspension and 0.25 g of Triton are added into the solution and stirred overnight. The solution can be electrospun with the same voltage and solution-to-substrate distance as the lab-synthesized PPy/PEO solution.

2.4 Flexible micro supercapacitor fabrication

To demonstrate flexible micro supercapacitor, the Kapton® polyimide film is used as a flexible plastic substrate. As illustrated in Figure 2-1b to d, micro supercapacitors are fabricated by NFES of PPy nanofibers on patterned gold electrodes. The thermally evaporated gold layer is 100 nm thick. The flat-end syringe tip is 22 gauge, and is ~2 mm above the gold pattern. The voltage source is fixed at 1 kV for the direct-write process.

Figure 2-3a shows the optical photo of the electrode pattern. Each gold "finger" in the pattern is 200 μm wide, 1300 μm long, with 200 μm-wide gap in between. The total area of the comb-shape interdigital electrodes is 2.2 mm × 1.9 mm. Figures 2-3b and c show microscopic photos of an electrode finger before and after the NFES process. It can be seen that the gold surface is uniformly covered with nanofibers after the electrospinning.

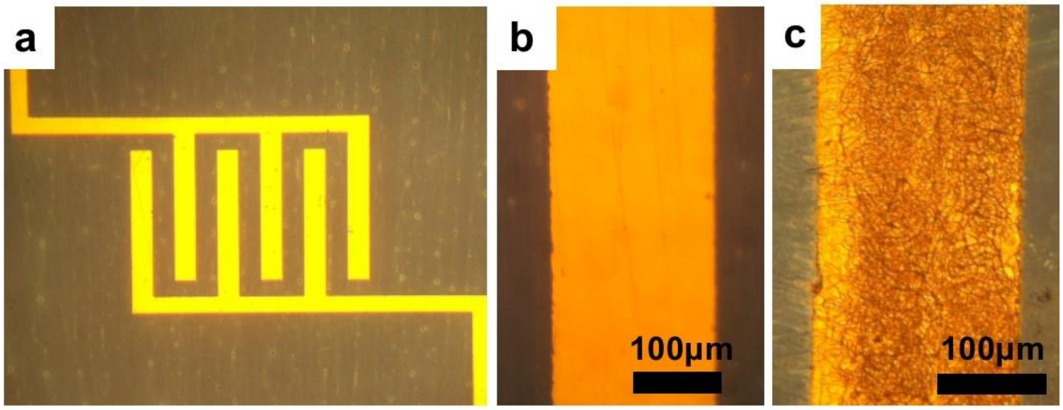

Figure 2-3. Optical photos of (a) comb-shape interdigital gold electrodes, (b) a blank electrode surface, and (c) an electrode that is covered by electrospun nanofibers.

SEM image in Figure 2-4a shows a 1 μm thick layer of nanofibers with the average diameter of 200 nm electrospun from commercial PPy dispersion on a Si wafer. The samples on a plastic substrate, however, display poor SEM image because of the low conductivities of both the substrate and the commercial PPy material. In the prototype we use to test the electrochemical performance, the thickness of the nanofiber network is about 5 μm. Figure 2-4b shows the SEM image of the nanofibers made of lab-synthesized PPy with an average diameter of 700 nm and the average thickness of about 5 μm on the plastic substrate. The image quality is better in this case, since the conductivity of lab-synthesized PPy is higher and the nanofibers are thicker. Nano-sized roughness is seen on the surface of the nanofibers and it helps to increase the total surface area of the network.

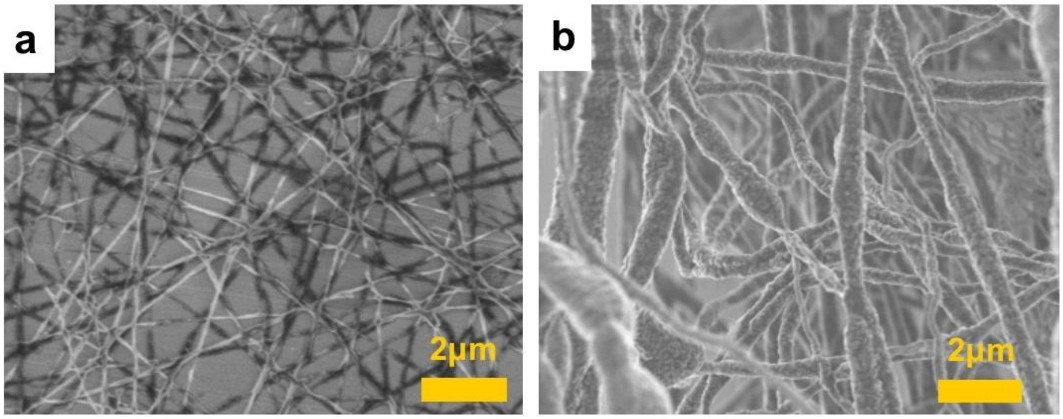

Figure 2-4. Scanning electron microscopic (SEM) images of (a) electrospun nanofibers of commercial PPy, and (b) electrospun nanofibers of lab-synthesized PPy.

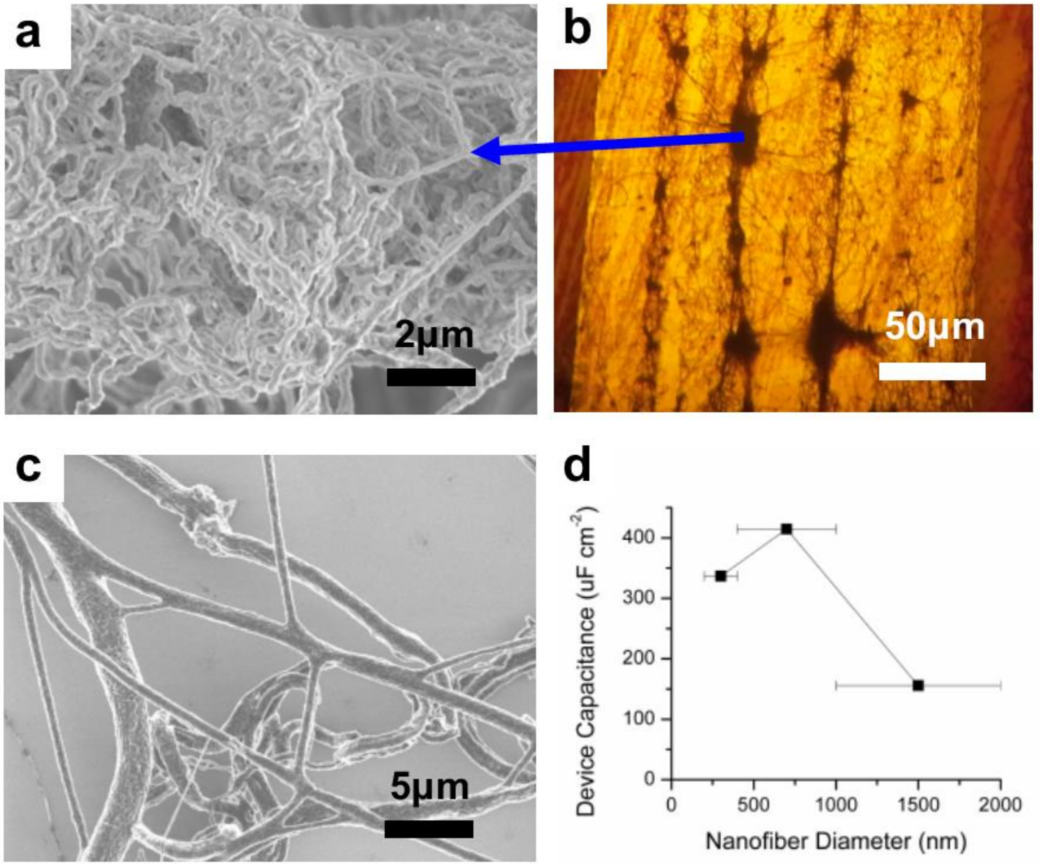

Figure 2-5. (a) SEM image of nanofibers that are electrospun from the solution in which the weight ratio of lab-synthesized PPy and PEO is 7:3. (b) Optical photo of the gold electrode with nanofibers deposited on it, where nanofibers tend to aggregate on random locations. (c) SEM image of nanofibers that are electrospun from the solution in which the weight ratio of lab-synthesized PPy and PEO is 4:6. (d) Device capacitances of nanofibers deposited from different solutions.

The diameter of the nanfibers can be tuned by adjusting the viscosity and the surface tension of the polymer solution, as well as the NFES parameters such as the voltage and tip-to-substrate distance. For example, nanofibers that are 300 ± 100 nm in diameter are spun form the solution in which the weight ratio of lab-synthesized PPy and PEO is 7:3 (Figure 2-5a). However, the electrospinning process of such a solution is not stable, and nanofibers tend to aggregate on random locations on metal electrodes (Figure 2-5b). Thicker nanofibers with diameters of 1500 ± 500 nm are spun from a more viscous solution (PPy : PEO = 4:6, Figure 2-5c). Such nanofibers are sparsely distributed on metal electrodes, and result in relatively low capacitance (Figure 2-5d). The optimized process results in nanofibers that are uniformly deposited on metal electrodes, as indicated by Figures 2-3c and 2-4b, and is considered as the most reliable condition for the deposition of lab-synthesized PPy.

Figure 2-6a shows a photo of the plastic substrate with multiple cells of micro supercapacitor on it. The fabrication process is applicable to various substrates with larger arrays, even substrates with other components on them, as illustrated in Figure 1a. To test the electrochemical performance of the prototype, a solid-state polymer electrolyte is applied to complete the device. The electrolyte is prepared by first dissolving 1g of polyvinyl alcohol (PVA, Mw~90,000) in 8g of de-ionized water at 80 ^{o}C under stirring until it becomes clear, and then 1 g of 85 wt% H_3PO_4 is added into the solution. The solution is applied onto the active electrode area and dried in the air. Figure 2-6b shows a complete prototype ready for testing, where a thin and transparent layer of polymer electrolyte covers the electrode area. Three kinds of cells are prepared for comparison: a blank cell without nanofibers on the gold electrodes, a cell with nanofibers of commercial PPy, and a cell with nanofibers of lab-synthesized PPy.

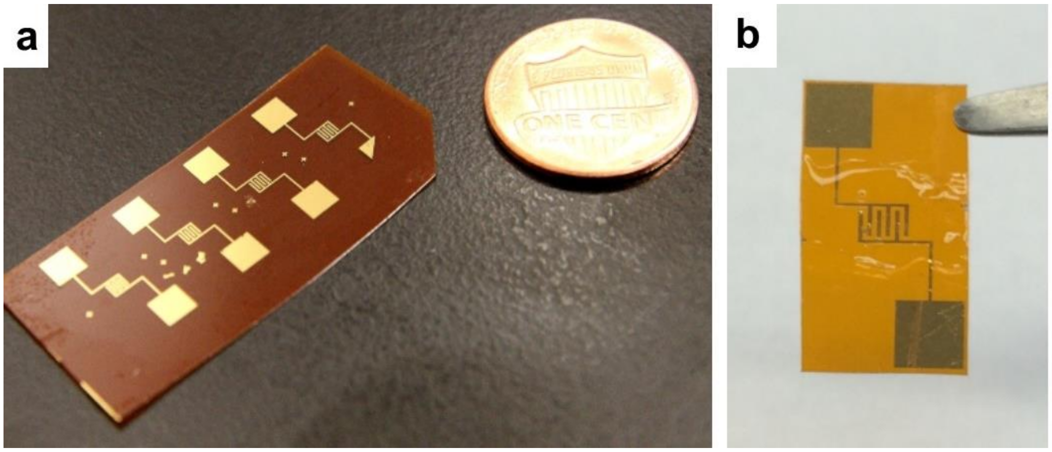

Figure 2-6. Optical photos of (a) multiple micro supercapacitor cells on a piece of plastic substrate and a one-cent US coin at the background, and (b) a prototype with a thin layer of polymer electrolyte.

2.5 Electrochemical performance

The supercapacitor performances are characterized and recorded by a Gamry Reference 600 potentiostat. Figures 2-7a and 2-7b show the cyclic voltammetry (CV) curves of the prototypes using commercial PPy and lab-synthesized PPy, respectively. Both cells show capacitive energy storage behavior indicated by the symmetric parallelogram shapes under different scan rates and the increase of currents with scan rates. Since the devices are charged and discharged at a higher rate when the scan rate is higher, the excellent capacitive performances preserved at 1 V s^{-1} imply their potential applications for fast charge and discharge systems. Figure 2-7c compares the CV curves of three cells at the same scan rate of 20 mV s^{-1}. The blank cell shows a small current caused by the electrical double layer effect of the gold layer. The prototypes with nanofibers have much larger current density than the blank one, which proves that their supercapacitor performances are mainly contributed by electrospun nanofibers instead of the gold electrodes. Moreover, the cell using lab-synthesized PPy shows obviously larger current than the other ones, indicating its larger capacity.

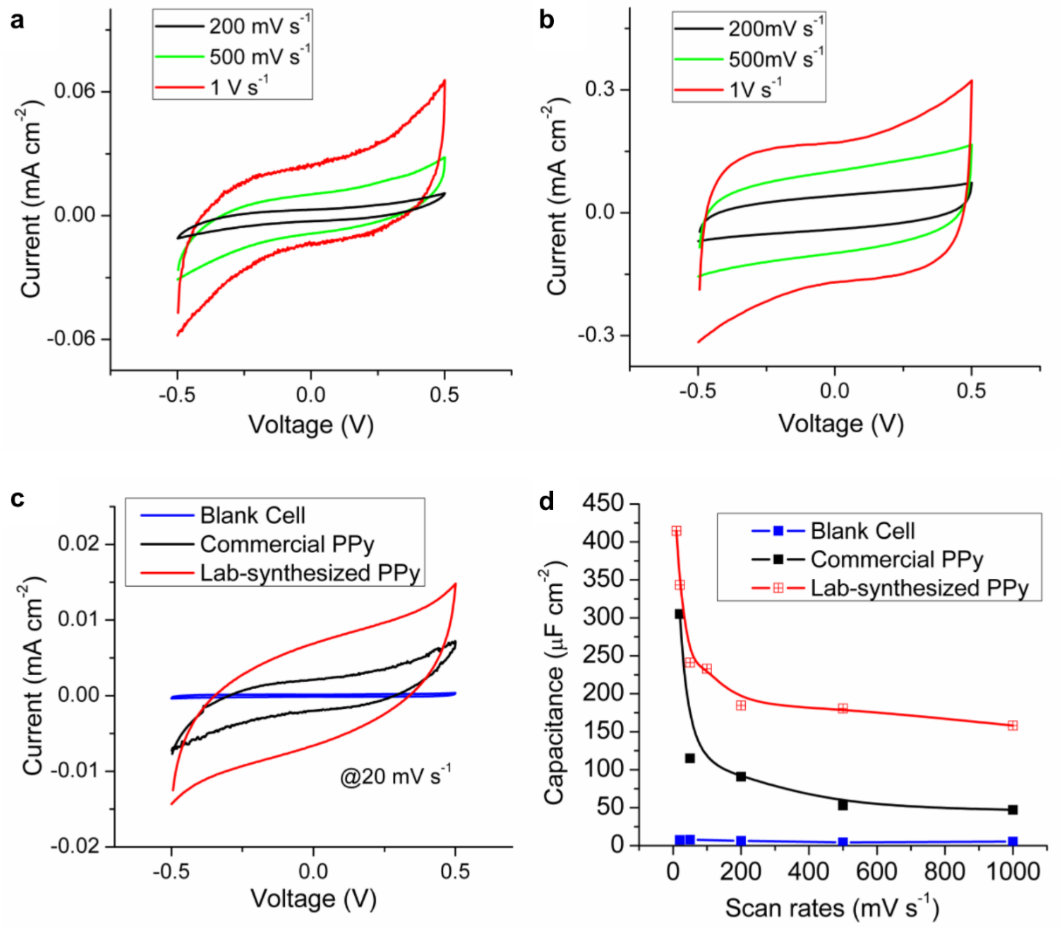

Figure 2-7. Cyclic voltammetry curves of the micro supercapacitor cells (a) using commercial PPy based nanofibers, and (b) using lab-synthesized PPy based nanofibers,

under different scan rates. (c) Comparison of CV curves of three cells at the same scan rate of 20 mV s^{-1}. (d) Calculated areal capacitances of three cells versus scan rates. [37]

The capacitances per unit area of the devices can be calculated from the CV curves by using the following formula:

$$C_{area} = \frac{\int Idt}{A \cdot \Delta V}$$

where I is the measured current on the CV curves, t is the time, A is the working area including both electrodes and electrolyte, and ΔV is the voltage range. Figure 2-7d compares the calculation results of three prototypes under different scan rates. The cell using lab-synthesized PPy exhibits the capacitance of 0.42 mF cm^{-2} at a scan rate of 10 mV s^{-1}, which is 40 % higher than the one using commercial PPy and almost two orders of magnitude higher than the blank cell without nanofibers. The cell with lab-synthesized PPy also shows better power performance, since its capacitance is about 3 times higher than the one with commercial PPy at a high scan rate of 1 V s^{-1}. The better performance of lab-synthesized PPy is mostly attributed to the better conductivity of the material. To evaluate the conductivities of the electrode materials, we drop cast the solutions used for NFES onto a glass substrate and test the conductivities of the thin films when they are completely dried by using a four-probe ohmmeter. The conductivity of the dried cast film of the commercial PPy dispersion is about 0.5 S m^{-1}, but since PEO is used to enhance the processability of the solution, the conductivity of the dry film containing commercial PPy/PEO is measure to be 0.03 ± 0.01 S m^{-1}. The film of lab-synthesized PPy/PEO, however, shows a much higher conductivity of 1.1 ± 0.2 S m^{-1}. The conductivity of the conducting polymer is highly dependent on the dopant and doping level. To further improve the performance of the lab-synthesized PPy, one way is to design a better synthetic process as the conductivity of PPy can be more than 10^4 S m^{-1} according to the literature [71].

On the other hand, a number of papers have demonstrated that performances including the capacitance and power per unit area can also be improved, by better designing of the electrode sizes and by increasing the thickness of the functional materials [72], [73]. The capacity of the prototype characterized in this paper can also be directly increased by repeating the NFES process, i.e. by depositing thicker layer of nanofibers. Our current experimental setup allows the uniform deposition of up to 5 μm-thick nanofiber network onto 200 μm-wide electrodes. This is because the control precision of the motion stage limits the writing precision, and nanofibers may not fall onto the exact position when the writing is repeated multiple times. But thicker layers are still achievable on wider electrodes with the same setup.

We have also conducted bending tests of the prototypes to evaluate their flexibility. Photos in figure 2-8a to c are the bending conditions, in which the prototype is kept straight, bent forward, and bent backward, respectively. Cyclic voltammetry curves of two cells with nanofibers are recorded at each bending state, as plotted in figures 2-8d and e. The curves show that the performances of both prototypes don't change much when they are bent. For the cell using commercial PPy, a minor drop in the current occurs when it’s bent backward. This phenomenon doesn’t happen on the other cell using lab-synthesized PPy, which shows almost exactly the same performance under different bending states. The reason for the slightly different responses is mainly due to the surface property of the nanofibers. The commercial PPy is hydrophilic such that nanofibers attach to the electrolyte layer better than the substrate. Small portion of the nanofibers loses contact with the gold electrode when the device is bent backward and the electrolyte layer is stretched. As a result, the testing current drops when less electrode material is connected to the metal layer. The lab-synthesized PPy, however, is bonded well with the gold electrode and not affected by the bending and deformation of the solid electrolyte. Both nanofibers are ultra-flexible due to the nature of the 1D nanostructures, which make them suitable as functional materials for applications in flexible systems.

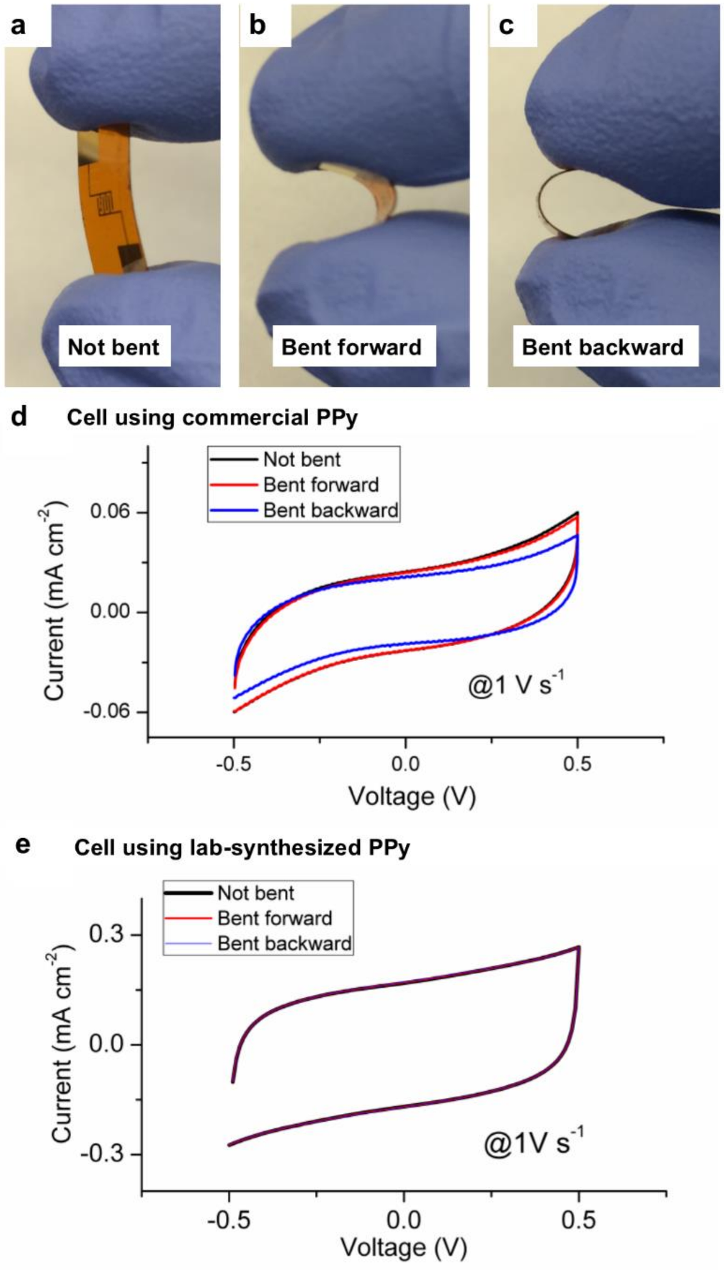

Figure 2-8. Photos of the micro supercapacitor with electrodes facing left when it's (a) straight, (b) bent forward, and (c) bent backward. The bending radius of curvature is kept at 3 mm during all tests. Cyclic voltammetry curves of the cells (d) using commercial PPy based nanofibers and (e) using lab-synthesized PPy based nanofibers, when they are bent at different directions.

Further characterizations including constant current charge-discharge test, impedance measurement and cycling test of the prototypes using lab-synthesized PPy are conducted, and the results are summarized in Figure 2-9. Cyclic voltammetry curves at low scan rates are tested from 0 to 1V as shown in Figure 5a. The capacitive behavior still dominates at 2 mV s^{-1} and no battery-like redox reactions are shown in the curves. Figure 2-9b shows the charge-discharge curves of the prototype under constant currents from 5 to 50 μA cm^{-2}. The nearly straight lines also indicate excellent capacitive behavior of the device. The internal resistance is estimated to be 3.1±0.1 kΩ cm^2 from the IR drops of the curves. A capacitance of 0.48 mF cm^{-2} is calculated at a charging current of 5 μA cm^{-2}, slightly higher than the value obtained from cyclic voltammetry curves (0.42 mF cm^{-2}). A volumetric capacitance of 0.96 F cm^{-3} is derived if the thickness of electrodes is considered. Most of the micro supercapacitors reported in the literature show areal capacitances between 0.1 and 10 mF cm^{-2}, and volumetric capacitances between 0.1 and 10 F cm^{-3} [74]. In addition to our nanofiber-based electrodes, various works have used 1D nanomaterials to build 3D porous networks for on-chip energy storage because such structures offer easily accessible high surface area. Most of them, such as SiC nanowires (0.24 mF cm^{-2}, or 0.24 F cm^{-3} [52]) and carbon nanotube forests (0.428 mF cm^{-2}, or 0.053 F cm^{-3} [75]), are based on EDL capacitance only. Our capacitance is relatively high compared to those structures with similar porosity because the EDL and the pseudo capacitance effect coexist in the PPy nanofibers. Some 2D structured materials, such as laser written graphene oxide (0.106 mF cm^{-2}, or 0.479 F cm^{-3} [63]), are also used for micro supercapacitor, and the capacitance is also limited by the single EDL effect. Besides EDL capacitors, our prototype shows better flexibility and areal capacitance than some pseudo capacitors using rigid material. For example, in a MnO_x/Au supercapacitor (0.39 mF cm^{-2} [56]), very thin 2D MnO_x/Au layers has to be used to improve the conductivity and keep the flexibility of the electrodes.

The energy densities and power densities of the prototype are calculated and plotted in Figure 2-9c, in which the points are derived from cyclic voltammetry tests at different scan rates. Most of the micro supercapacitors report energy densities between 0.01 and 10 mWh cm^{-3} [22], [74]. Our device shows the ability to uptake/deliver a wide range of power densities with energy densities around 0.1 mWh cm^{-3}. Considering that the fabrication method is simple, versatile, and avoids high temperature and processes that immerse substrates in complex solutions, our direct-write micro supercapacitor is promising for applications in a self-powered integrated system such as illustrated in Figure 2-1a. Usually, a micro electromechanical system (MEMS) based energy harvester generate power density smaller than 1 mW cm^{-3} [5], and it is difficult to power a wireless sensor node constantly. Our micro supercapacitor with comparable size is able to store such generated power and provide higher power to sensors or transmitters when necessary.

Figure 2-9d shows the Nyquist plot of the impedance, which shows capacitive behavior of the device within large frequency range. The crossover frequency at a phase angle of -45 ° is about 60 Hz, which is even higher than micro supercapacitors based on highly conductive graphene [62], [76]. The excellent frequency response is attributed to the fast ion transport within the porous nanofiber network, which is also proved by the absence of semicircle in the Nyquist plot of high frequency region.

One drawback of the typical conducting polymer-based supercapacitor is their poor cycling stability caused by the insertion/de-insertion of ions in the polymer matrix. The use of nanostructures can greatly improve the stability because of the shortened transport distances within the material. Figure 2-9e shows cycling experimental results and the calculated relative capacitances of the prototypes using different active materials for 1000 cycles. The capacitance retention is 92.6 % after 1000 cycling for lab-synthesized PPy, indicating excellent stability for a pseudo capacitor based on the fast redox reactions.

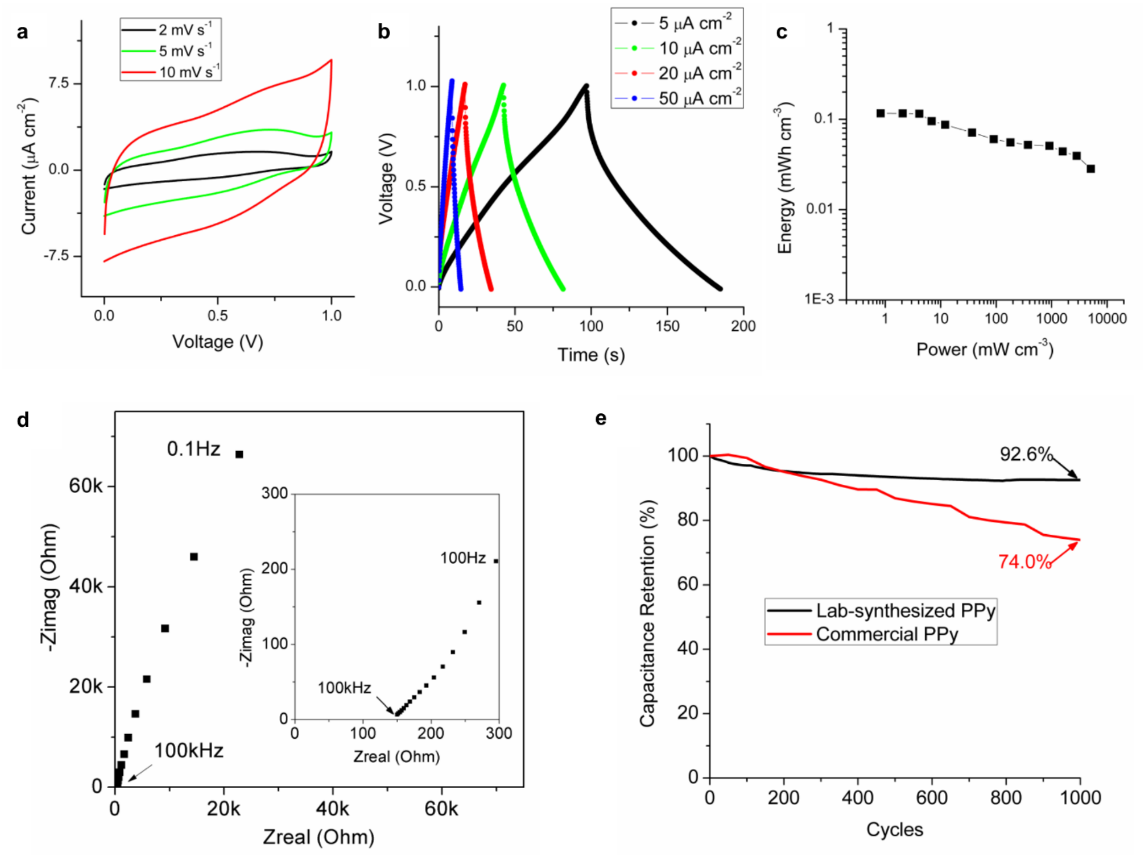

Figure 2-9. Further characterizations of the micro supercapacitor using lab-synthesized PPy. (a) Cyclic voltammetry curves at low scan rates within 1V range. (b) Constant current charge-discharge curves. (c) Calculated energy density versus power density. (d) Nyquist plot showing the impedance spectrum. Inset shows the zoom-in view of the impedance spectrum in the high frequency region. (e) Cycling tests of cells using

different active material, in which the cells are charged and discharged 1000 cycles at a scan rate of 100 mV s^{-1} from 0 to 1V. [37]

2.6 Summary

In this chapter, a solid-state flexible micro supercapacitors based on polymer nanofibers is successfully demonstrated. The nanofibers can be directly written onto micro-sized electrode patterns on various substrates including flexible polymer films. Characterizations of prototypes show that the nanofiber network exhibits two orders larger capacitance as compared with a flat electrode surface. The nanostructure also benefits the power performance and frequency response of the device by facilitating ion transport within the porous electrode. The prototype based on the lab-synthesized PPy nanofibers shows a high capacitance of up to 0.48 mF cm^{-2} and the same performances when it’s bent at different states. Overall, the micro supercapacitor is highly flexible with excellent electrochemical performance and cycling stability. The approach is simple, versatile, and compatible with different substrates for direct integration of energy storage devices in flexible micro systems.

3 Ultrathin coaxial fiber supercapacitor

3.1 Introduction

While two-dimensional (2D) flexible electronics such as printed electronics and flexible displays have been ready for commercialization in recent years, fiber-based electronics are attracting growing interest because they represent the next level of ministrations and flexibility from the current 2D systems to one-dimensional (1D) structures [77]. Clearly, both 1D power generation sources [68], [78], [79] and energy storage devices [3], [35] will be indispensable components in systems based on 1D structures. For example, flexible fiber supercapacitors [35], [80]–[82] and batteries [83], [84] have been developed for the possible integrations with electronics such as the “smart textiles” [85]. Traditionally, supercapacitors have two parallel planar electrodes sandwiching an electrolyte layer in between. Such supercapacitors can be made flexible by using thin layers of solid electrolyte and electrodes or flexible conductive materials such as carbon nanotubes [86] and graphene [62]. However, these 2D structures won’t allow water or air to pass through and their mechanical properties and fabrication processes are not compatible with textiles. On the other hand, fiber-based supercapacitors are flexible with higher degrees of freedom when compared with 2D films and they are potentially compatible with textiles in terms of similar geometric dimensions, mechanical properties and fabrication processes.

Previously, three configurations of fiber supercapacitors have been reported based on: (1) parallel electrodes [81], [82], [87]–[90], (2) twisted electrodes [91]–[97], and (3) coaxial electrodes [98]–[108], respectively. For supercapacitors using parallel electrodes, a flexible substrate is used to assemble the electrodes and a layer of electrolyte is applied afterwards. For supercapacitors using either twisted or coaxial electrodes with electrolyte in between, they could be directly woven into textiles. Since the coaxial fiber supercapacitors generally have larger interface areas, shorter ion transport path, and better stability upon mechanical bending (such as illustrated in Figure 3-1), they have been the focuses of several prior works.

However, factors and choices in sizes, materials, and fabrication processes in the state-of-art coaxial fiber supercapacitors have limited their performances in energy density, power density, mechanical strength, and manufacturing cost. Specifically, the layer thicknesses and fiber diameter have great influences on the electrochemical performances and mechanical properties. Electrodes and electrolyte layers with small thicknesses may result in higher power density by shortening the ion transport pathes [12] but small size fibers may also cause poor structural rigidity. As such, several reported coaxial fiber supercapacitors have diameters of 100 microns to several millimeters [98], [101], [102], [109], which are much larger than those of wearable fibers of 10-50 μm in diameter such as cotton, silk, and polyester. For metal-wire based coaxial supercapacitors

[98], [101], heavy mass lowers their energy density based on the total weight of the system. For carbon nanotubes (CNTs) based coaxial supercapacitors [99], low mechanical tensile strength (0.01-0.1 GPa) is a major concern. On the other hand, highly graphitized carbon fibers have high tensile strength (4-8 GPa) but they have small electric double-layer capacitance (EDLC) due to low surface areas. Finally, coaxial supercapacitors with electrolyte [102] or electrode [99], [109] fabricated by laboratory-based wrapping processes won't be compatible with the large-scale, low-cost fabrication processes in the textile industries.

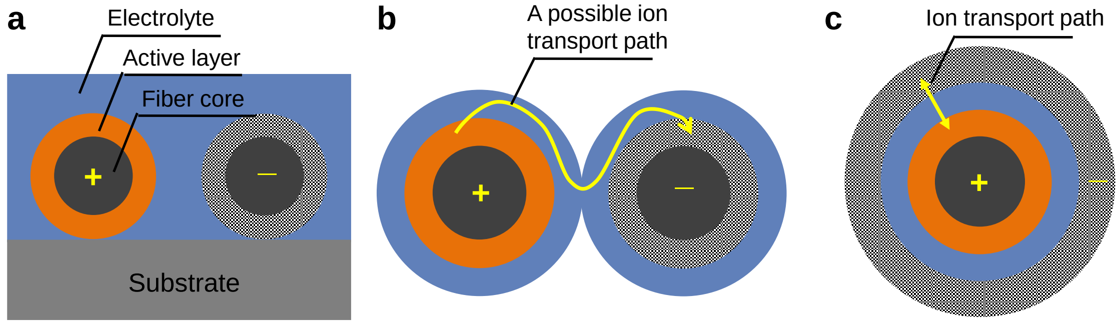

Figure 3-1. Cross-section schematics of three configurations of fiber-based supercapacitors. For the same thicknesses of the electrodes and the electrolyte layer, the coaxial structure requires minimum amount of electrolyte and provides the shortest ions transport path as compared with electrodes that are in parallel or twisted.

In this chapter, we demonstrate high-performance (both high energy and power densities), flexible, and mechanically strong micro coaxial fiber supercapacitors (μCFSCs) via a potentially scalable fabrication process to achieve an overall diameter of ~13 μm - the smallest fiber supercapacitor device in the literature. The small size and proper design of each active layer not only guarantee high flexibility, but also benefit both energy and power densities, as further supported by simulation of a general electrochemical model of 1D CFSCs. As such, this micro coaxial fiber supercapacitor could be a promising building block as flexible energy storage systems for applications in wearable electronics.

3.2 Equivalent circuit model of coaxial fiber supercapacitors

3.2.1 Description of the equivalent circuit model

As CFSCs are long and thin devices with axial dimensions much larger than diameter, they can be modeled as 1D device that is described by a transmission line circuit model, as illustrated in Figure 3-2. To a first-order approximation, the local EDLC and pseudo capacitance are lumped into a single capacitor at the electrode-electrolyte interfaces as dC_i and dC_o for the inner and outer electrode, respectively. The local electrical and ionic resistances are represented as dR_i, dR_o, dR_e for the inner electrode, outer electrode, and electrolyte (including electrolyte in porous electrodes), respectively.

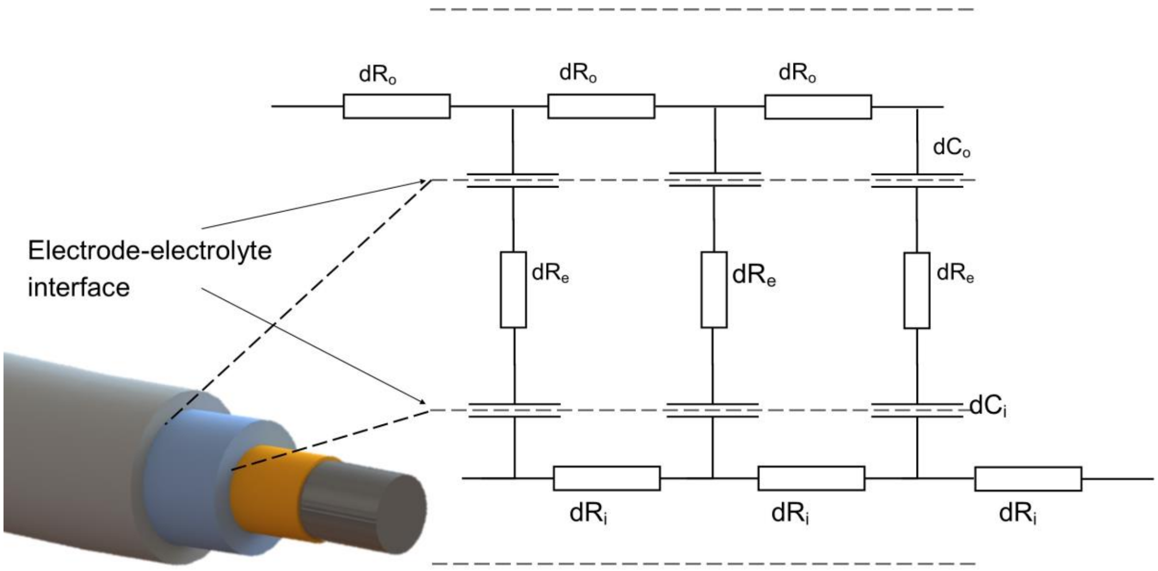

Figure 3-2. A transmission line circuit model of 1D CFSC, in which the differential capacitors at the electrode-electrolyte interface represent local capacitance effects, and differential resistors are local electrical and ionic resistances in the radial and axial directions.

To numerically describe the model, the axial direction is defined as x-axis. One end of the outer electrode of the device is assumed to be grounded, and voltage and current are applied to the other end of the inner electrode to charge and discharge the CFSC, as illustrated in Figure 3-3. Parameters for calculation are defined as the following:

$$dr_i = \frac{dx}{\sigma_i \cdot \pi R_i^2}$$

$$dr_o = \frac{dx}{\sigma_o \cdot \pi (R_o^2 - R_i^2)}$$

$$dr_e = \frac{R_o - R_i}{\sigma_e \cdot \pi (R_i + R_o) \cdot dx}$$

$$dc = C' dx$$

where σ_i, σ_o, σ_e are conductivity constants (S/m) for inner electrode, outer electrode, and electrolyte, respectively; C' is the lumped capacitance per fiber length (F/m); R_i, R_o are radii (m) for inner and outer electrodes, respectively.

A set of differential equations can be derived for voltage distribution (voltages at inner electrode V_i and outer electrode V_o, respectively) in CFSC to solve the circuit model under various charge-discharge conditions (boundary conditions). Here the constant scan rate voltammetry is used to simulate cyclic voltammetry tests of CFSCs.

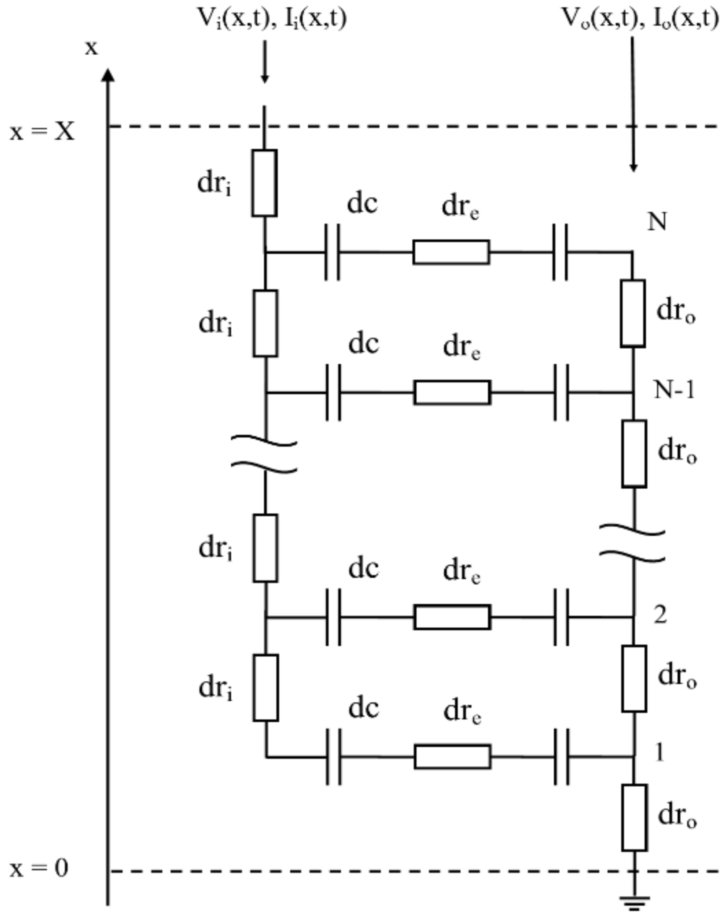

Figure 3-3. Definition of parameters in the transmission line circuit model of 1D CFSC.

Governing equations for voltage distribution in 1D CFSC are:

$$A_1 \cdot \frac{\partial^2 V_i}{\partial x^2} + A_2 \cdot \frac{\partial^2 V_o}{\partial x^2} = 0 \tag{3.1}$$

$$\frac{\partial (V_i - V_o)}{\partial t} = A_3 \cdot \frac{\partial^2 V_i}{\partial x^2} + A_4 \cdot \frac{\partial}{\partial t}\left(\frac{\partial^2 V_i}{\partial x^2}\right) \tag{3.2}$$

where $A_1 = \sigma_i \cdot \pi R_i^2$, $A_2 = \sigma_o \cdot \pi (R_o^2 - R_i^2)$, $A_3 = \frac{\sigma_i \cdot \pi R_i^2}{C'' \cdot \pi R_i^2} = \frac{\sigma_i}{C''}$ (C'' is the volumetric capacitance (F/m^3) of the electrode material), $A_4 = \frac{(R_o - R_i) \cdot \sigma_i \cdot \pi R_i^2}{\sigma_e \cdot \pi (R_i + R_o)} = \frac{\sigma_i \cdot (R_o - R_i) \cdot R_i^2}{\sigma_e \cdot (R_i + R_o)}$, are all constants determined by the dimension of the CFSC and electrical and electrochemical properties of the electrode materials used.

Boundary conditions for constant scan rate voltammetry are:

(B-1) $V_o(0, t) = 0$

(B-2) $\frac{\partial V_i(0,t)}{\partial x} = 0$

(B-3) $\frac{\partial V_o(X,t)}{\partial x} = 0$

(B-4) $\frac{\partial V_i(X,t)}{\partial t} = \delta$ (scan rate)

3.2.2 Calculation and simulation of the equivalent circuit model

The electrochemical performance (e.g. energy density, power density) of a CFSC model can be calculated as long as the sizes and material properties are all known. Here we assume the CFSC to be 4 layers with known material properties [34]: First, the carbon fiber with radius of R_i is used as the core for mechanical support (ultimate strength ~4.9 GPa) and current collector (conductivity ~0.7×10^5 S/m). Second, a layer of MnO_2/Polypyrrole (PPy) composite with a thickness of T_i coated on carbon fiber is used as the inner electrode material (volumetric capacitance ~350 F/cm^3). Third, a layer of polyvinyl alcohol (PVA)/H_3PO_4 with a thickness of T_e is coated as the solid-state electrolyte (ionic conductivity ~10^{-2} S/m). Fourth, a layer of CNTs with a thickness of T_o is coated as the outer electrode (conductivity ~10^5 S/m, volumetric capacitance ~95 F/cm^3). To avoid exploring too many variables, the following assumptions are made for all calculations:

Assumption 1: the capacitance of carbon fiber is negligible compared with the MnO_2/PPy layer and the CNT layer.

Assumption 2: the layer thicknesses of MnO_2/PPy and CNT (T_i and T_o) are always adjusted so that the capacitances of inner and outer electrodes are equal.

Assumption 3: the layer thickness of electrolyte (T_e) is adjusted so that the volume of electrolyte is proportional to that of two active electrodes.

In the following paragraphs, the device performance as a function of sizes of each layer will be examined.

(1) Maximum volumetric capacitance and mechanical strength of CFSC:

The maximum possible energy density of the CFSC is estimated based on the series capacitance of the total inner electrode capacitance (C_i) and the total outer electrode capacitance (C_o), which are determined by the volumetric capacitance and the volume fraction of each electrode. For a carbon fiber core with a fixed base radius, thicker coating layers provide larger capacitance per overall volume due to higher ratios of active energy storage materials (Figure 3-4a). However, thicker coating materials result in lower mechanical strength per cross-section area since the coating materials are weaker than the carbon fiber core.

In Figure 3-4b, we estimate the overall volumetric capacitance and mechanical strength as functions of the total thickness of the coating layers, while the radius of the carbon fiber core is fixed to be 3.35 μm. For the size of choice in this work, the total thickness of three coating layers is ~3.15 μm, which corresponds to 73 % of the total volume for high capacitance. Meanwhile, a high overall mechanical strength of 1.3 GPa is guaranteed, which is 27% of that of a bare carbon fiber.

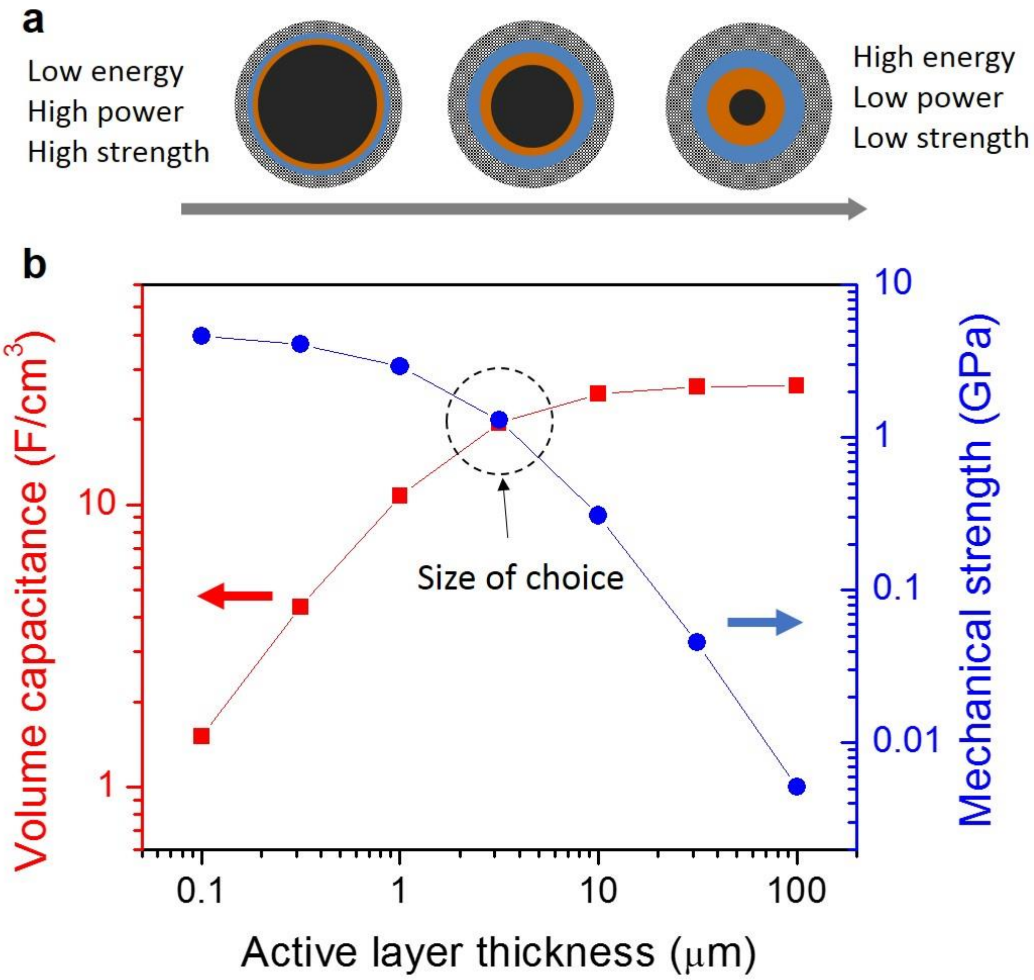

Figure 3-4. (a) Cross-section schematics of CFSC with different volume ratio of coating layers and carbon fiber core. (b) Calculations of the volume capacitance and mechanical strength of the CFSC as functions of the total thickness of coating layers (including inner electrode layer, electrolyte, and outer electrode layer), when the radius of the fiber core is fixed at 3.35 mm.

(2) Power density dependency on coating layer thickness:

The maximum power density and rate dependency of the device, on the other hand, are greatly affected by the electrical resistance of inner electrode (R_i) and outer electrode (R_o), and ionic resistance of electrolyte (R_e), which are determined by the geometry of each layer and the electrical or ionic conductivity of each material. The electrical conductivity of carbon or metal-based electrodes is typically in the ranges of 10^4-10^8 S/m, while the ionic conductivity of solid electrolyte is generally lower than 10^{-1} S/m (about 10^{-2} S/m for PVA/H_3PO_4 used here) [16], [110]. Therefore, R_e is the limiting resistance even in CFSC where the geometry is in favor of ion transports. Intuitively, thinner electrode and electrolyte coatings result in higher power performance because of shorter ion transport paths between two electrodes.

We use the circuit model to investigate the energy density and power density of CFSCs with different total thicknesses of coating layers (T_{CL}, Figure 3-5a) and a fixed carbon fiber core radius of 3.35 μm. In this way, we are changing the volume ratio of the coating layers in the whole device. The calculated results are plotted (known as Ragone plots) in Figure 3-5b. It can be seen that thinner total coating layers only slightly improve the power density, but drastically lower the energy density. In addition, if the thickness of the electrolyte layer (T_e) is approaching zero, the energy density does go up due to the higher volume fraction of the electrode materials, while the improvements in power density is negligible. These calculations suggest that our size choice represents a reasonable volume ratio between the carbon fiber core and coating layers to balance the mechanical strength, energy density, and power density.

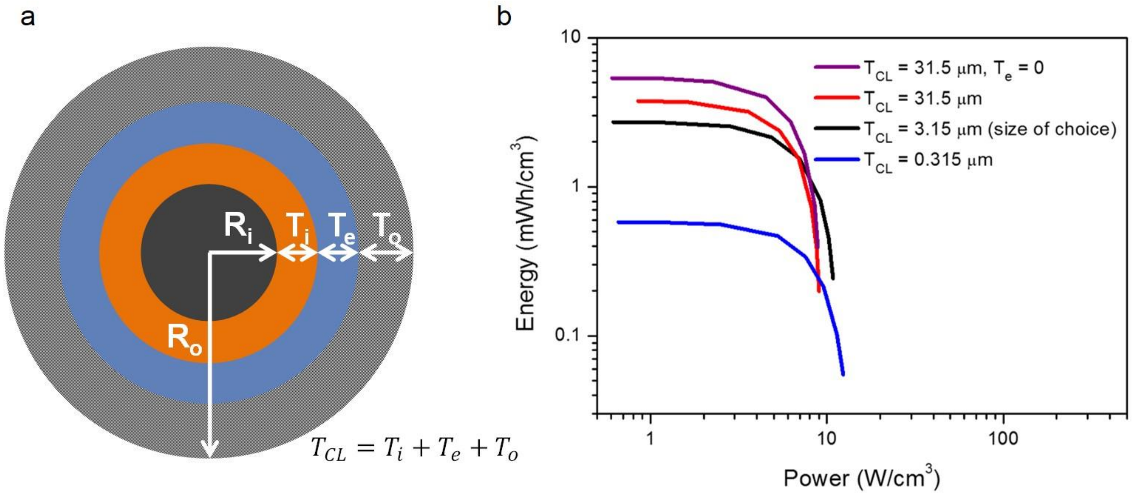

Figure 3-5. (a) Cross-section schematics of CFSC and the definition of coating lay thickness T_{CL}. (b) Energy density versus power density (Ragone plots) calculated by the model of CFSCs with different thicknesses of coating layers.

(3) Power density dependency on scaled CFSC sizes:

Instead of fixing the core size, another interesting question is whether we should make thinner or thicker CFSCs if we can choose the size of all layers. It is without doubt that thinner fibers of the same material will bring higher flexibility. Fibers used in wearable textiles are usually 10-100 μm in diameter, and thinner fibers make more flexible and softer garments.

Here, we keep the volume ratio of each layer of the CFSCs and calculate their performances with scaled overall size of the device (Figure 3-6a). The results are plotted in Figure 3-6b. It is found that: First, the maximum energy density remains about the same, because the volume ratio of electrode materials that provide capacitance is unchanged. Second, the power density increases with smaller fiber sizes, because the resistance of the electrolyte layer, R_e, decreases with layer thickness. Third, the power density saturates around the size of 13 μm - our size of choice. The reason is that, while the power performance is limited by the ionic resistance, R_e, for CFSCs with large diameters, the contribution of the electrical resistances, R_i and R_o, could become comparable to that of R_e for smaller radial dimensions, such that further reduction of R_e won't make large improvements of the power density.

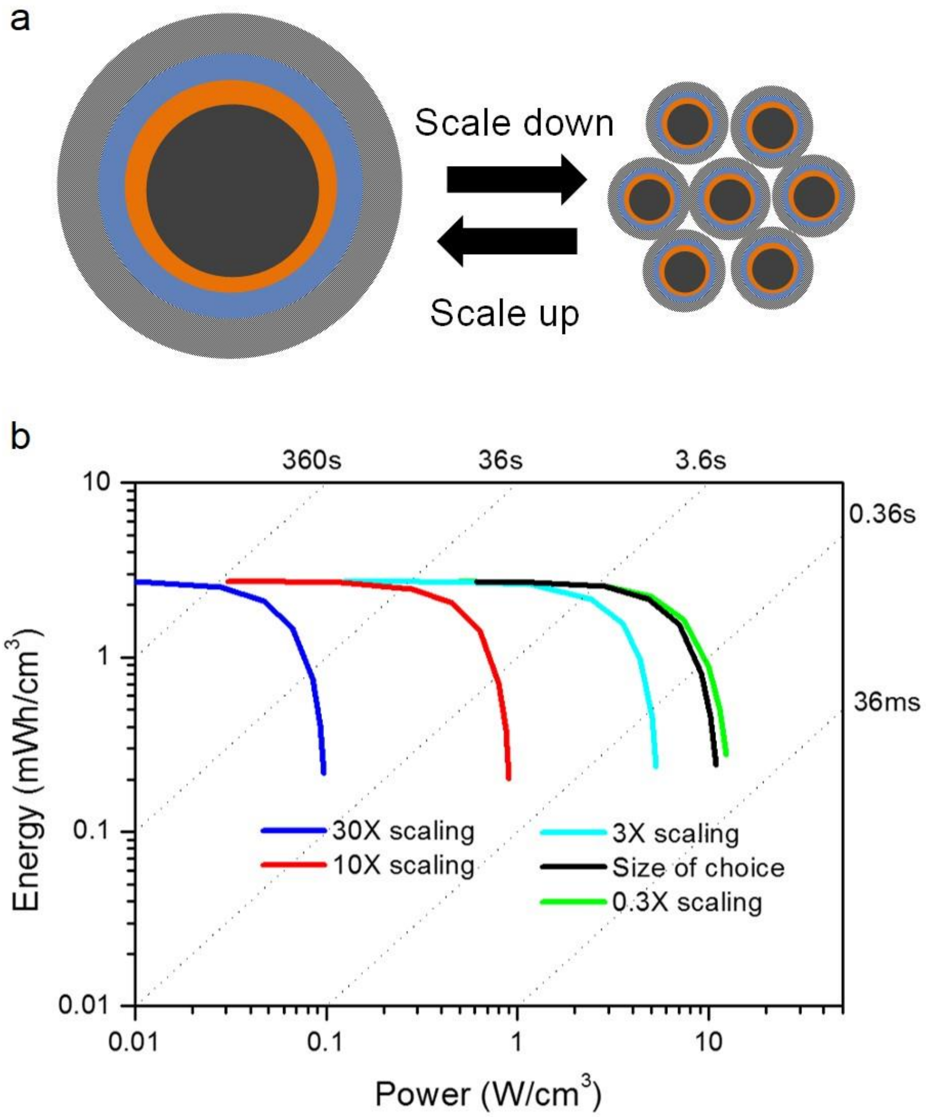

Figure 3-6. (a) Cross-section schematics illustrating the scaling of CFSC. (b) Ragone plots showing the simulation results of CFSCs with scaled sizes, in which the volume ratio of each layer with respect to the fiber core is fixed.

The above calculations have suggested an optimized design choice for CFSC. By starting with a carbon fiber core of a diameter of 3.35 μm, a total coating thickness of ~3.15 μm results in balance between mechanical strength and energy density, as well as the almost highest possible power density. The total diameter of such a CFSC is ~13 μm, which is as thin as a single cotton fiber and much thinner than a human hair. In the next section, the fabrication of such ultrathin CFSC will be introduced.

3.3 Design and fabrication of ultrathin coaxial fiber supercapacitors

3.3.1 Materials and process design

The structure of the designed ultrathin CFSC is illustrated in Figure 3-7a. The fabrication process starts with a low-cost, commercially available micro carbon fiber [111] with a measured diameter of 6.7±0.2 μm as the core material with high electrical conductivity (0.7 x 10^5 S/m), light weight (1.8 g/cm^3), and large mechanical strength (4.9 GPa). While the fiber core serves as both mechanical support and current collector, a thin layer of MnO_2/Polypyrrole (PPy) composite is electrodeposited as the inner electrode coating in which MnO_2 provides ultrahigh capacitance [13], [112]–[114] and PPy protects and stabilizes the MnO_2 [115], [116] (Figure 3-7b). The 650 nm-thick composite layer improves the capacitance of a bare carbon fiber by 1000 times without increasing much volume (See section 3.3.2). A layer of polyvinyl alcohol (PVA)/H_3PO_4 (1.0±0.5 μm thick) and a layer of CNTs (Figure 3-7c, 1.5±0.5 μm thick) are dip-coated as the solid-state electrolyte and the outer electrode coating, respectively (See sections 3.3.3 and 3.3.4). Such processes result in a thin and pinhole-free layer of electrolyte with a very short ion transport path, and a porous and conductive network of CNTs with high capacitance.

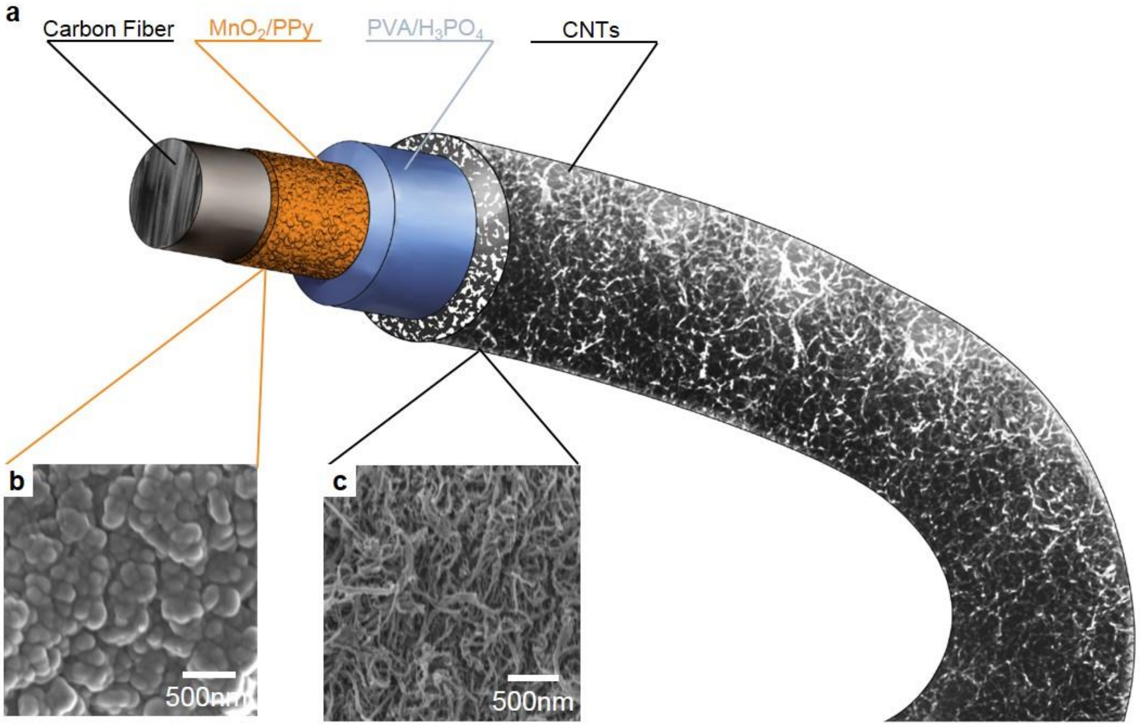

Figure 3-7. (a) Schematic of the μCFSC composed of a carbon fiber as the core, a layer of MnO_2/PPy as the inner electrode coating, a layer of PVA/H_3PO_4 as the solid-state electrolyte, and a layer of CNTs as the outer electrode coating. SEM images of the surface of (b) the MnO_2/PPy layer, and (c) the CNTs layer. [34]

As the proposed fabrication process is based on the electrodeposition and dip-coating of continuous carbon fibers, it is potentially compatible with a roll-to-roll process to mass production of such CFSCs, as illustrated in Figure 3-8a. Threads made of ultrathin CFSCs in parallel can be produced at the end of the process, and various forms of macro-scale flexible supercapacitors can be braided or woven by the CFSC threads, as illustrated in Figure 3-8b. In the following sections, we first start with separated single carbon fiber filaments to demonstrate the feasibility of each fabrication step.

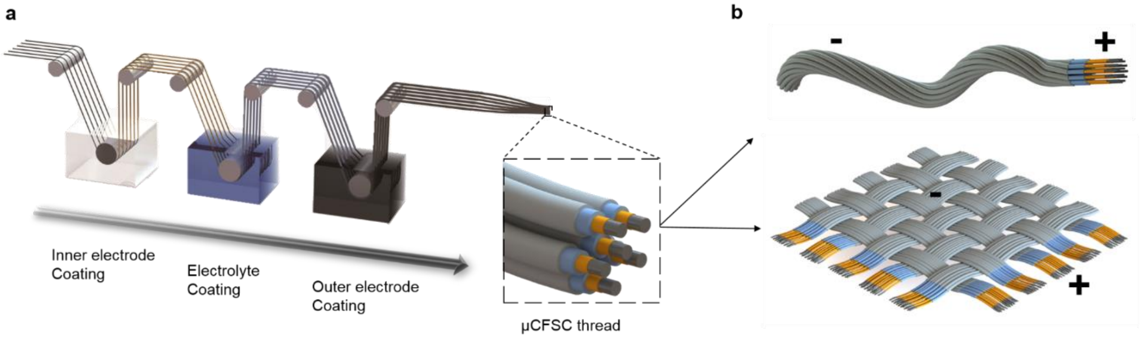

Figure 3-8. Schematics of (a) potential fabrication steps of a future roll-to-roll process to continuously produce ultrathin CFSCs, and (b) possible future forms of flexible supercapacitors using threads made of ultrathin CFSCs.

3.3.2 Electrodeposition of the inner electrode

The bare carbon fiber has smooth surface and provides a specific surface area of only ~0.2 m^2/g, which does not offer much EDL capacitance. While it perfectly serves as both mechanical support and current collector, additional active layers should be coated on it to provide higher electrochemical capacitance for energy storage. Electrodeposition of pseudo-capacitive materials is chosen because the thickness of the deposited layers can be uniform and well-controlled, and the attachment of the layers are usually strong. MnO_2 is first selected as the active layer as it provides a high theoretical capacitance of ~1350 F/g [13] and is compatible with electrodeposition. However, a single MnO_2 layer is not compatible with common solid-state electrolyte, which is usually acidic. Therefore, the MnO_2/PPy composite layer as the active inner electrode is proposed, in which the PPy protects and stabilizes the MnO_2, and provides additional capacitance and conductivity.

To deposit the MnO_2/PPy composite layer on carbon fiber, two approaches are examined, including constant potential deposition and constant current deposition. In both approaches, single carbon fiber filaments (TORAYCA® T700S) with 6.7±0.2 μm diameter and 4-6 cm long are used as the inner core material. The carbon fibers are immersed in acetone overnight and activated by 65 wt% nitric acid in 200 °C for 2 hours to make their surface more hydrophilic before further processes. The water solution of 20 mM $Mn(NO_3)_2$ and 100 mM $NaNO_3$ is used for the MnO_2 deposition. The water solution of 0.1 M $LiClO_4$ and 5 vol% pyrrole monomer is used for the PPy deposition [116].

First, the constant potential deposition is applied by using a three-electrode setup. One carbon fiber filament as the working electrode, an Ag/AgCl reference electrode, and a Pt wire as the counter electrode are immersed in the deposition solution. A constant potential vs. Ag/AgCl is applied to carbon fiber to deposit MnO_2 and then PPy on its surface. Figure 3-9a shows the typical deposition current measured over time as a constant potential is applied to a carbon fiber. The current decreases dramatically over time, meaning that the MnO_2 grows much slower when more MnO_2 is deposited, or the deposited MnO_2 is passivating the carbon fiber surface and making the further deposition much more difficult. As a result, not much MnO_2 is coated on carbon fiber surface, as indicated in the SEM image in Figure 3-9b. Higher deposition potential also shows the same tendency, and bubbles are generated when the potential is too high, probably due to the oxygen evolution. The deposition of PPy, however, shows another phenomenon in Figure 3-9c. The deposition current (an indication of the growth rate) first decreases, then increases. This can be explained as that the deposited PPy is making the fiber more conductive and also creating more surface area for faster deposition rate. The resulting PPy layer, however, is not uniform as shown in Figure 3-9d. PPy may grow much faster at certain sites while much slower at other ones.

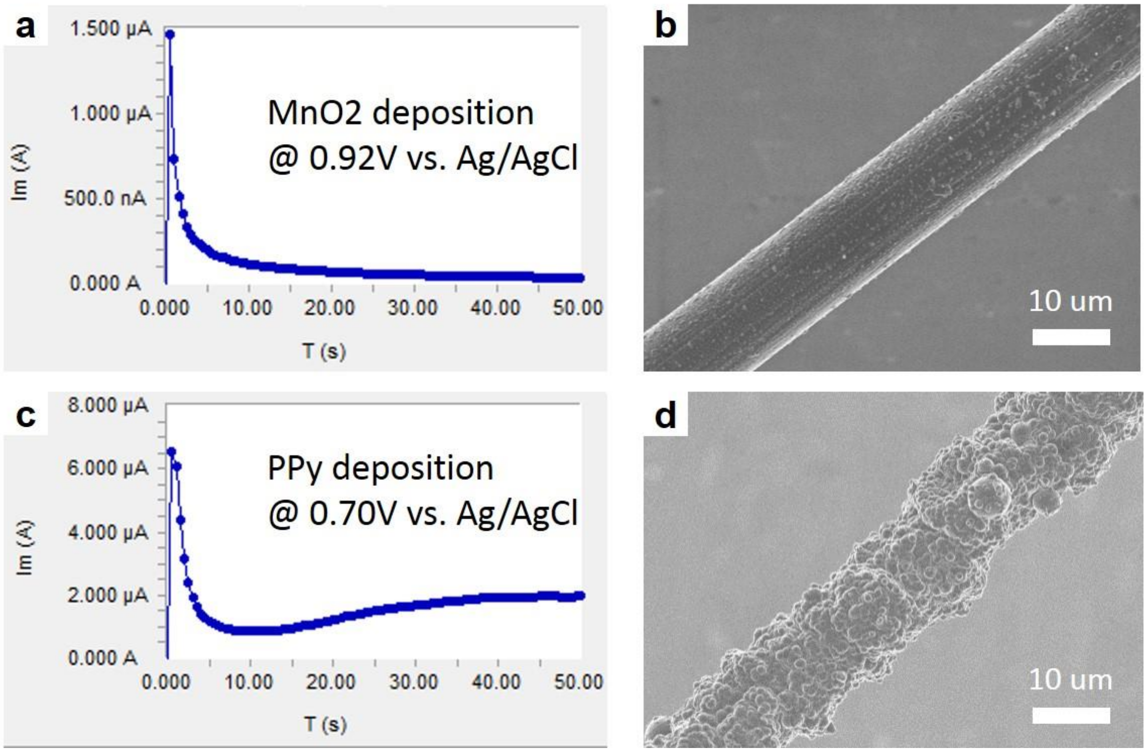

Figure 3-9. Typical (a) deposition current curve and (b) SEM image for MnO_2 deposition at constant potential. Typical (c) deposition current curve and (d) SEM image for PPy deposition at constant potential.

The above experimental results imply that the growth rates of MnO_2 and PPy cannot be controlled by applying constant potentials. Therefore, constant current deposition is proposed for uniform coating of both layers. A simpler two-electrode setup, including a carbon fiber as the working electrode and a Pt wire as the counter electrode, can be used, because the potential does not need to be monitored by using a standard reference electrode. To ensure the same current density for samples with different lengths, a constant current per carbon fiber length is applied for each deposition. The typical voltage measured over time for MnO_2 deposition is shown in Figure 3-10a, and the carbon fiber surface after the process is shown in Figure 3-10b. Nanoflakes of MnO_2 with the size of ~10nm are uniformly grown on the carbon fiber surface. The voltage curve for PPy deposition is shown in Figure 3-10c, and the PPy coating surface is shown in Figure 3-10d. The PPy layer fully covers MnO_2 with nanostructure of spheres of ~100nm. Such results suggest that the constant current deposition can control the growth rate of the deposited material and make functional coatings with controlled thickness and uniformity at the level of ~100nm. Therefore, the constant current deposition is applied in all later experiments.

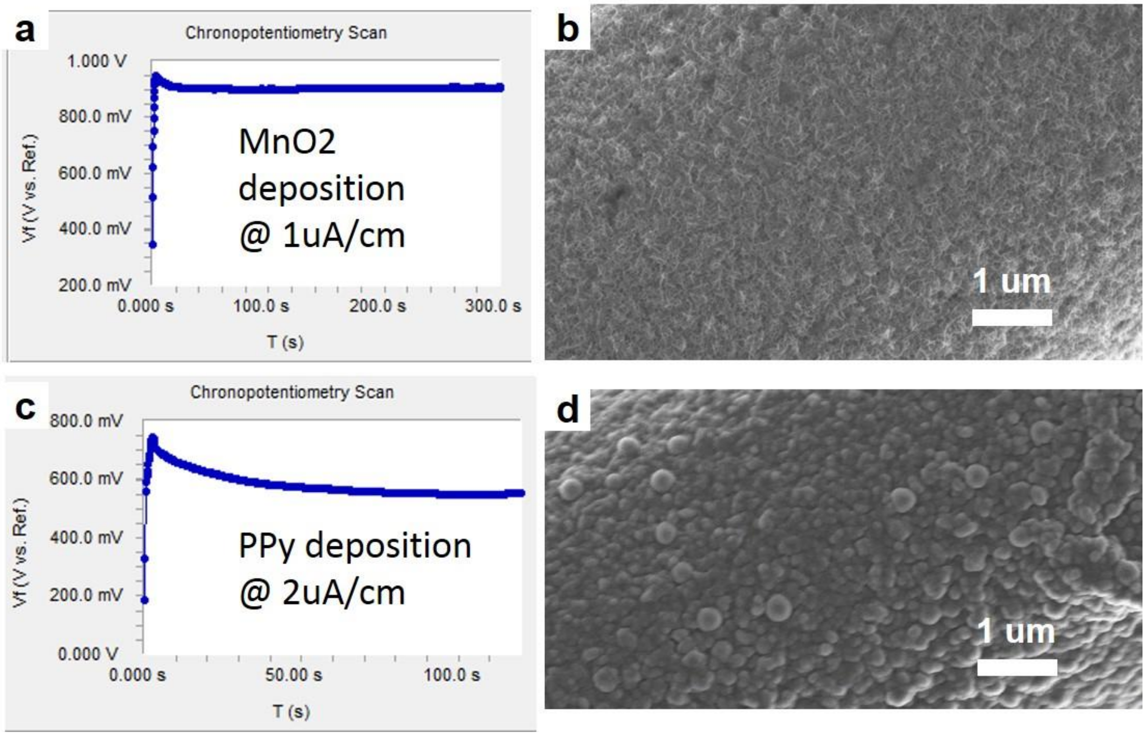

Figure 3-10. Typical (a) measured voltage curve and (b) SEM image for MnO_2 deposition at constant current per length of the carbon fiber filament. Typical (c) measured voltage curve and (d) SEM image for PPy deposition at constant current per length of the carbon fiber filament.

The composition of the deposited layers is verified by X-ray photoelectron spectroscopy (XPS, Figure 3-11) and energy dispersive X-ray Spectroscopy (EDS, Figure 3-12). In Figure 3-11, the XPS results show that the bare carbon fiber sample only shows peaks of carbon (C) and oxygen (O). After the deposition of MnO_2, the CF-MnO_2 sample shows additional Mn $2p_{1/2}$ and Mn $2p_{3/2}$ peaks and higher signal intensity of oxygen, indicating the successful growth of manganese oxides. After the PPy deposition, the CF-MnO_2-PPy sample shows an additional peak of nitrogen (N) on the surface, which should come from pyrrole in the chemicals used. Mn is almost fully covered by PPy, because only very weak Mn peaks are seen. In Figure 3-12, the EDS shows similar results that the CF sample is mainly composed of Carbon, while the CF-MnO_2 sample is composed of Carbon, Oxygen, and Manganese, and the CF-MnO_2-PPy sample has additional Nitrogen and Chlorine, because of ClO_4^- group doped in PPy.

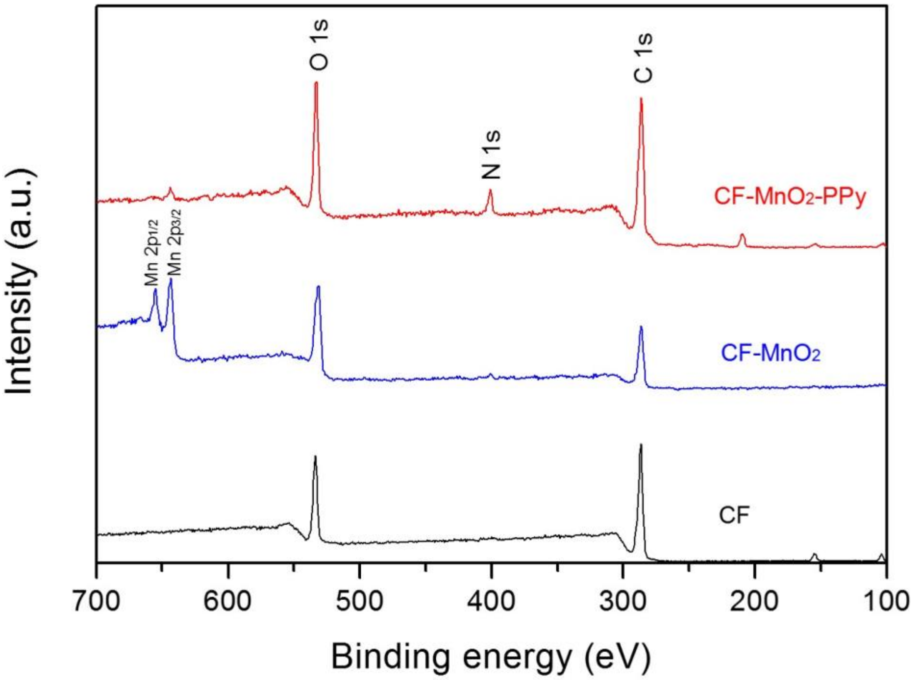

Figure 3-11. X-ray photoelectron spectroscopy (XPS) of the inner electrode materials composed of bare carbon fiber (CF), carbon fiber deposited with MnO_2 (CF-MnO_2), and carbon fiber deposited with MnO_2 and PPy (CF-MnO_2-PPy), respectively.

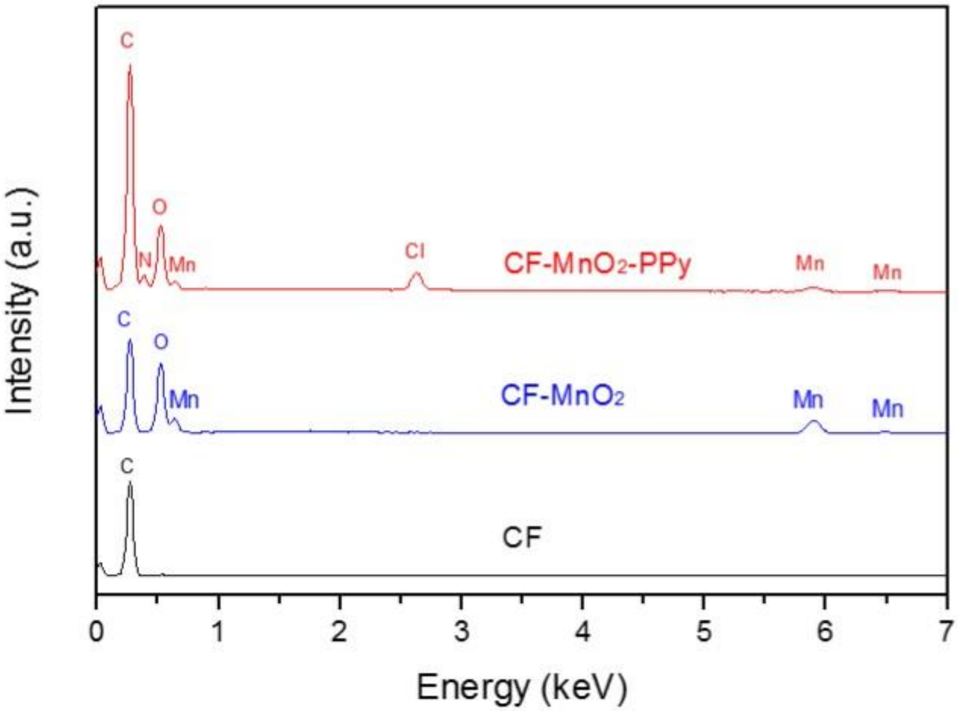

Figure 3-12. Energy Dispersive X-ray Spectroscopy (EDS) of the inner electrodes composed of bare carbon fiber (CF), carbon fiber deposited with MnO_2 (CF-MnO_2), and carbon fiber deposited with MnO_2 and PPy (CF-MnO_2-PPy) , respectively.

To find out the proper deposition time for each active layer, we test the electrochemical performance of the inner electrode (including carbon fiber core and active layers) by using a three-electrode system with the fiber as the working electrode, a platinum wire as the counter electrode, and an Ag/AgCl reference electrode. The water solution of 1 M H_3PO_4 is used as the electrolyte. The capacitances per length and per volume of fiber electrodes with different layers deposited with different times are summarized in Table 3-1, and some typical CV curves are plotted in Figure 3-13.

Table 3-1. Capacitance summary of different fiber electrodes

Fiber electrode	Capacitance per length (μF/cm)[a]	Average diameter (μm)	Capacitance of Active Layers (F/cm^3)[b]	Capacitance of Total Electrode (F/cm^3)[c]
Bare carbon fiber (CF)	0.03	6.7±0.2	N/A	0.085
CF treated in HNO_3	0.3	6.7±0.2	N/A	0.85
CF-MnO_2 (0.5 μA/cm, 5 min)	2	7.8±0.2	16	4.19
CF-MnO_2 (0.5 μA/cm, 5 min)-Ppy (2 μA/cm, 0.5 min)	31	7.8±0.3	247	64.9
CF-MnO_2 (0.5 μA/cm, 5 min)-Ppy (2 μA/cm, 2 min)	58	8.0±0.3	386	115
CF-MnO_2 (0.5 μA/cm, 5 min)-Ppy (2 μA/cm, 5 min)	110	12.5±1.0	126	89.6

[a] Calculated from CV curve at 100mV/s scan rate; 20% error from length measurement

[b] Capacitance divided by the volume of active layers

[c] Capacitance divided by the total volume of carbon fiber and active layers

From Table 3-1, the capacitance of bare carbon fiber is very low because of its low surface area. After treated by nitric acid, the average diameter of the fiber doesn't change, indicating that nitric acid doesn't etch the carbon away. An increase of capacitance is probably due to the oxidized carbon fiber surface with chemical groups providing additional pseudocapacitance. After the deposition of MnO_2, the capacitance further increases, but only a few times higher. This is because the MnO_2 layer is unstable in acidic electrolyte. It starts dissolving in acids when immersed in the electrolyte solution. After a thin layer of PPy is deposited for 0.5 min, the capacitance of the whole electrode further increases by more than 1 order, indicating that the PPy layer is protecting the MnO_2 and the composite layer is more stable. The average diameter of the electrode doesn't change much with small amount of PPy coating, and the deposited PPy is covering and filling the pores between MnO_2 nanoflakes. Further deposition of PPy for 2 min improves the capacitance again, and the diameter of the fiber is slightly increased. More deposition of PPy (e.g. 5 min) will continue to improve the capacitance per fiber length, but will decrease the volumetric capacitance of the whole electrode. This is probably because of the increase of the fiber diameter as well as the increased difficulty of ions to penetrate thick PPy layer to conduct pseudocapacitive reactions. Therefore, we consider the carbon fiber with MnO_2 deposited at 0.5 μA/cm for 5 min and PPy deposited at 2 μA/cm for 2 min as the optimized inner electrode.

The CV curves of bare CF, HNO_3 treated CF, and the optimized electrode are plotted and compared in Figure 3-13. The currents of bare CF and treated CF are enlarged by 100 times to be comparable with the optimized CF-MnO_2-PPy electrode at the same scan rate of 100 mV/s.

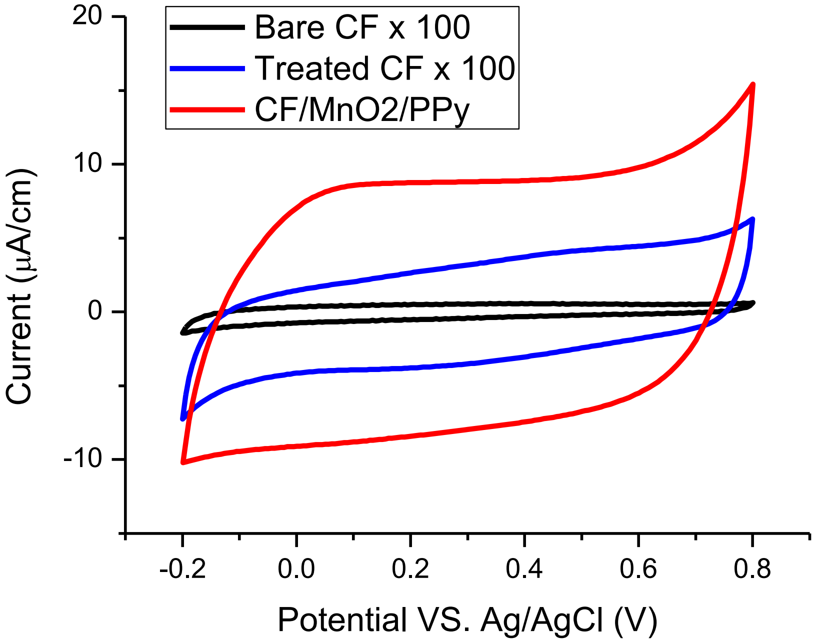

Figure 3-13. Typical CV curves of electrodes of bare CF, HNO_3 treated CF, and CF-MnO_2 (0.5 μA/cm, 5 min)-PPy (2 μA/cm, 2 min) tested in a three-electrode system.

3.3.3 Dip-coating of the electrolyte

The solid-state electrolyte layer between the inner electrode and outer electrode of CFSC should not only conduct ions but also fully separate the two electrodes to prevent them from short circuit. The thinner electrolyte layer provides shorter ion transport path for lower ionic impedance and higher power density. Moreover, as charges are not stored in electrolyte layer, thinner electrolyte also makes the overall energy density of the whole device higher. Therefore, the goal of electrolyte coating is to make the layer pinhole-free and as thin as possible.

Dip-coating is a simple and efficient way to coat polymer electrolyte on continuous fibers. The process of coating a viscous polymer solution onto a fiber is illustrated in Figure 3-14. The coating thickness can be controlled by the properties of the polymer solution as well as the pulling speed.

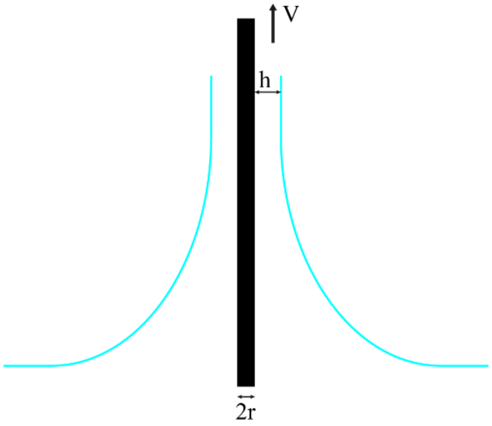

Figure 3-14. Schematic of the coating of polymer solution onto a carbon fiber with a radius of r at a pulling up speed of V.

In the dip-coating process, the electrolyte near the fiber must move at the same velocity as the fiber due to the liquid viscosity. The viscosity of the liquid, the gravity force and the capillary force all affect the dip-coating process. Researchers have proposed the relationship between the coating layer thickness and other parameters as:

$$h = \frac{1.34rCa^{\frac{2}{3}}}{1-1.34Ca^{\frac{2}{3}}} \tag{3.3}$$

where h is the coating layer thickness, r is the radius of the fiber, and Ca is the capillary number, which is computed by

$$Ca = \frac{\eta V}{\gamma} \tag{3.4}$$

where η and γ are the electrolyte viscosity and surface tension, respectively, and V is the pulling speed [117], [118].

Pulling up a carbon fiber from a polymer solution will form thinner coating with lower speed. The coating formed under lower pulling speed is also more uniform. Photos in Figure 3-15 show that beaded structures are formed if the fiber is pulled up at a relatively high speed, while smooth and uniform coating is found at low pulling speed.

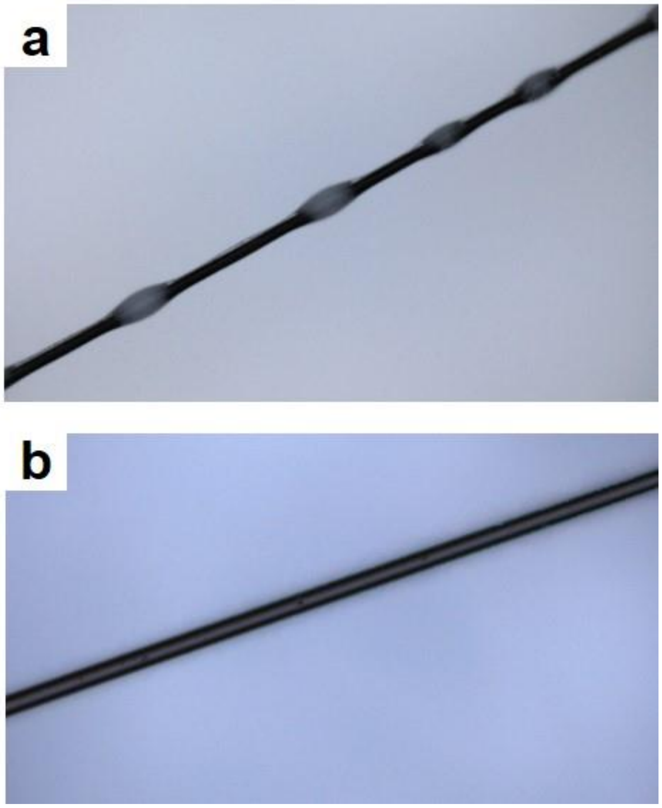

Figure 3-15. Optical photos of carbon fiber with polymer electrolyte coatings formed at (a) fast pulling speed and (b) slow pulling speed.

To check if the polymer coating on carbon fiber is pinhole free to prevent short circuit between inner and outer electrode, we fix one end of the carbon fiber (no coating) and cover the other polymer-coated end with a piece of low-melt alloy and heat it up until the alloy melts (at ~ 50 ^{o}C). The sample is then cooled down to solidify the alloy, and the resistance between the carbon fiber and the alloy is measured. If there are pinholes on the polymer coating, the alloy will be in contact with carbon fiber core. The resistance will be around 1 kΩ in this case, which is considered short-circuit. Otherwise, the resistance will outrange the ohmmeter.

Polymer solutions with different molecule weights of polymer and different concentrations are tested to find out a best solution. Some of the results are summarized in Table 3-2. At the beginning, a polyvinyl alcohol (PVA) solution with low PVA molecule weight (~45,000) is tested. The coating thickness of such solution is less than 0.1μm, and all tested samples are short-circuit. The solution of PVA with higher molecule weight (~180,000) is tested. The coating thickness becomes thicker, but most of the samples are still short-circuit. Later experiments show that the dip-coating process has to be repeated to reduce the short-circuit rate. For example, to dip the carbon fiber into 12.5 % PVA (Mw=180,000) solution twice will reduce the short-circuit rate to 16.7%, and result in coating thickness of 1-2μm. More experiments show that to use solution with lower concentration (8.3 wt% PVA, Mw=180,000) but repeat the dip-coating for 3 times result in both thin (~1 μm), uniform, and pinhole-free coatings.

Table 3-2. Electrical contact experiments of carbon fiber coated with different polymer solutions.

Concentration	Carbon fiber treatment	Short-circuit rate	Coating thickness
10 wt% PVA (Mw=45,000)	HNO3 Overnight	100%	< 0.1μm
10 wt% PVA (Mw=180,000)	HNO3 Overnight	90%	< 0.5μm
10 wt% PVA (Mw=180,000)	Ppy coat 60-90s	100%	< 0.5μm
12.5 wt% PVA (Mw=180,000) (dip 2 times)	HNO3 Overnight	16.7%	1-2μm

3.3.4 Dip-coating of the outer electrode

Dip-coating can also be used to coat outer electrode onto the coaxial fiber. The outer electrode material doesn’t have to form conformal and pinhole-free structure, but should be porous for ion transport and energy storage. Two carbon-based materials in the powder form are coated and tested as the outer electrodes for the CFSC in this section.

First, carbon black nanoparticles bound by polytetrafluoroethylene (PTFE) are coated as the outer electrode [39]. In a typical process, after coated with an electrolyte layer, the fiber is put into the carbon black and PTFE dispersion (the weight ratio of carbon black, PTFE, water is 9:1:90) for ~1 s and pulled out. The dispersion will attach on the fiber surface and the solvent will evaporate in minutes. The dried PTFE will bind the carbon black nanoparticles together, as shown in the SEM images in Figure 3-16a and b. The thickness of the layer is controlled by the number of dip-coating. More coating procedures will result in more nanoparticles attached on the surface. Typically, a 500nm-thick layer of carbon black can be formed after two dip-coatings.

Such electrode composed of carbon black stores energy by using the surface area of the nanoparticles. While other carbon-based particles, such as activated carbon powders, have higher surface area, they usually show much lower electrical conductivity, which can affect the performance of CFSC a lot, especially when the coating layer is ultrathin. Carbon nanotubes (CNTs), on the other hand, show both high surface area and high conductivity and are compatible with such dip-coating process, and are also experimented for comparison in this section.

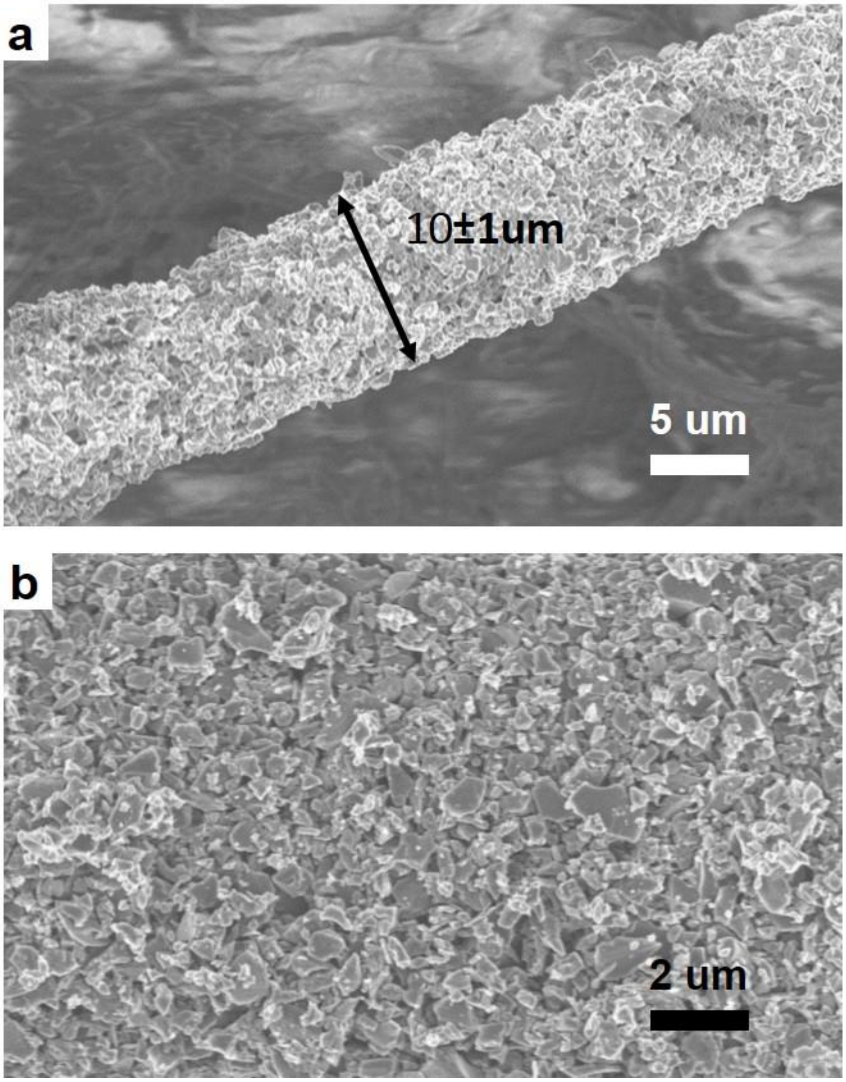

Figure 3-16. (a) SEM image of a fiber coated with carbon black nanoparticles. (b) Enlarged view of (a).

To coat CNTs as the outer electrode, uniform dispersion of CNTs is prepared. The optimized dispersion in this case is to use carboxylic acid functionalized multi-walled CNTs dispersed in Dimethylformamide (7-8 wt%). No binder is needed as CNTs entangle with each other and attach tightly on the electrolyte layer surface after the solvent of the dispersion is dried. The concentration of CNTs and the number of coatings can be adjusted to coat outer electrode with desired thickness. A typical sample after 5 times coating is shown in Figure 3-17.

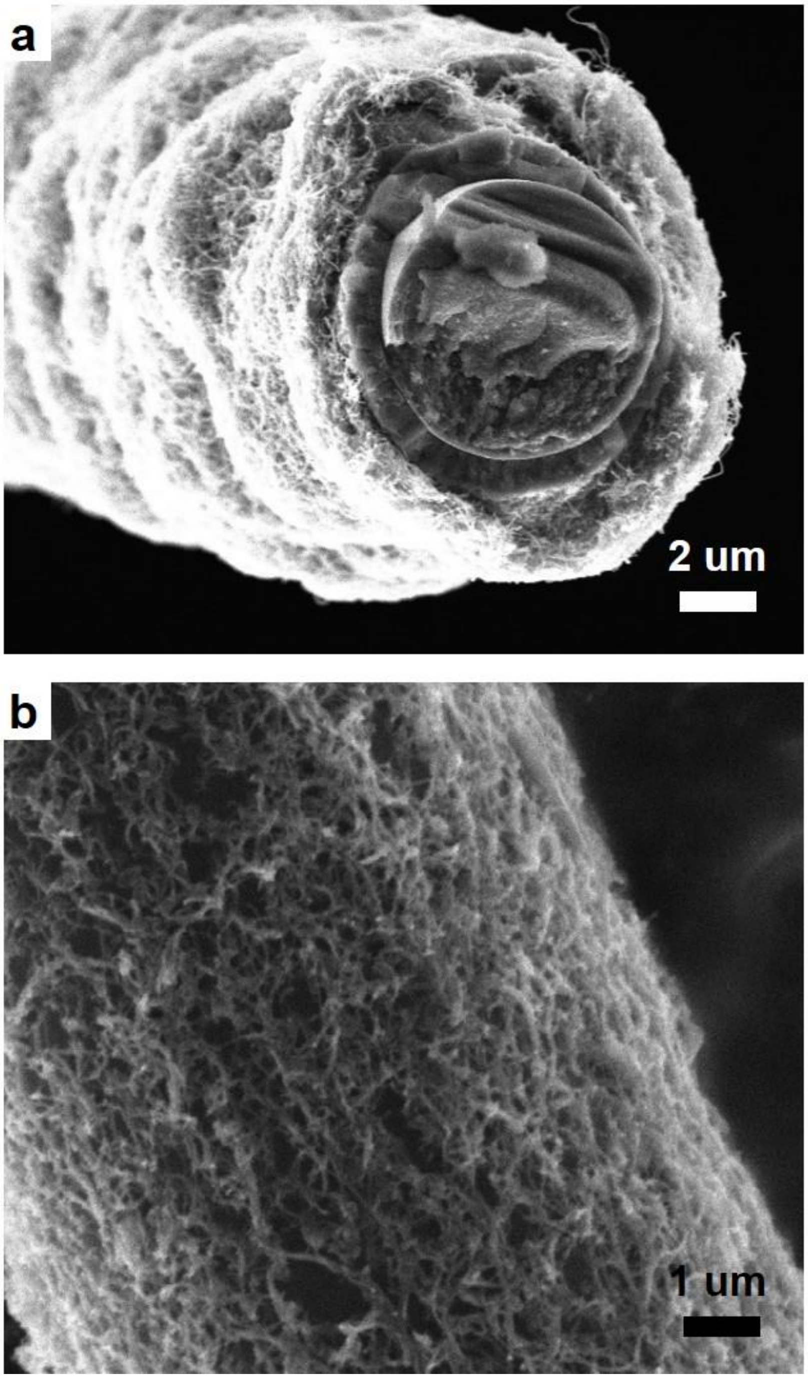

Figure 3-17. (a) SEM image of the cross-section of a fiber coated with CNTs. (b) SEM image of the surface of coated CNTs.

The electrochemical performance of different outer electrode materials are compared in complete CFSC prototypes. Three samples are prepared, all of which use the inner electrode and electrolyte layers described in the previous sections. In the first CFSC cell, silver paint is applied directly onto the fiber with electrolyte. In the other two cells, carbon black and CNTs are coated as the outer electrode, respectively. The silver paint is then applied onto the outer electrode to make electrical connection. The tested volumetric capacitances of the three CFSCs as a function of scan rate are plotted in Figure 3-18. Clearly, the cell with CNTs as the outer electrode shows much larger capacitance, which is 1 order higher than the one with carbon black outer electrode and 2 orders higher than the one with silver paint only. Therefore, CNTs are selected as the outer electrode for further investigation.

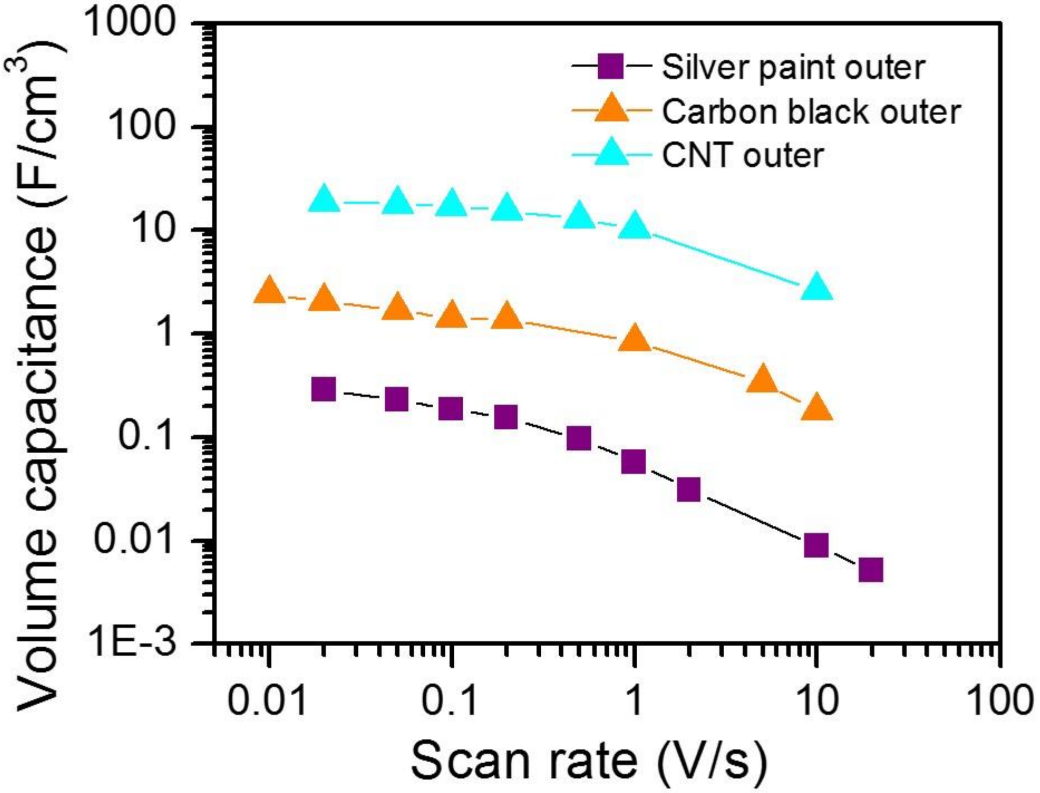

Figure 3-18. The volumetric capacitances of CFSCs with different outer electrodes as a function of scan rate.

To estimate the volumetric capacitance of the selected outer electrode (dip-coated CNTs) for ultrathin CFSCs, a two-electrode symmetric supercapacitor cell using only CNTs is prepared. A thin PVA/H_3PO_4 solid electrolyte film of ~10 μm is first prepared by drying of the electrolyte solution in a Petri dish. Then the film is dipped into the CNT dispersion, so that both sides of the film are coated with CNT (7±4 μm-thick in a typical coating). The CNT-coated electrolyte film is dried, dipped into 85 wt% H_3PO_4 for a few seconds, and cut into squares of ~1 cm^2. Silver paint and metal wires are used to connect the CNT electrodes on two sides of the film. The capacitance of such a symmetric cell is tested, and the volumetric capacitance of such a CNT layer is calculated to be ~95 F/cm^3.

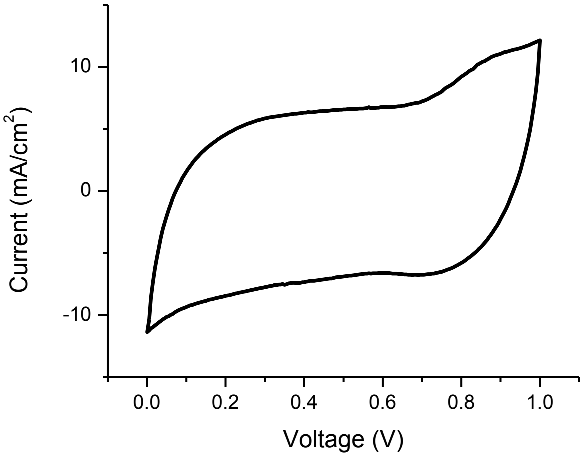

Figure 3-19. CV curve of a two-electrode symmetric supercapacitor cell using CNT electrodes and PVA/H_3PO_4 solid electrolyte film at a scan rate of 100 mV/s.

3.3.5 Final device fabrication

The optimized, complete fabrication process for an ultrathin CFSC is detailed as the following steps:

(1) Synthesis and Fabrication of the inner electrode layer:

One single carbon fiber (CF, TORAYCA® T700S) with 6.7 ± 0.2 μm diameter and 4-6 cm long was used as the inner core material. The CF was immersed in acetone overnight and activated by 65 wt% nitric acid in 200 °C for 2 hours before further processes. The MnO_2 nanoflakes and PPy nanolayer were deposited on the CF via the electrochemical deposition process. A solution of 20 mM $Mn(NO_3)_2$ and 100 mM $NaNO_3$ is used for the MnO_2 nanoflakes coating, 0.1 M $LiClO_4$ and 5wt% pyrrole monomer is used for the PPy nanolayer coating respectively. The two-electrode configuration was used in the deposition process with a platinum wire as the counter electrode, and the CF as the working electrode. A constant current of 0.5 μA/cm is used for 5 minutes to electrochemically deposit MnO_2 nanoflakes, and a 2 μA/cm current is used for 2 minutes to electrochemically deposit the PPy layer. Then the CF was washed by deionized water (DI water) and dried between each process.

(2) Fabrication of the electrolyte layer:

The gel electrolyte was prepared by adding 1 g of Phosphoric acid (H_3PO_4), and 1 g of polyvinyl alcohol (PVA, Mw=180,000) powder into 11 g of deionized water. The mixture was heated to 100°C with stirring until the solution became clear. To coat the electrolyte onto the MnO_2/PPy-coated CF, the CF was dipped into the gel electrolyte and pulled up vertically at the speed of 0.2 mm/s. After the electrolyte was solidified, the dip coating process was repeated 3 times.

(3) Fabrication of the outer electrode layer:

Multi-walled carbon nanotubes were dispersion in Dimethylformamide (7-8wt%, carboxylic acid functionalized) and used as outer electrode. To coat the outer electrode onto the electrolyte-coated CF, the CF was dipped into the carbon nanotubes dispersion and pulled up 3 to 4 times before drying in ambient temperature.

Figure 3-20 shows the SEM images of the ultrathin CFSC fabricated at different steps. A bare carbon fiber is shown in Figure 3-20a. The fiber surface is smooth at first, and becomes rough after successive electrodeposition of MnO_2 and PPy (Figure 3-20b and c). The thickness of the inner electrode coating is 650±150 nm to achieve a capacitance of 58 μF/cm, which corresponds to a volumetric capacitance of 386 F/cm^3 for the inner electrode coating only, or 115 F/cm^3 including the carbon fiber core. A 1.0±0.5 μm-thick layer of PVA/H_3PO_4 is dip-coated as the electrolyte layer, which looks transparent under optical microscope (Figure 3-21) and smooth under SEM (Figure 3-20d). A 1.5±0.5 μm-thick layer of CNTs is then dip-coated (Figure 3-20e). For better performance, the final ultrathin CFSC device is dipped into 85 wt% H_3PO_4 to soak the nanoporous CNTs layer with sufficient electrolyte. Figure 3-20f shows the SEM image of the cross-section of the CFSC, in which the coaxial structure of the carbon fiber core, the inner electrode coating, the electrolyte, and the outer electrode coating are clearly seen and distinguishable.

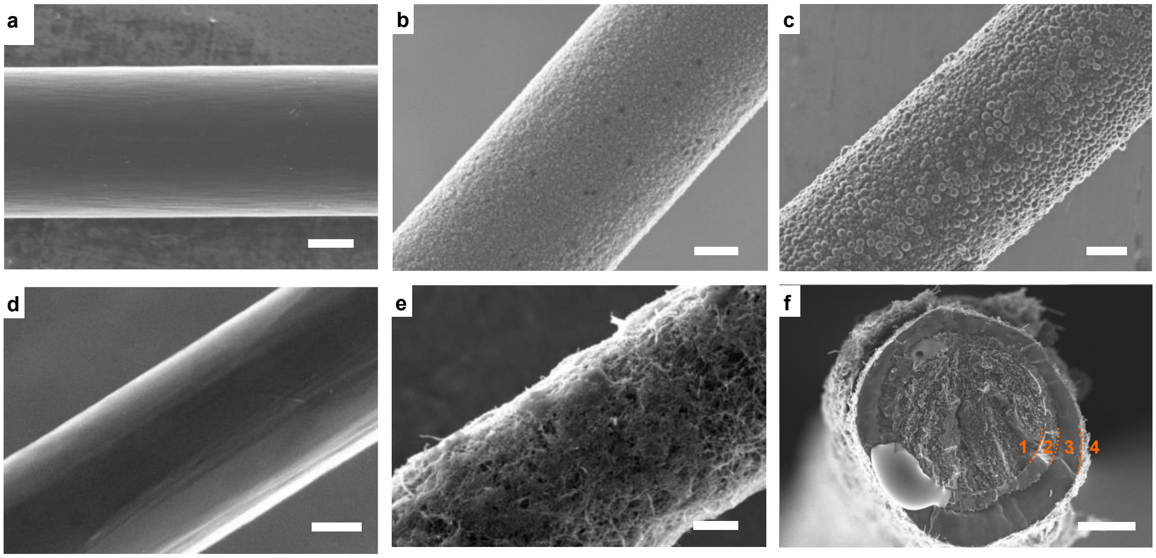

Figure 3-20. SEM images of: (a) a bare carbon fiber, (b) a carbon fiber coated with MnO_2, (c) a carbon fiber coated with MnO_2/PPy as the inner electrode, (d) after the electrolyte coating, (e) after the CNTs coating layer as the outer electrode, and (f) the cross-section of the μCFSC showing clear boundaries between the four layers. 1- carbon fiber core; 2- MnO_2/PPy; 3- electrolyte; and 4- CNTs layer. Scale bars are 2μm in all figures.

The corresponding optical photos of the ultrathin CFSC fabricated at each step is shown in Figure 3-21. The optical photos show that the uniform coatings can be achieved at long range (~1 mm in a single photo, > 1 cm for photos taken at different positons), indicating that the process can be extended to continuous roll-to-roll fabrication.

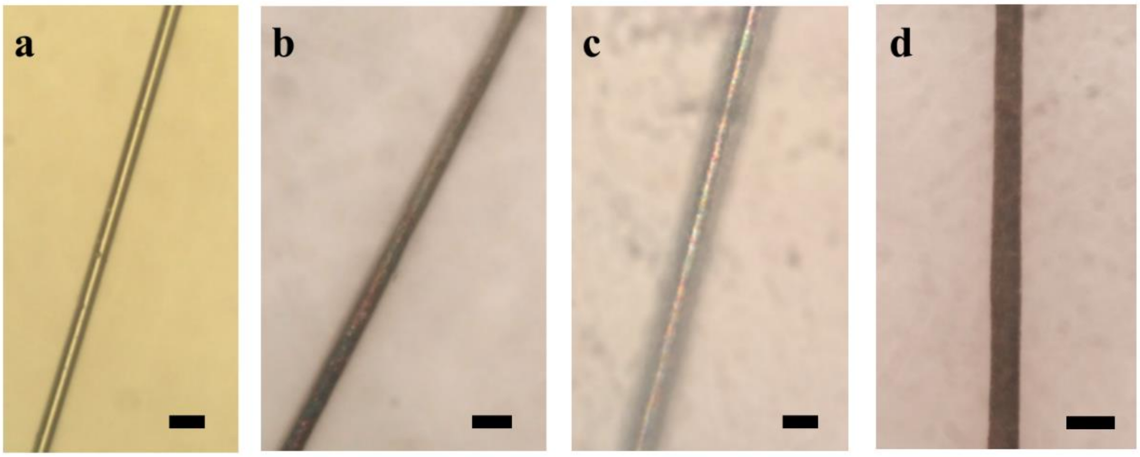

Figure 3-21. Optical photos of (a) the carbon fiber core; (b) after the electrodeposition of polypyrrole; (c) after the dip-coating of electrolyte; (d) after the dip-coating of outer electrode. All scale bars are 20µm.

The final µCFSC device has a diameter of about 13 µm, even thinner than the cotton fibers in wearable fabrics (Figure 3-22a). Such a small size guarantees a high bending flexibility of the device. Moreover, a single µCFSC is strong enough to lift a US quarter coin of 5.67 g, which corresponds to a tensile strength of at least 0.42 GPa (Figure 3-22b).

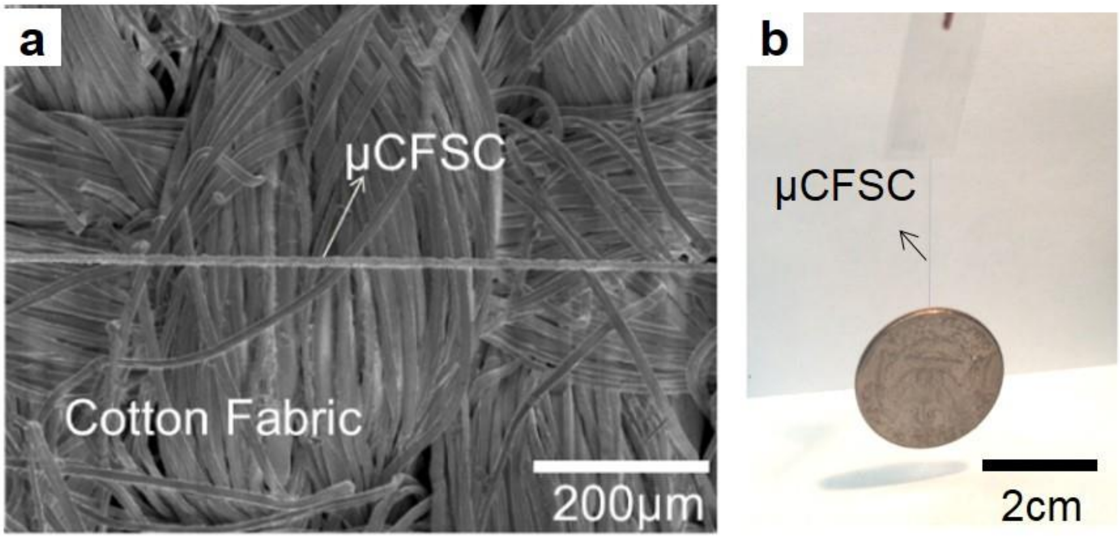

Figure 3-22. (a) SEM image of a µCFSC put on a wearable cotton fabric. (b) Photo of a US quarter coin (5.67g) lifted by a µCFSC.

To make electrical connections to the two electrodes of a single μCFSC, one end of the carbon fiber is fixed by a metal clip during the whole fabrication and testing process (Figure 3-23a). The other end with outer electrode layer is connected by the soldering process to a conductive wire. Figure 3-23a also compares the CFSC with a human hair, showing its small size and high flexibility. The ultrathin device shows no mechanical failure even at a small bending radius of ~50 μm (Figure 3-23b).

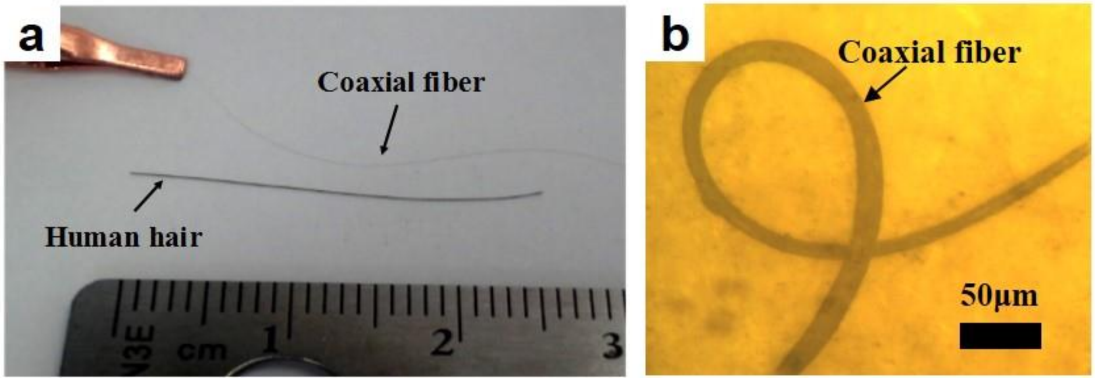

Figure 3-23. (a) Optical photo the μCFSC as compared with a human hair. (b) Optical microscope photo of a twisted μCFSC.

3.4 Electrochemical characterizations

3.4.1 Performance of a single ultrathin CFSC

Cyclic voltammetry (CV) tests are conducted to characterize the electrochemical performance of the device. Figure 3-24a shows the CV curves of a single μCFSC at scan rates from 20 mV/s to 1000 mV/s, which indicate excellent capacitive behavior of the prototype since the shapes of the curves are nearly rectangular and the currents are almost proportional to the scan rates (Figure 3-24b). The volumetric capacitance as a function of scan rate is plotted in Figure 3-25, together with the results simulated by using the 1D transmission line circuit model. The μCFSC shows a capacitance of 25.8 μF/cm, or 19.4 F/cm^3, or 2.7 mWh/cm^3 at the scan rate of 20 mV/s, which is a very high value since the total volume of the two electrodes, the electrolyte, and even the mechanical support (carbon fiber core) are all included. The predictions from the circuit model are not far from the experimental results, and the deviation is probably due to the uncertainties in the dimension measurements and the simplified electrochemical impedances used in the circuit model.

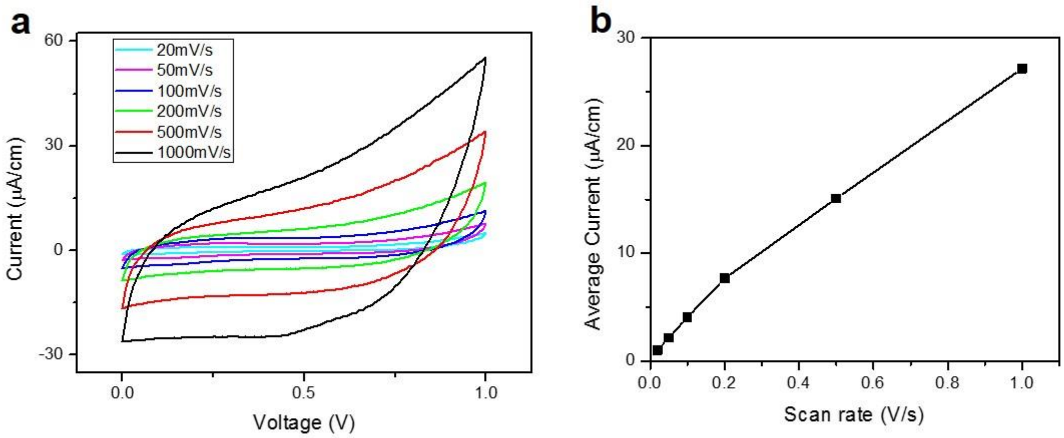

Figure 3-24. (a) Cyclic voltammetry (CV) curves of a μCFSC prototype under different scan rates from 20 to 1000 mV/s. (b) The current as the function of scan rate for the μCFSC prototype.

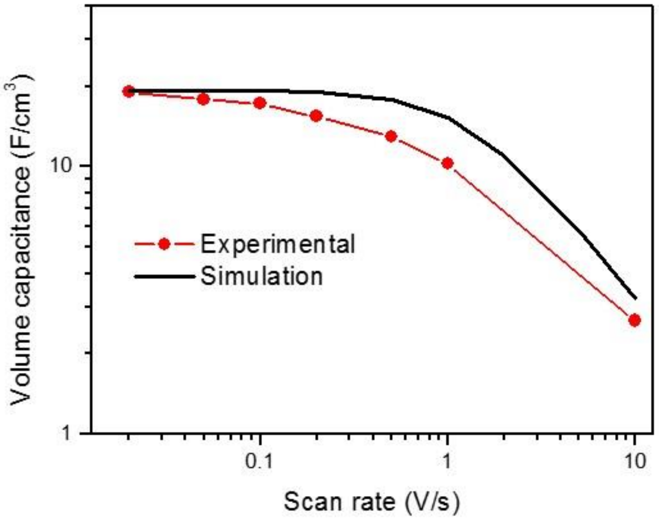

Figure 3-25. Volume capacitances calculated from experimental results and the circuit model versus scan rate.

The energy and power densities of our μCFSC are plotted in Figure 3-26, including experimental results from other reported CFSCs, and simulation results using our circuit model and reported parameters [34]. From both experimental and simulation results, our μCFSCs show higher energy and power densities than other reported CFSCs [98], [99], [101]–[109], [119]. The high values are mainly due to the high capacitance of the active materials and the compact design with short paths for ion transports between electrodes. Specifically, our design has positive and negative electrodes occupying over 52 % of the total volume using thin layers of MnO_2/PPy and CNTs with measured high capacitances of 386 F/cm^3 and 95 F/cm^3, respectively. Other CFSCs have larger sizes but lower performances, such as the ones using CuO/AuPd/MnO_2 nanowires (410 μm in diameter, 37 F/cm^3 and 31 vol% for the electrodes) [98], multiwalled carbon nanotubes/carbon fibers (800 μm in diameter, 14.1 F/cm^3 and 27 vol% for the electrodes) [102], or carbon nanotubes (43 μm in diameter, ~32 F/cm^3 and 25 vol% for the electrodes) [99], For other fiber-based supercapacitors using twisted electrodes and parallel electrodes, researchers often ignore the sizes of separator, electrolyte, and mechanical support in the performance calculations to achieve capacitances between 2.5 to 300 F/cm^3, and energy density up to 6.3 mWh/cm^3 in the literature [35], [89]. As a result, the comparison of those work with coaxial fiber supercapacitors, which have separator, electrolyte, and mechanical support all included in a single 1D device, is difficult.

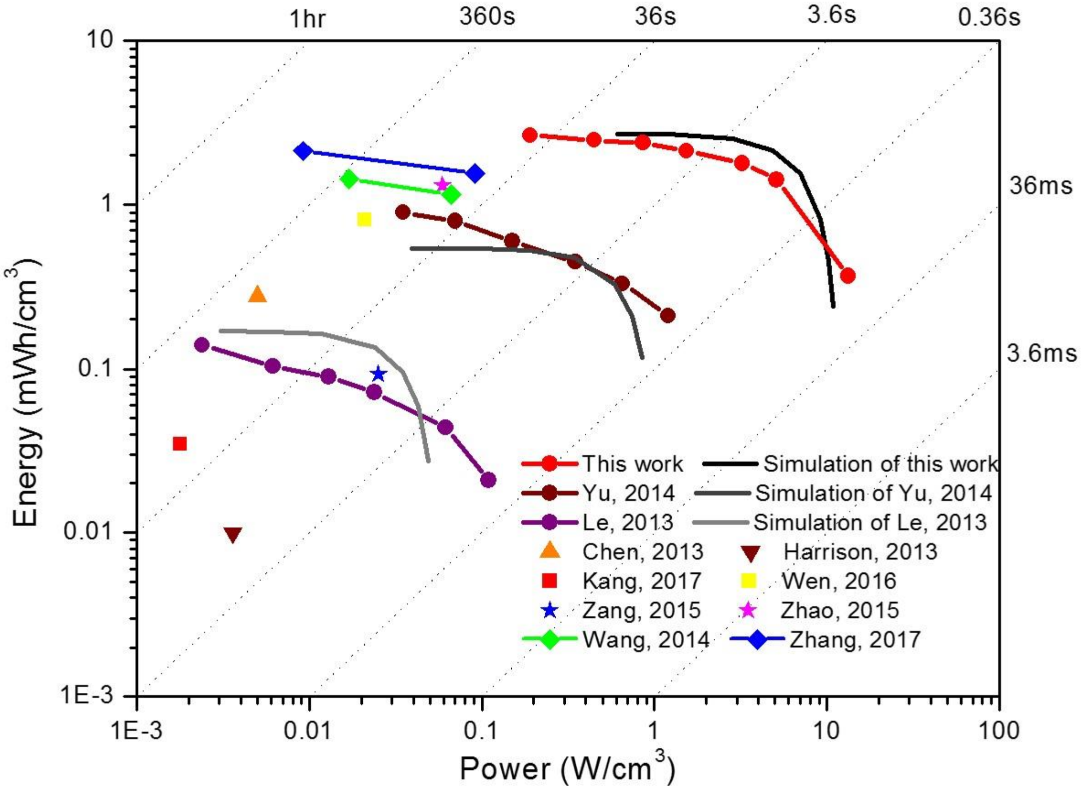

Figure 3-26. Ragone plots of results from our experiments, simulations from our circuit model, and experimental results from prior works.

Other electrochemical measurements, such as cycling tests and impedance spectroscopy of a single μCFSC are recorded. Figure 3-27a shows the capacitance retention of the μCFSC during 20,000 charge/discharge cycles. The device shows an increase of capacitance in the first 10,000 cycles, which is probably due to the gradual infiltration of electrolyte into the nanoporous structures of both electrodes, as similar tendency is observed in other works [81], [92], [120], [121]. Over 85% of the initial capacitance is retained after 20,000 cycles, demonstrating an excellent cycle stability of the device.

Figure 3-27b shows the Nyquist plots before and after 20,000 charge/discharge cycles with the frequency range from 0.1 to 100k Hz. The impedance doesn't change much even after long-term cycling. For the initial impedance, the crossover frequency at a phase angle of -45° is 160 Hz, which corresponds to a relaxation time of only 6.3 ms.

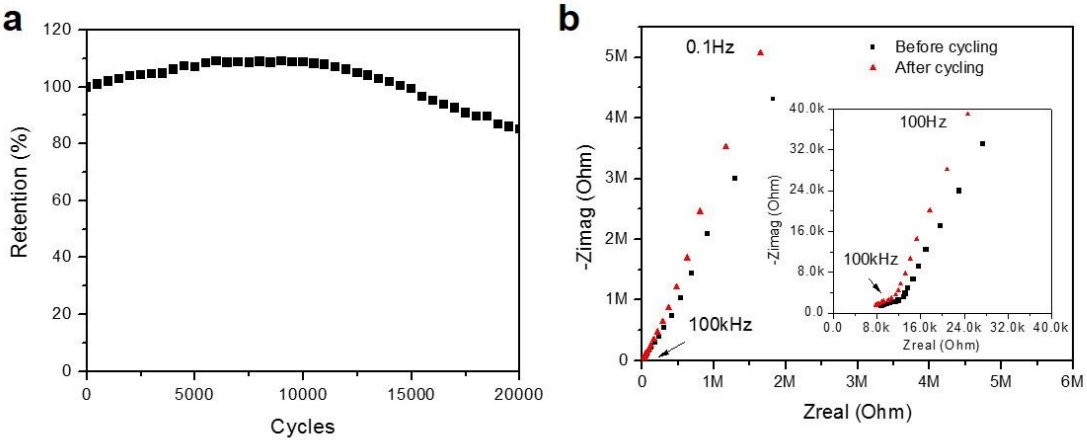

Figure 3-27. (a) Capacitance retention results of the μCFSC during the 20,000 charge/discharge cycling tests. (b) Nyquist plot of the impedance of a single μCFSC with the frequency range from 0.1 to 100k Hz.

The same result can also be obtained through evolution of the imaginary part of capacitance as a function of frequency (Figure 3-28a). An equivalent circuit model is used to fit the Nyquist polt (Figure 3-28b). The circuit is composed of a series resistance (R_s=9.3 kΩ), a capacitance (C=11.3 μF), a charge transfer resistance (R_{ct}=0.13 kΩ), a Warburg impedance (Z_W=0.32 $\mu S \cdot s^{1/2}$), and a constant phase element (CPE=0.63 $\mu S \cdot s^{0.617}$). Relatively small charge transfer resistance and diffusion impedance are due to the shortened distance between two electrodes of the device. Although the impedance at high frequency and the fitted result both show a series resistance of ~9 kΩ for a single μCFSC device, the impedance should be inversely proportional to the cross-section area for one dimensional fiber-shaped supercapacitors. Considering that the diameter of our device is only ~13μm (cross-section area = 1.3×10^{-6} cm^2), the normalized series resistance should be ~0.01 $\Omega \cdot cm^2$. For the potential applications, many μCFSCs will be connected in parallel to reduce the overall impedance.

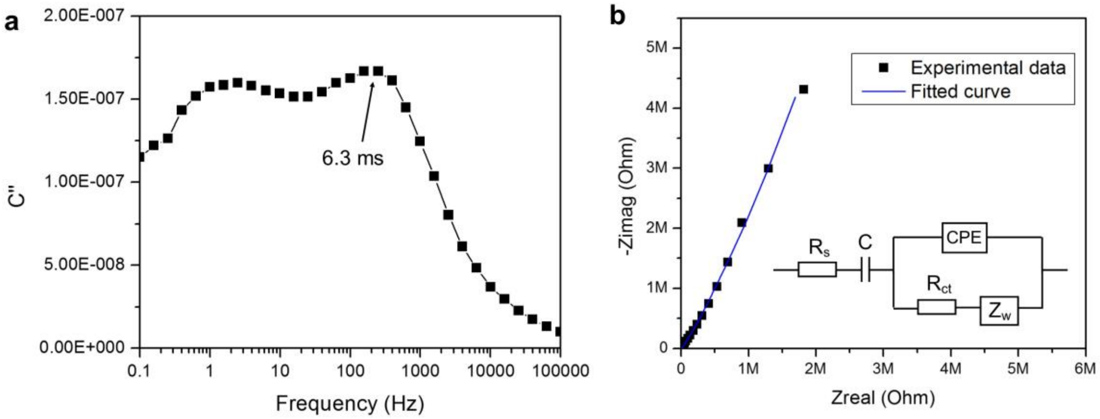

Figure 3-28. (a) Evolution of the imaginary part of capacitance vs. frequency for the μCFSC, in which the peak at ~160 Hz corresponds to a relaxation time of 6.3 ms. (b) Fitting result of the impedance spectrum of the μCFSC using an equivalent circuit model.

In addition to the high electrochemical performance, the ultra-thin μCFSC shows intrinsically high mechanical flexibility. All 1D fibers may be bent in any direction with any angle, while the bending radius is limited by the size and flexibility of the fiber. Our μCFSC can be bent at a radius of less than 50 μm without breaking, as shown in the optical photo in Figure 3-23b. We can also tie the μCFSC into a knot with a radius of ~100 μm, as shown in the SEM image in Figure 3-29a.

We tested the performance of a μCFSC with a bending radius of ~100 μm in the middle and compared the results with that of a straight μCFSC in Figure 3-29b. The two curves are very close to each other, and the bent device works as good as the straight one. The slight deviation of the performance may be caused by the errors during the coating of CNT layer, which shows a performance error of ±20% for different samples. Such a small bending radius means that the device is very difficult to break through bending, and this value can hardly be achieved by fibers with large diameters in the range of a few hundred microns. The small size and high flexibility make our μCFSC promising in realizing energy storage systems to be integrated with clothes, as clothes are usually woven by fibers with dimeters of tens of microns for comfortableness and softness.

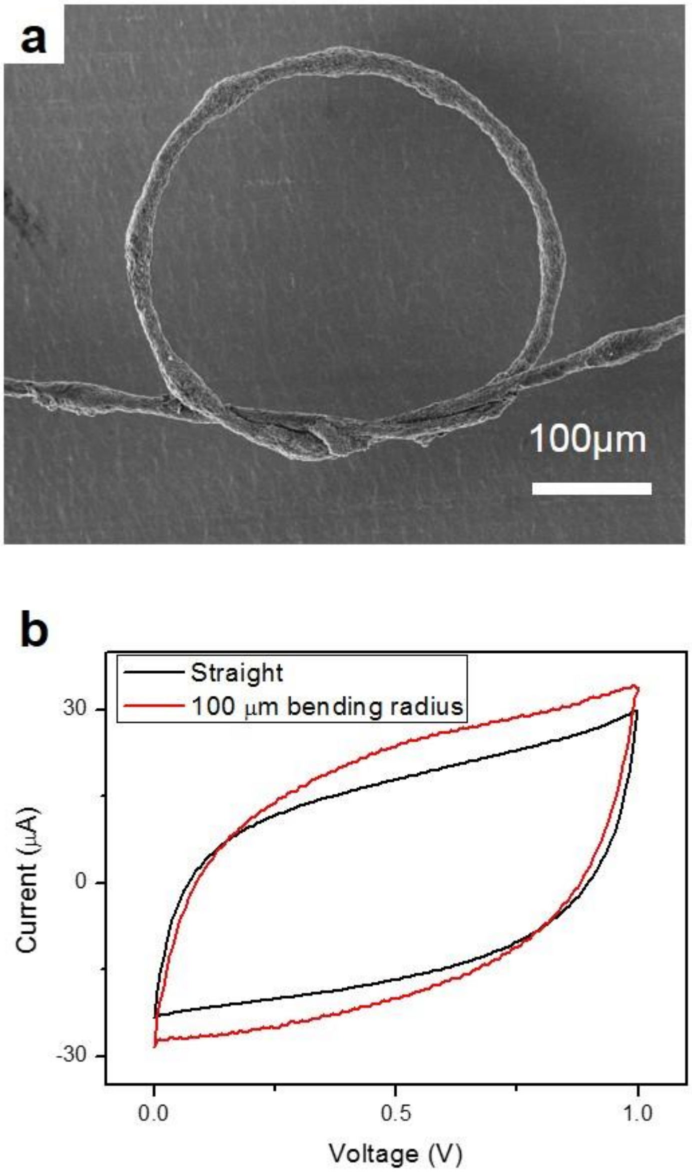

Figure 3-29. (a) SEM image of a μCFSC with a knot in the middle. (b) CV curves of a straight μCFSC and a μCFSC that is bent with a radius of about 100 μm in the middle.

3.4.2 Performance of multiple connected ultrathin CFSCs

For practical applications, threads composed of many μCFSCs in parallel have to be used to increase the overall current. Here we twist 7 μCFSCs (Figure 3-30a) and test the CV curve (Figure 3-30b) and Galvanostatic charge–discharge curve (Figure 3-30c) of the thread. The thread shows a capacitance of more than 5 times of a single μCFSC due to variations in each μCFSC.

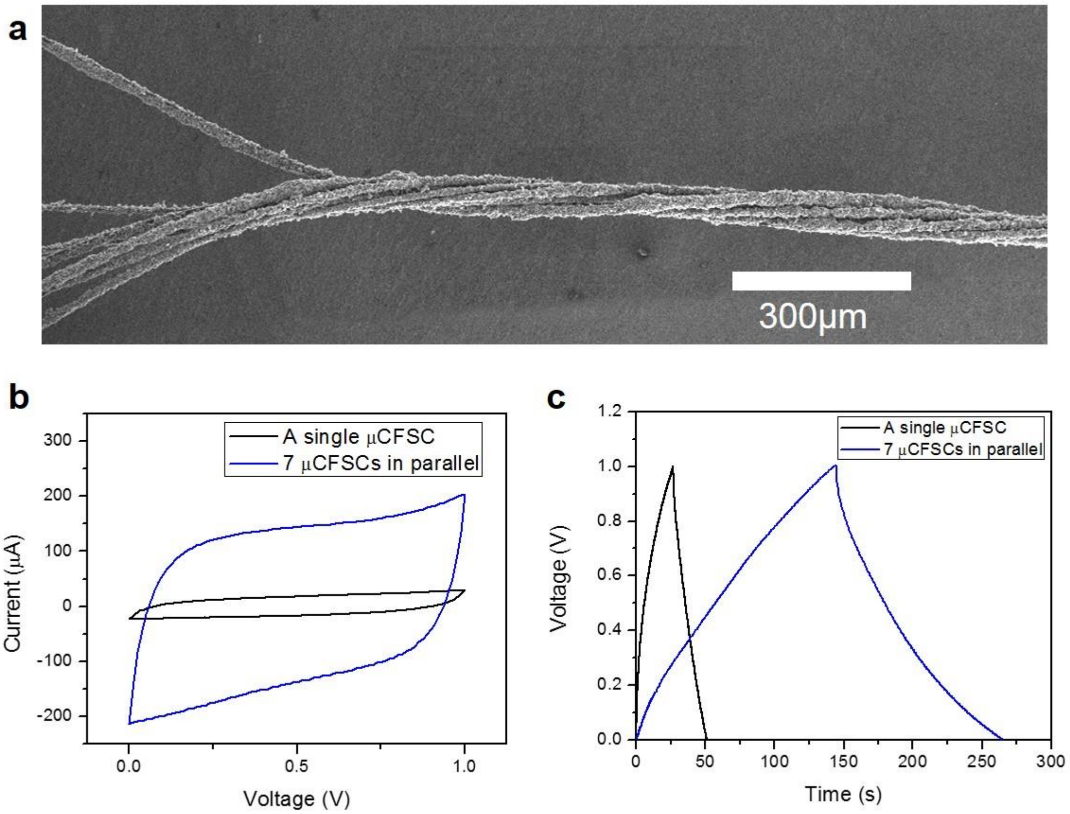

Figure 3-30. (a) SEM image of a thread made of seven twisted μCFSCs. (b) CV curves of a single μCFSC and seven μCFSCs in parallel at the scan rate of 1 V/s. (c) Galvanostatic charge–discharge curves of a single μCFSC and seven μCFSCs in parallel at the current density of 1 μA/cm.

We also test three μCFSCs connected in series to achieve a higher voltage compared with a single one. Figure 3-31a shows the schematic of how three μCFSCs are connected, and Figure 3-31b shows the photo of the real setup, in which the metal connections are much bigger than the μCFSCs. Figures 3-31c and d compare the CV and galvanostatic curves of a single μCFSC and three in series at the same test conditions, respectively. The operation voltage is tripled and the capacitance becomes one third when three fibers are in series.

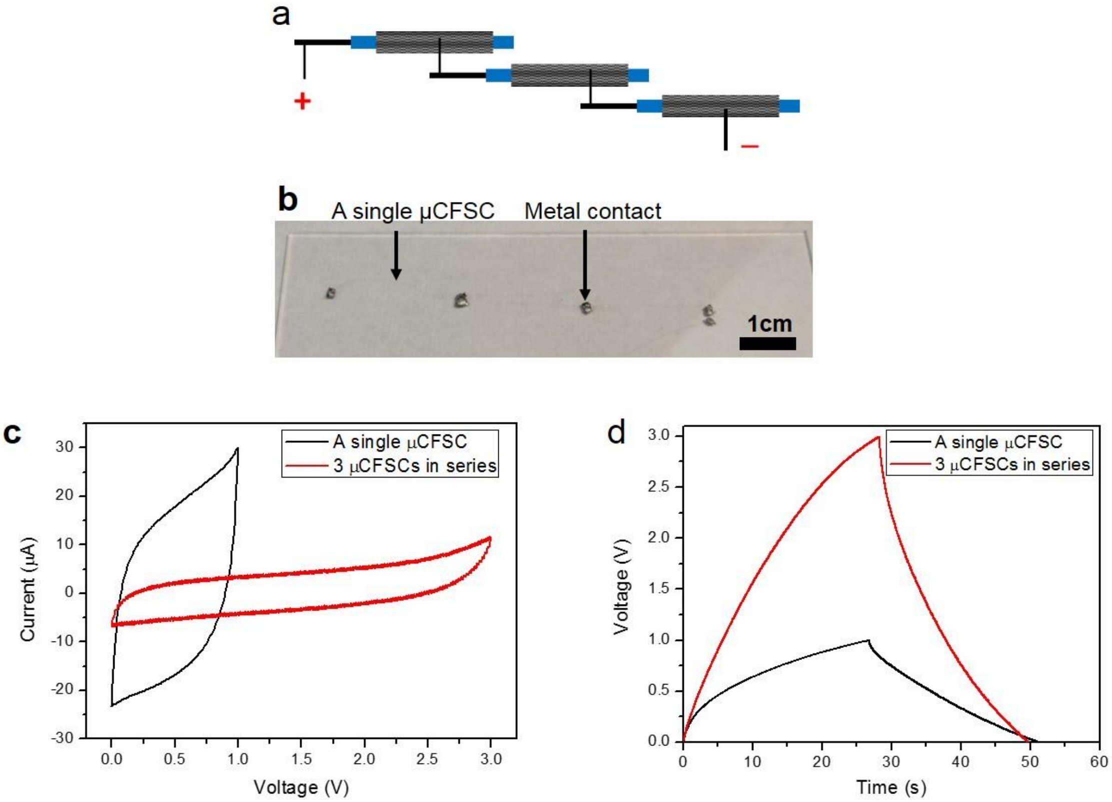

Figure 3-31. (a) Schematic of three µCFSCs connected in series. (b) Photo of three µCFSCs connected in series. (c) CV curves of a single µCFSC and three serial ones at the scan rate of 1 V/s. (d) Galvanostatic charge–discharge curves of a single µCFSC and three serial ones at the current density of 1 µA/cm.

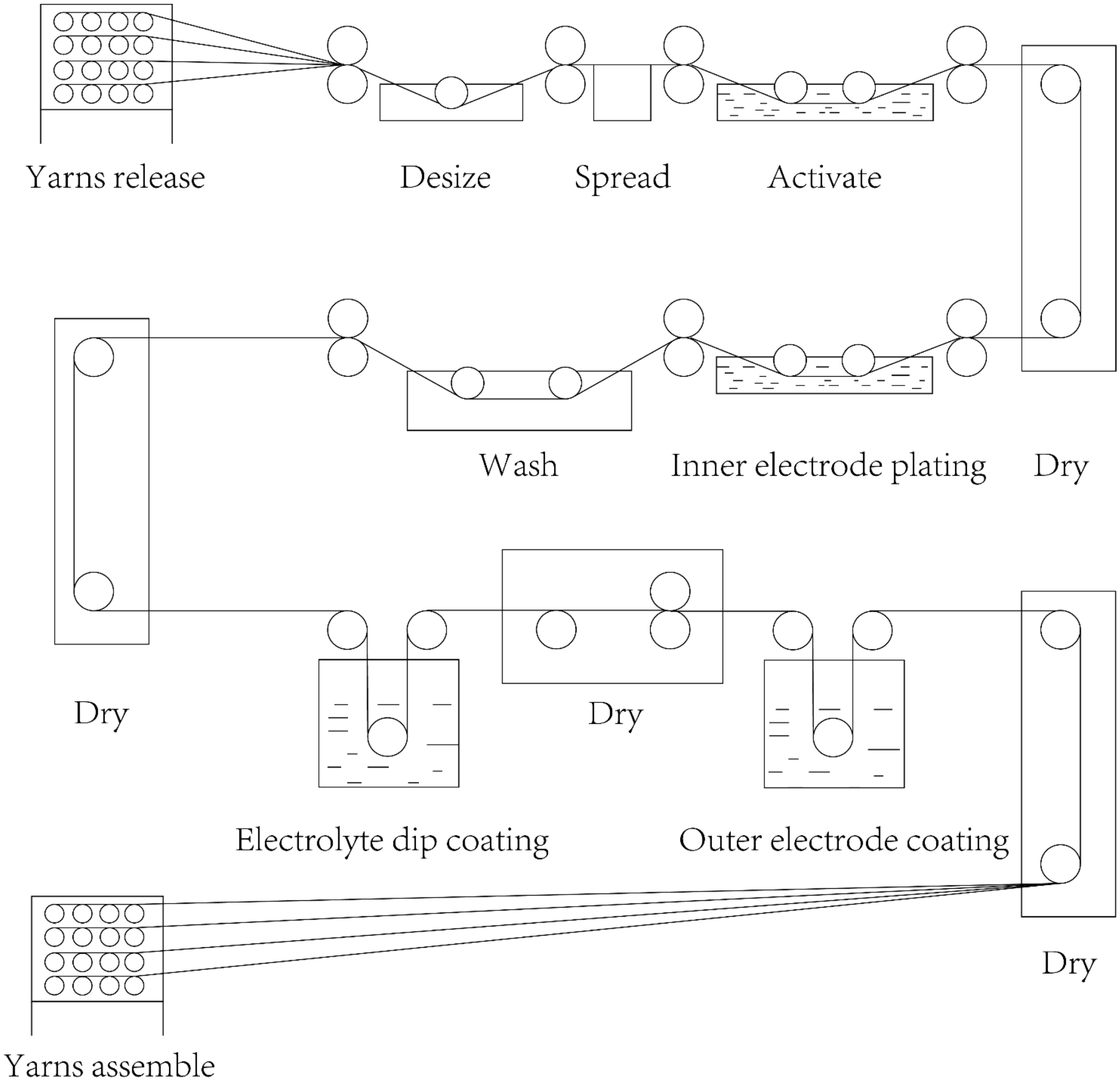

Figure 3-32. A possible roll-to-roll process design for continuous production of μCFSCs as future work.

3.5 Summary

In summary, we propose and demonstrate an ultra-thin micro coaxial fiber supercapacitor with the smallest reported overall diameter (~13 μm) achieving high energy density (up to 2.7 mWh/cm^3) and power density (up to 13 W/cm^3). We also develop a simplified circuit model which agrees with our experiments. The model can be used to simulate fiber supercapacitors with coaxial structure of any size. It reveals that scaling down the diameter of CFSCs by using thinner layers of active materials while fixing the volume ratios of each layer will improve the performances, especially the energy density, power density and flexibility. With the use of scalable fabrication process, such as a detailed future roll-to-roll process illustrated in Figure 3-32, we believe such μCFSCs are promising building blocks for future flexible and wearable power systems.

4 Woven supercapacitor fabrics

4.1 Introduction

While the ultrathin CFSC introduced in Chapter 3 provide high power and energy densities, as well as excellent flexibility, the integration of such flexible supercapacitors into wearable textiles also requires the compatibility with weaving technology and mechanical durability for the device. A lot of work needs to be done to realize the batch fabrication of defect-free ultrathin CFSCs. At the same time, this chapter will consider other solutions to scalable, safe, and durable energy storage for wearable applications.

In fact, the safety risks and poor mechanical compatibility with flexible systems are major obstacles for the use of lithium-ion batteries in different wearable electronics. Therefore, even with lower energy densities than rigid lithium-ion batteries, flexible supercapacitors (SCs) have the potential to enable new flexible and wearable electronics where flexibility and safety are of particular importance.

In terms of and mechanical stability and durability, which are highly related to the safety of electrochemical energy storage, two types of flexible SCs with either two-dimensional (2D) or one-dimensional (1D) electrode configurations are considered separately. Flexible SCs using sandwiched or in-plane interdigital 2D thin-film electrodes usually use fragile electrode materials supported by flexible substrates such as plastic membranes and textiles [2], [15], [16], [18]. Though much progress has been made on the electrochemical performances of the electrode materials, the flexibility, mechanical strength, and stability of these devices rely heavily on additional mechanical support. For example, in practical applications, the substrates and packaging materials of these devices occupy a large portion of the total weight/volume and greatly diminish the overall energy density. The electrochemical performance has to be sacrificed for better mechanical properties.

On the other hand, the flexible SCs based on coaxial, twisted, or parallel 1D electrodes integrate mechanical support, current collector, and capacitive electrode materials in a single fiber/yarn/thread [35], [100], [122]. However, similar issues such as high proportion of mechanical support still exist by coating functional nanomaterials onto heavy metal wires [98], [123], [124] or non-conductive wearable fibers [90], [95], [96], [109], [125], [126]. A promising approach is to develop dual-functional electrode materials that provide energy storage and mechanical support simultaneously. For example, researchers have demonstrated free-standing yarn electrodes by the spinning of carbon nanotubes, graphene oxide, conducting polymers, and so on [80], [81], [89], [92], [99], [120], [127]–[129]. Such yarns achieve high capacitances (up to ~300 F cm^{-3} per electrode) because of the absence of binder materials, current collector, and other supporting compositions [89]. However, their tensile strength, which decreases with the increase of porosity, is usually around 100 MPa, which is much lower than that of typical wearable fibers (~1000 MPa for cotton and polyester fibers [4.30]). As a result, they have to be assembled on a plastic substrate or woven into other textiles for practical applications. Commercial carbon fibers (CF) with high mechanical strength (over 1000 MPa), light weight, and high conductivity are another promising structural material as 1D electrode for flexible SCs [97], [102], [116], [130]. However, pristine CF has low surface area (< 1 m^2 g^{-1}) and is usually used as an electrode to load other capacitive nanomaterials, while surface-activated CF has a higher surface area but limited to less than 100 m^2 g^{-1} [131].

In this chapter, woven SC fabrics using nanoporous CF thread electrodes with both high surface area (340 m^2 g^{-1}) and high strength (1955 MPa) through a scalable fabrication process are demonstrated. The flexible SCs show a high energy density (2.58 mWh g^{-1} or 3.6 mWh cm^{-3}, normalized by the whole weight/volume of the device) comparable to rigid commercial supercapacitors and can work under a high tensile strength of 1000 MPa or a high pressure of 100 MPa without noticeable performance degradations. The versatile SC configurations allow for a variety of form-factor designs of energy storage fabrics with excellent flexibility and mechanical durability.

4.2 Structure and process design

A SC device comprises of two electrodes and electrolyte connecting two electrodes. In almost all reported SC devices, the two electrodes are in parallel configuration. For example, when 1D fiber-based electrodes are assembled to be a SC device, the positive and negative electrodes are usually arranged in the same direction with maximum area facing each other (as illustrated in Figure 4-1a) no matter whether a coaxial, twisted, or parallel structure is applied. Such configuration makes the ion transport between two electrodes most efficient. However, the fabrication of such SCs is not compatible with woven textiles, and the electrical connection can be difficult when a lot of such devices are assembled for larger-area flexible SCs.

Another arrangement of electrodes, in which two thread-like electrodes are perpendicular to each other and have contact at any electrolyte-coated area (Figure 4-1b), is seldom considered in the literature. In fact, each electrode coated with electrolyte can be considered as a half cell of a SC. As long as the electrolyte of two half cells is in contact, ion path will form and a complete SC cell will be working. The ion transport path, however, is very large in this case and will lead to very slow charging and discharging of the device.

An advanced design using perpendicular electrodes is illustrated in Figure 4-1c. Multiple parallel electrodes are connected as a single positive or negative electrode and the other ones in the perpendicular direction is used as the counter electrode. The contact points between positive and negative electrodes are growing in a parabolic way when more and more parallel electrodes are used. The average ion transport distance will also be reduced with more densely arranged "threads". Obviously, such electrode configuration is compatible with the fabrication of woven fabrics. Moreover, the woven supercapacitor fabrics provide breathable feature that allows water and air to pass through space between threads, which is not achieved with 2D thin film flexible supercapacitors.

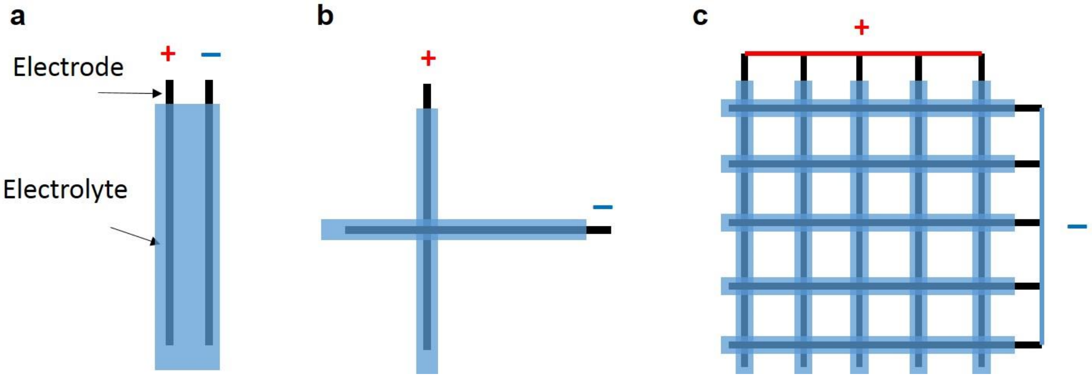

Figure 4-1. Schematics of (a) two thread electrodes in parallel to form a supercapacitor cell, (b) two thread electrodes in perpendicular, and (c) 5 parallel thread electrodes in perpendicular with other 5 parallel thread electrodes.

A simple experiment is conducted to verify the feasibility of a SC using two perpendicular thread electrodes, as shown in Figure 4-2a. Each thread electrode comprises of ~1000 carbon fiber (CF) filaments. Two CF threads coated with solid electrolyte are in contact at one point. The schematic of the cross section view of the contact is illustrated in Figure 4-2b. The ends of the threads with no electrolyte are connected with metal clips. Cyclic voltammetry curve measured for the setup is plotted in Figure 4-2c. The curve shows a combination of capacitive and resistive behavior, in which the capacitance is proportional to the enclosed area of the curve and the slow increase/decrease of the current in the charging/discharging curve indicates a large time constant determined by RC (resistance multiplies capacitance). The result verifies that the one point contact of electrolyte connects two half cells of SC and leads to a measureable capacitance, but it provides long ion transport distance with relatively high resistance.

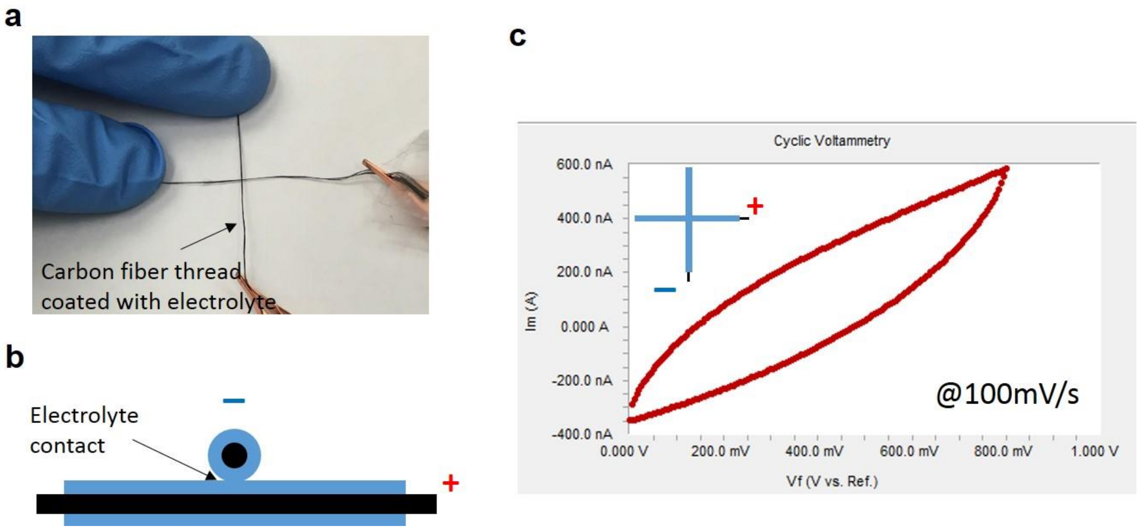

Figure 4-2. (a) Photo of the setup to test two electrolyte-coated thread electrodes in contact at one point. (b) Schematic of the cross section of two electrolyte-coated thread in contact. (c) Cyclic voltammetry curve of the device shown in (a).

CF threads are used in this chapter because of their high conductivity, high strength, light weight, and reasonable flexibility, as explained in Chapter 3. Commercial CF threads usually comprise of 1,000 to 48,000 CF filaments per thread and each filament is ~7 μm in diameter (the same as the ones used in the previous chapter). For convenience, the thread consists of x,000 CF filaments is referred as "xk thread", where x=1, 3, or 12 indicating the three sizes of threads used in this chapter. Figure 4-3 shows a photo of a 3k thread coiled on a carton tube.

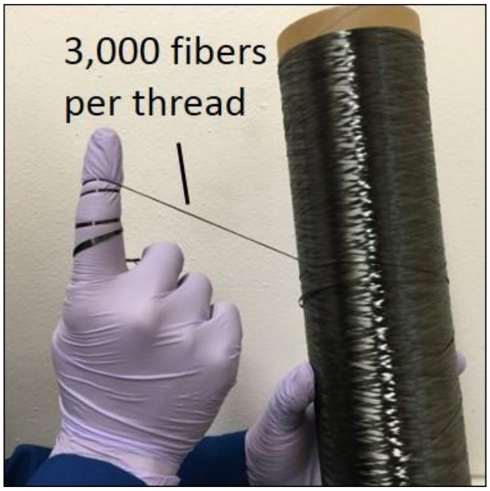

Figure 4-3. Photo of the as-received commercial flexible 3k CF thread.

As mentioned in Chapter 3, bare CFs have smooth surface with low surface area and do not store much charge as supercapacitor electrodes. While electrodeposition of high-performance pseudocapacitive materials on CF surface can greatly improve its capacitance, the approach only works well when filaments in the thread are completely separated. Coatings by electrodeposition are not uniform on threads with thousands of filaments. The fibers close to the fringe of the thread will have active material deposited on surface first, which will then block the inside ones. A better way to create high surface area for the entire thread is to etch the surface of CF to make it nanoporous. Electrochemical and chemical etching are tested for the purpose of creating higher surface area on CF, which will be explained in details in the following section. It is found that the chemical etching of CF using potassium hydroxide (KOH) results in nanoporous structure with the highest surface area, and mechanical strength comparable to original CF threads.

By combining the surface activation of CF threads and the weaving technology, the process of fabricating woven SC fabrics with high capacitance, high strength, and high mechanical stability is illustrated in Figure 4-4a. The nanoporous CF threads are prepared by a chemical activation process with KOH (Figure 4-4b). The crossing threads in the fabrics, between which ions can shuttle through contacted electrolyte layers, are used as positive and negative electrodes, respectively (Figure 4-4c) and the whole fabrics can be used as an electrochemical double layer (EDL) supercapacitor with symmetric electrodes.

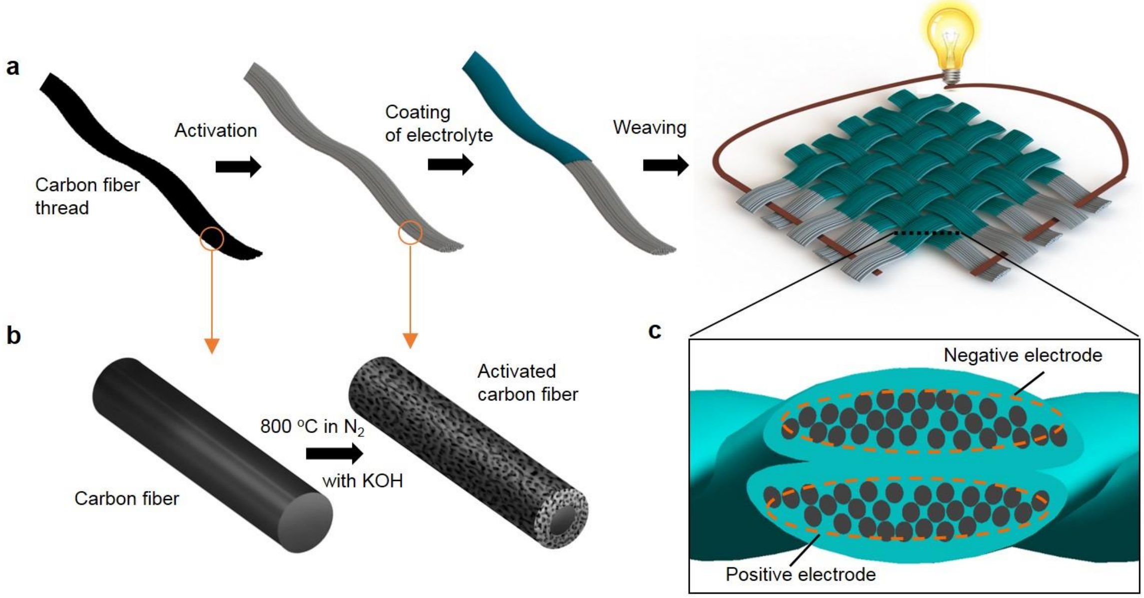

Figure 4-4. (a) Fabrication process for the woven supercapacitor fabrics by using activated carbon fiber threads. (b) The activation process of a carbon fiber, after which the carbon fiber has a nanoporous surface and a solid core with high mechanical strength. (c) Cross-section schematics of the supercapacitor fabrics showing two crossing threads as positive and negative electrodes, respectively, with a solid electrolyte layer in between. [40]

4.3 Activation of carbon fiber threads

4.3.1 Selection of activation process

Three approaches have been applied to activate the carbon fiber, including (1) chemical activation by using HNO_3, (2) electrochemical activation by using H_2SO_4, and (3) chemical activation by using KOH. 12k threads are used for all approaches. Samples of different approaches are first prepared for electrochemical tests before further characterization. All electrochemical tests are conducted in two-electrode setup, in which two identical threads are used as positive and negative electrodes, respectively. Capacitance of the activated threads are calculated using data from cyclic voltammetry (CV) curves. Detailed methods and results are described as below.

(1) Chemical activation by using HNO_3:

To activate CF threads by using HNO_3, the threads are immersed into 70 wt% HNO_3 and sealed in an autoclave. The autoclave is heated up to 120 ^{o}C for 2 hr and naturally cool down to room temperature. The activated CF is then washed by water until the PH value of water reaches 7.

Typical CV curves of CF threads before and after HNO_3 activation are compared in Figure 4-5. Calculation shows that the capacitance of the threads increases for about 1 order after the activation. However, observation finds that many of the filaments breaks after the process. The whole thread is also a lot easier to break with HNO_3 treatment.

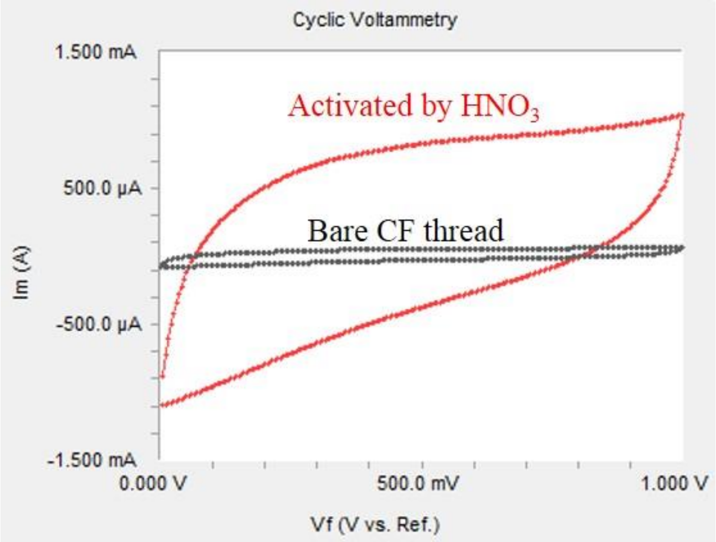

Figure 4-5. CV curves of CF thread electrodes before and after HNO_3 activation, tested in symmetric two-electrode setup at a scan rate of 100 mV/s.

(2) Electrochemical activation by using H_2SO_4:

To perform electrochemical activation by using H_2SO_4, a three-electrode system is applied. CF thread immersed in 0.5 M H_2SO_4 is used as the working electrode, Ag/AgCl is used as the reference electrode, and a Pt wire is used as the counter electrode. A potential of 2 V versus Ag/AgCl is applied to CF thread for different amount of time. The threads are then washed in water and tested.

Figure 4-6a shows CV curves of CF threads activated for 10s, 60s, and 300s, respectively. Clearly, longer activation time results in higher capacitance of the threads. Figure 4-6b plots the calculated capacitance per thread length versus activation time. The result shows that the initial activation (~10s) increases the capacitance much faster than later time. Another observation is that, after more than 600s of activation, the mechanical strength of the thread also diminishes a lot, and many filaments break during the handling and washing process.

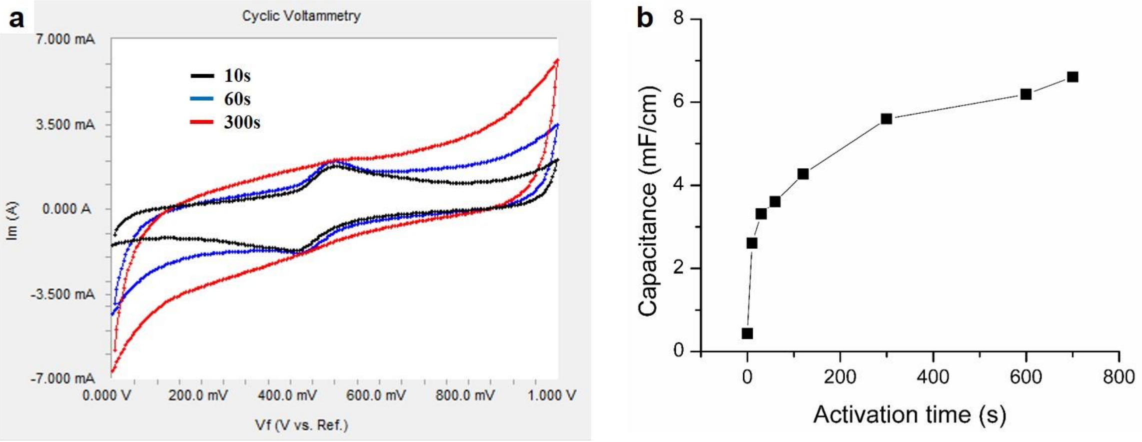

Figure 4-6. (a) CV curves of CF thread electrodes after H_2SO_4 activation for 10s, 60s, and 300s, at a scan rate of 100 mV/s. (b) The calculated capacitance per thread length versus activation time.

(3) Chemical activation by using KOH:

To activate CF threads by using KOH, the threads are first dipped into a saturated KOH water solution (~20 M at room temperature) and dried at 80 ^{o}C to load KOH on CF surface. The thread is then heated to 800 ^{o}C for 1hr in N_2 in a tube furnace. After cooling down of the sample, it is washed in water. The above process may be repeated for twice or three times. The activated samples are tested in the symmetric two-electrode setup.

The preliminary electrochemical test results are plotted in Figure 4-7. From the CV curves shown in Figure 4-7a, the samples activated by KOH for 1 time or 2 times provide much larger capacitances, which are proportional to the currents measured at the same scan rate. The values are 2 orders more than that of the original CF threads, and the twice activated one shows about twice of the capacitance of the 1-time activated one. Compared with the results of HNO_3 and H_2SO_4 activations (Figures 4-5 and 4-6a), KOH activation clearly improves more capacitance for CF threads. Figure 4-7b compares the charge-discharge curves of the threads with no activation, after 1 activation and 2 activations. Similar conclusions can be drawn, as activated CF threads need over 10 times longer to be charged/discharged at 10 times higher currents, indicating over 100 times larger capacitance.

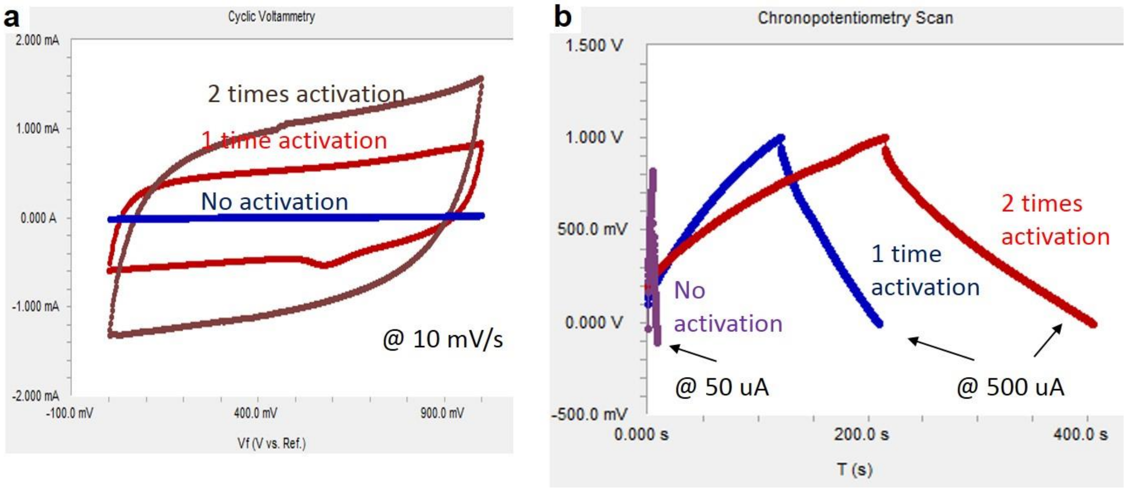

Figure 4-7. (a) CV curves of CF thread electrodes after KOH activation for 1 time and 2 times. (b) The constant current charge-discharge curves for different samples.

The calculated capacitances of CF threads after different activation methods are summarized in Table 4-1. The much larger capacitance derived by KOH activation suggests that it is a better approach to improve the capacitance of CF threads. Moreover, it is observed that the strength of the CF threads remains high after KOH activation. Therefore, KOH activation of CF threads is further studied and optimized in this chapter to produce high-performance thread electrodes for woven supercapacitor fabrics.

Table 4-1. Summary of capacitances of thread samples using different activation processes

12k CF thread electrode	Capacitance per thread length	Mechanical property
Bare CF threads	~0.38 mF/cm	Strong
Chemically activated by HNO_3	~5 mF/cm	Many broken fibers, weak
Electrochemically activated by H_2SO_4	2.6 - 6.6 mF/cm	Easily broken when handled by tweezers
Chemically activated by KOH	50 – 110 mF/cm	Strong

4.3.2 Optimization of KOH activation

This section tries to optimize the KOH activation process of CF threads by adjusting different parameters. The amount of KOH loaded on CF threads, the type of CF threads, and the number of activations are mainly studied.

(1) The amount of KOH loaded on CF threads:

The KOH activation of carbon at high temperature is based on the reaction, $6KOH + C \leftrightarrow 2K + 3H_2 + 2K_2CO_3$, followed by decomposition of K_2CO_3 and/or reaction of $K/K_2CO_3/CO_2$ with carbon [20]. However, it is difficult to determine the proper amount of KOH for the activation of CF by calculations. We find that significant amount of KOH will be evaporated during the high temperature process. As the mechanical property of the activated sample is considered, it is better to etch a proper portion of the CF fiber so that the strength remains high with the rest of the carbon.

A number of samples activated by different amount of KOH are prepared. The dip-coating of saturated KOH solution will randomly load 50 - 200 wt% of KOH onto a CF thread. To load more KOH, the KOH solution can be dropped onto the thread and dried quickly in an oven. The capacitances of CF thread calculated after activation are summarized in Table 4-2. The comparison of 5 samples shows that the amount of KOH loaded on CF thread will not affect the resulting capacitance. One possible explanation is that only certain amount of KOH has reacted with the surface of CF, and the rest of KOH is evaporated or blocked by the products of the initial reactions and cannot react with more carbon. Therefore, it is not necessary to load too much KOH on CF thread. Further activation of CF will not be achieved by loading more KOH, but can be done by repeating the activation process. It is also found that the weight of CF will change after activation. The gravimetric capacitance will be used for better comparison in the following sections.

Table 4-2. Summary of capacitances of thread samples activated by different amount of KOH

Sample number	KOH loaded	Capacitance per thread length (mF/cm)	Gravimetric capacitance (F/g)
1	82 wt%	45.3	5.94
2	160 wt%	43.1	5.06
3	268 wt%	50.5	5.58
4	374 wt%	37.6	4.07
5	492 wt%	58.5	6.47

(2) The type of carbon fiber threads:

There are different manufacturers and types of carbon fibers produced using various processes. Their composition is only slightly different, but their chemical and mechanical properties may vary a lot. We mainly examined two types of carbon fibers produced by Toray, Japan, including T-300 and T-700. The results are compared in Table 4-3. Here, a "reheating" process is introduced, which is to reheat the sample in N_2 at 800 ^oC for 1hr after activation and washing the sample. This process has no obvious effect on T-700 carbon fibers, but can greatly improve the capacitance of the activated T-300. The reheated activated T-300 shows 4 times higher capacitance than that of T-700. As T-700 is mechanically stronger than T-300 (4.9 GPa vs. 3.5 GPa), it may contain less defects and is more difficult for KOH to etch its carbon atoms away. As T-300 carbon fiber provides high enough mechanical strength and much higher capacitance after KOH activation, it is used in the rest of this chapter unless specified.

Table 4-3. Capacitances of different carbon fiber types after activation

CF type	Process	Weight loss	C (F/g)
T-700	1 activation	±15%	~6.3
	1 act. + reheating	±5%	~6.3
T-300	1 activation	±5%	~2.5
	1 act. + reheating	1~4%	~25

(3) The number of activations:

As briefly discussed in the previous section, twice activated CF threads show larger capacitance as compared with 1-time activated ones. Experiments are conducted to find the maximum capacitance after different numbers of activations. The results for two types of CF are listed in Table 4-4. Further etching of T-700 after 2 activations only result in small increase of capacitance. For T-300, however, the thread will break after 3 activation processes. Actually, the second activation process has already etched ~50 wt% of the carbon, and reaches a high capacitance of ~ 80 F/g.

Table 4-4. Capacitances of carbon fiber threads after different activation processes

CF type	Process	Weight loss	C (F/g)
T-700	1 activation	±15%	~6
	2 activations	~20%	~14
	3 activations	~25%	~16
T-300	1 act. + reheating	1~4%	~25

	2 act. + reheating	~50%	~80
	3 act.	Thread breaks	

For convenience, the original T-300 CF thread with no activation is denoted as CF-A0, the 1-time activated one is CF-A1, and the 2-time activated one is CF-A2, in the rest of this chapter. Figure 4-8 shows the typical CV curves of the three samples tested in a two-electrode setup. The current is normalized by the length of the thread electrode dipped into the electrolyte solution, and the result of CF-A0 is enlarged by 50 times to be comparable to other ones.

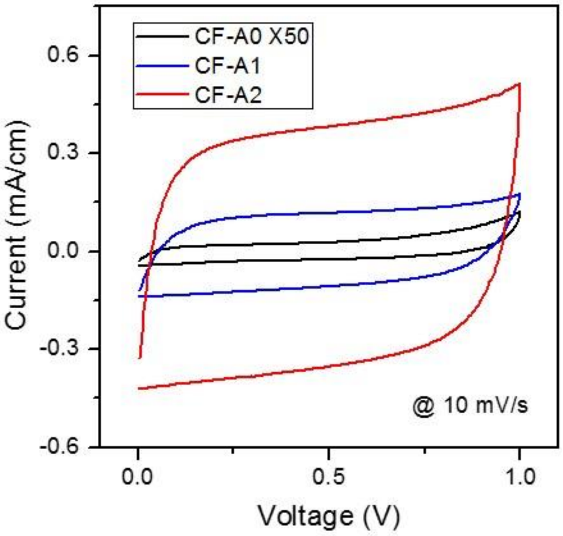

Figure 4-8. The cyclic voltammetry curves showing the EDL capacitances of two-electrode cells using different carbon fibers tested in 1M H_3PO_4 solution.

While the capacitance of CF-A2 tested in a symmetric two-electrode system is ~80 F/g, the value is as high as ~200 F/g when tested in a three-electrode setup using Ag/AgCl as reference and Pt wire as the counter electrode. A typical CV curve is shown in Figure 4-9. Despite higher value tested, two-electrode setup is mainly used in this work, as three-electrode configuration often overestimates the capacitance of electrodes working in a symmetric device [20].

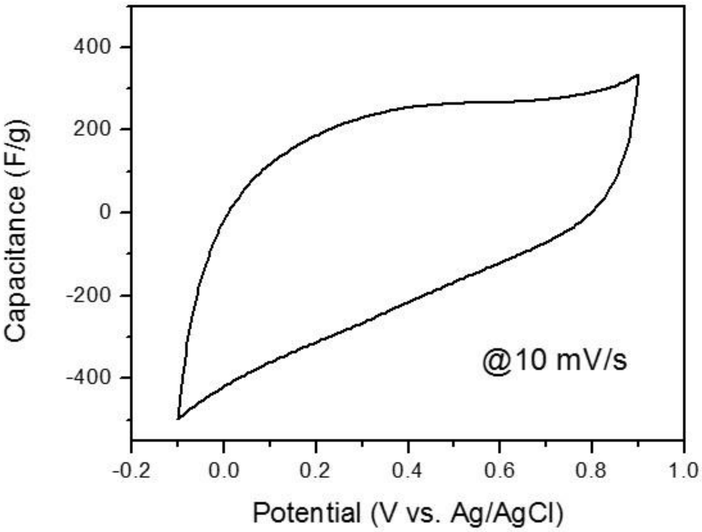

Figure 4-9. The cyclic voltammetry curve of CF-A2 tested in a three-electrode setup in 1M H_3PO_4 solution.

4.3.3 Morphology and surface area

The morphology of CF thread before and after activation is examined by SEM. As-received commercial carbon fibers have smooth surface (Figure 4-10a) and a measured SSA of 0.5 ± 0.3 m^2 g^{-1}. About 5 wt% of the carbon fiber is etched away after the one-time activation process, resulting in rough surface under the SEM (Figure 4-10b) and slight change in diameter distributions (Figure 4-10d). After the two-time activation process, about 50 wt% of the carbon fiber is lost, which creates rougher surface (Figure 4-10c) and thinner carbon fiber with wider diameter distributions (Figure 4-10d).

The N_2 adsorption/desorption experiments are conducted using QuadraSorb to analyze the surface area and pore size distribution. The Brunauer–Emmett–Teller (BET) SSAs calculated from isotherms in Figure 4-11a are 7.0 ± 1.5 m^2 g^{-1} and 340 ± 28 m^2 g^{-1} for CF-A1 and CF-A2, respectively, which are much larger than that of CF-A0. Cumulative pore volumes and pore-size distributions of CF-A1 and CF-A2 are compared in 4-11b, showing that CF-A2 has much larger pore volume. The pore size of CF-A1 is mostly around 1 nm, and that of CF-A2 is smaller in average. This indicates that most of the surface area is contributed by micropores created by KOH activation [20].

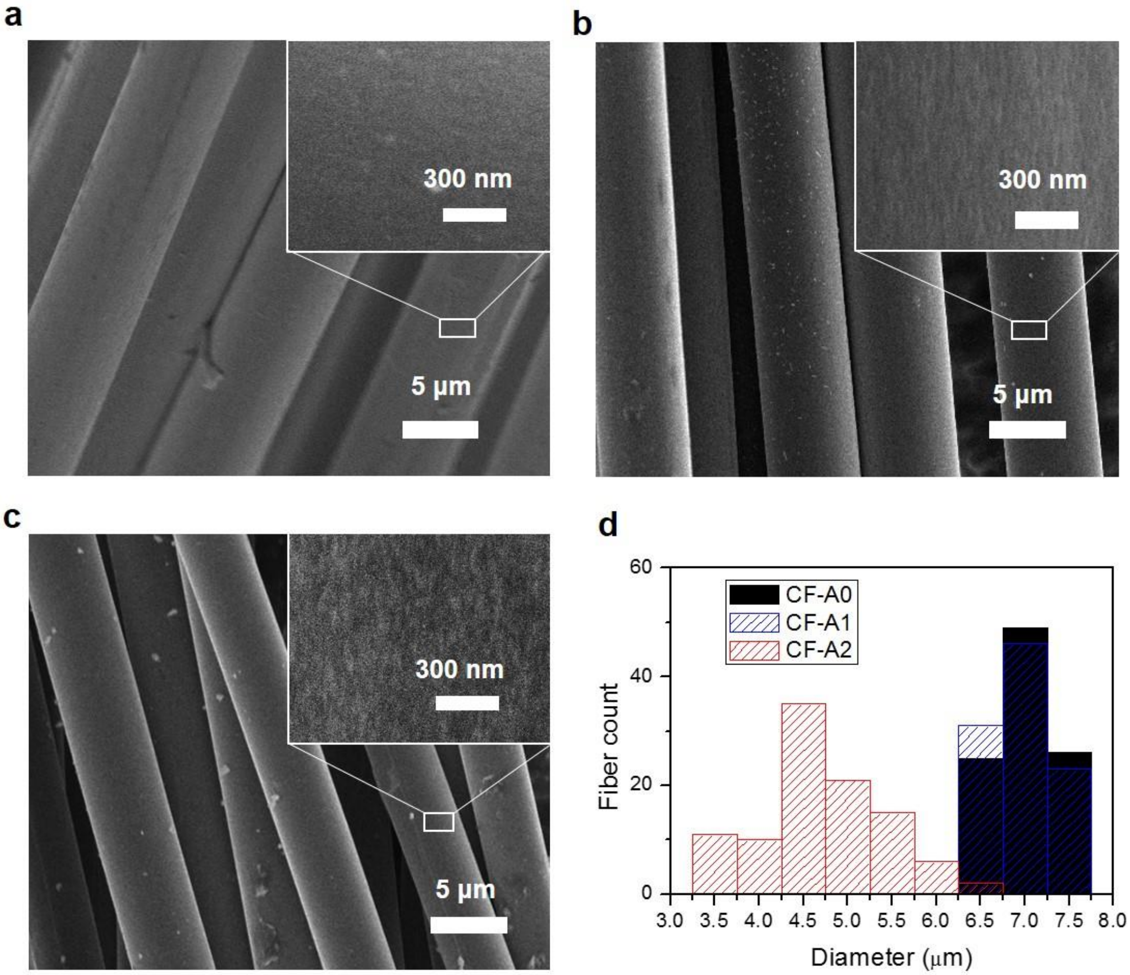

Figure 4-10. SEM images of carbon fiber threads: (a) with no activation (CF-A0), (b) after one activation (CF-A1), and (c) after two activations (CF-A2). (d) Diagram showing the diameter distribution of CF-A0, CF-A1, and CF-A2.

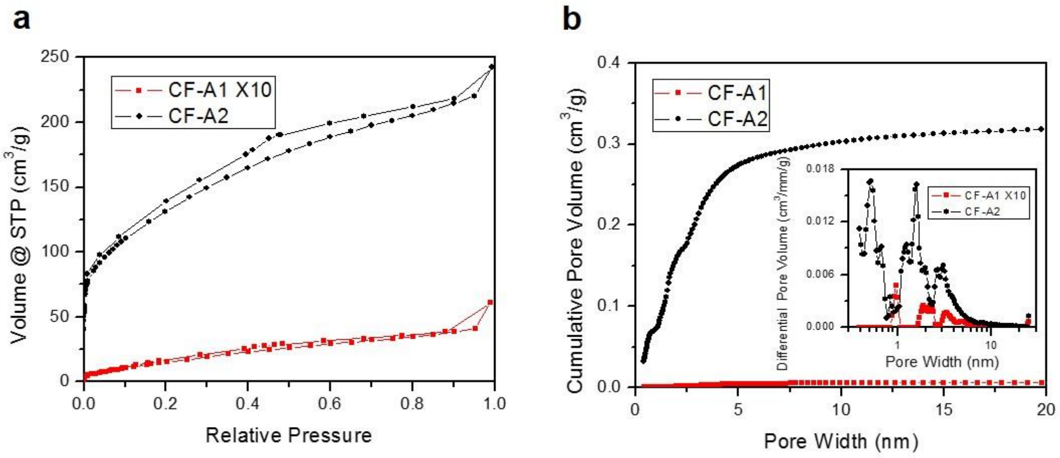

Figure 4-11. (a) N_2 adsorption/desorption isotherm of activated carbon fiber samples. (b) Cumulative pore volume and (inset) pore-size distribution of the samples calculated by using a slit/cylindrical nonlocal density functional theory (NLDFT) model.

4.3.4 Mechanical property of CF threads and electrolyte coating

The activation of CF involves the etching away of carbon atoms and should diminish its mechanical strength in principle. The effect of activation on the variation of mechanical strength is therefore quantitatively examined. A typical sample of CF thread for tensile test is shown in Figure 4-12a. Two ends of the thread are both bonded by epoxy, clamped by Al plates, and then loaded on a tensile test machine (Instron® Model 4483). The sample is then stretched until it breaks in the middle. Samples with or without electrolyte coating are both tested and no detectable difference is found, because the Young's modulus of the electrolyte is negligible compared to that of CF. The tensile stress was calculated by dividing the applied force by the cross-section area of carbon fiber threads. The cross-section area is estimated by the number of carbon fibers (3000 in this work) times the average cross-section area of a single carbon fiber filament (πr^2, where *r* is the root mean square of radii measured using SEM) with errors considered.

The typical stress-strain curves of threads using CF-A0, CF-A1, and CF-A2 are plotted in Figure 4-12b. Although the tensile strength of pristine CF is 3530 MPa from the data sheet of the product [132], the measured average strength of CF-A0 is ~2266 MPa because not all carbon fibers in a thread are stretched to the same extent during the test. Variations of up to ±18 % of the values are measured in different threads, as summarized in Figure 4-12c. For the same reason, each thread shows a slight difference in the stress-strain behavior and the failure strain. Decrease of tensile strength is found in the activated fibers as compared with original ones. The average tensile strengths of CF-A1 and CF-A2 are 1936 ± 173 MPa and 1955 ± 345 MPa, respectively, which are 85% and 86% of CF-A0, all much higher than those of wearable fibers [133].

Figure 4-12c also compares the surface areas of different samples together with the strength. It shows that the surface area increases dramatically after the two-activation process while the mechanical strength remains high. Such results indicate that the KOH tends to etch the surface atoms of CF first, so that the structure atoms inside the fiber are still maintaining the high strength.

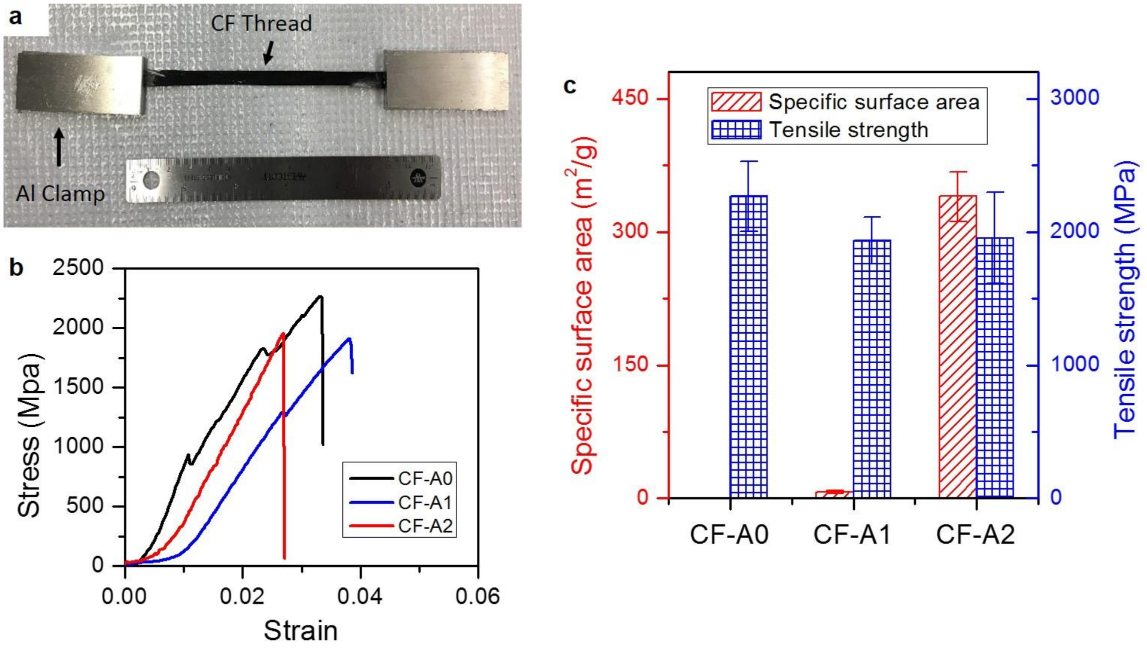

Figure 4-12. (a) A photo showing the sample used for tensile strength tests. (b) Typical tensile test curves of CF-A0, CF-A1, and CF-A2. (c) Measured specific surface area and tensile strength of CF-A0, CF-A1, and CF-A2.

In spite of tensile stress, the supercapacitor fabrics may fail due to compressive force that breaks the electrolyte layer and shorts the two electrodes. Therefore, solid electrolyte coating that can sustain high compressive stress is significant for the woven fabrics. To uniformly coat polymer-based electrolyte onto CF threads, a viscous solution of the electrolyte is first coated by impregnation and gradually dried to form a solid electrolyte layer that binds carbon fibers together (Figure 4-13a). A drum is rolled over the thread during the drying process to adjust the thickness of the electrode and the coating process can be repeated to coat a thicker electrolyte layer. Figure 4-13b shows the cross-section SEM image of a sample with ~70 μm-thick electrode (carbon fibers + electrolyte) and ~25 μm-thick electrolyte after twice coating of electrolyte. Such uniform electrolyte layer can prevent the crossing of electrodes in the woven supercapacitor fabrics from shorting such that no separator is needed.

The polymer with relatively high molecule weight (PVA, Mw=180,000) is chosen to provide high compressive strength. A simple setup is designed for experimental data (Figure 4-13c, d). In each test, two identical threads with electrolyte coating are overlapped and compressed until the electrolyte layer breaks and the two CF threads are in contact with each other to cause the electrical short circuit. The pressure at which two threads are shorted is recorded as the failure pressure.

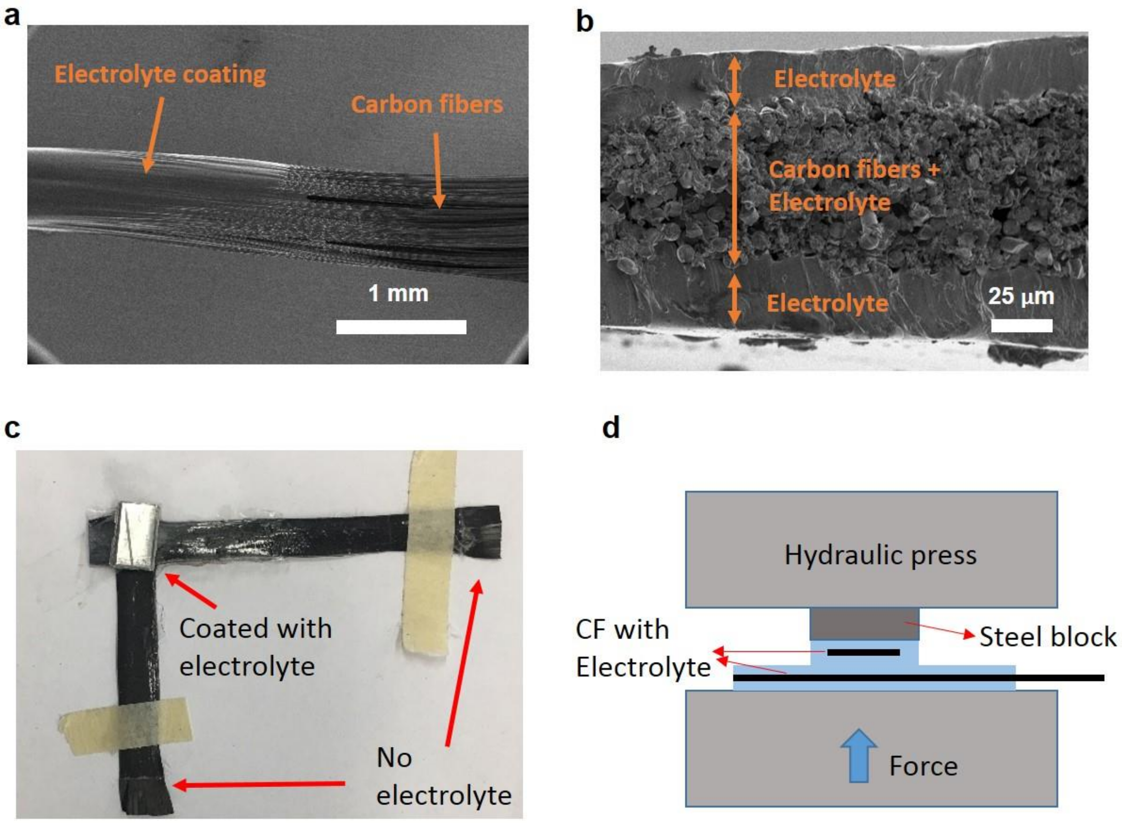

Figure 4-13. SEM images of (a) the top view and (b) the cross-section view of a 3k CF thread coated with solid electrolyte. (c) A photo of the top view of a sample used for compressive strength test. (d) Schematic of the cross-section of the compressive test setup.

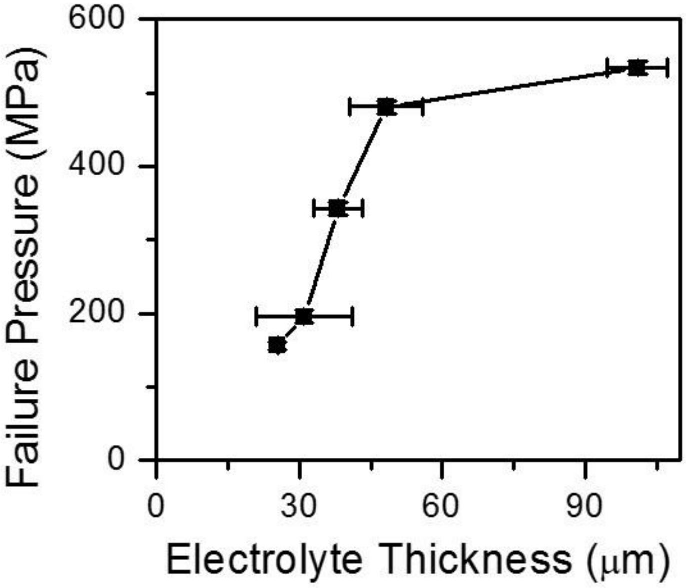

Figure 4-14. Failure pressure of the crossing point in supercapacitor fabrics as a function of electrolyte thickness.

Figure 4-14 plots the failure pressure of the electrolyte layer as a function of thickness. High failure pressures from 156 to 534 MPa are measured for electrolyte thicknesses from 25 to 100 μm, respectively. The increase of electrolyte thickness clearly reduces the probability of short between the crossing electrodes caused by compressive force. However, thick electrolyte layer can increase the ionic resistance and decrease the power performance. Therefore, the balance between high power density and high resistance for compressive strength should be designed based on the specific application.

4.4 Performance of the woven supercapacitor fabrics

As the solid electrolyte-coated CF threads are strong and flexible, they can be woven into supercapacitor fabrics by using a loom or by hand. Figure 4-15 shows photos of the weaving process by using a toy loom, a 3D-printed loom designed for weaving small samples, and by hand. Such process is clearly compatible with large-scale weaving technology. The electrochemical performance and mechanical property of the woven supercapacitor fabrics are examined in this section.

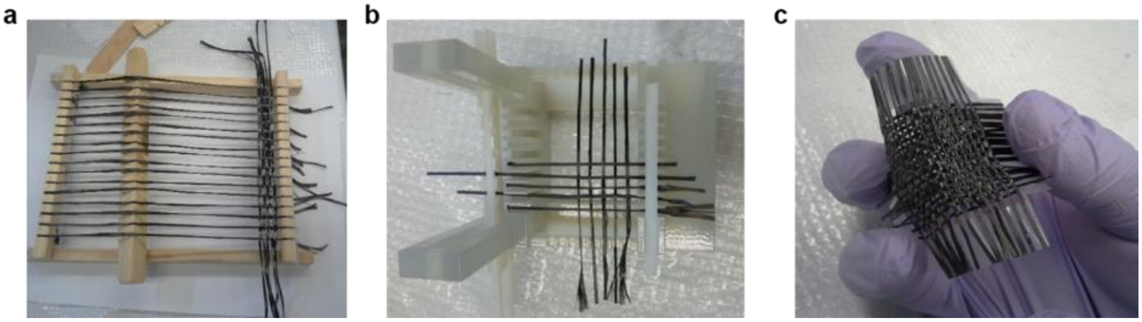

Figure 4-15. Photos showing the weaving of SC fabrics by using (a) a toy loom, (b) a small 3D-printed loom, and (c) a sample woven by hand.

4.4.1 Electrochemical performance of woven supercapacitor fabrics

The activated CF electrodes store energy based on EDL capacitance, which is proportional to the interface area between the electrode surface and the solid electrolyte. Therefore, woven samples with more CFs should provide larger electrode surface and show larger capacitance as a result.

Samples of various sizes are tested with representative results shown in Figure 4-16. Figure 4-16a shows the photo of two 5 × 5 fabrics woven by 3k and 12k threads, respectively. The CV curves of the two samples in Figure 4-16b show that the sample with 4 times of filaments per thread has 4 times of higher capacitance, proving that the capacitance is proportional to the total surface area of the electrodes. Figure 4-16c shows the capacitance as a function of the number of threads used to weave fabrics. The capacitance increases when more threads are used. Such increase is not linear, which can be explained by two reasons. First, the samples are all woven by hand so that the length of each thread and the distance between threads are not well controlled. Second, larger samples using longer thread could have larger resistance from electrode so that the measured capacitance is smaller at the same charge/discharge condition. Samples woven by hand can be easily scaled up with more work time. Figure 4-16d shows the photo of 18 × 18 fabrics with an area of ~100 cm^2.

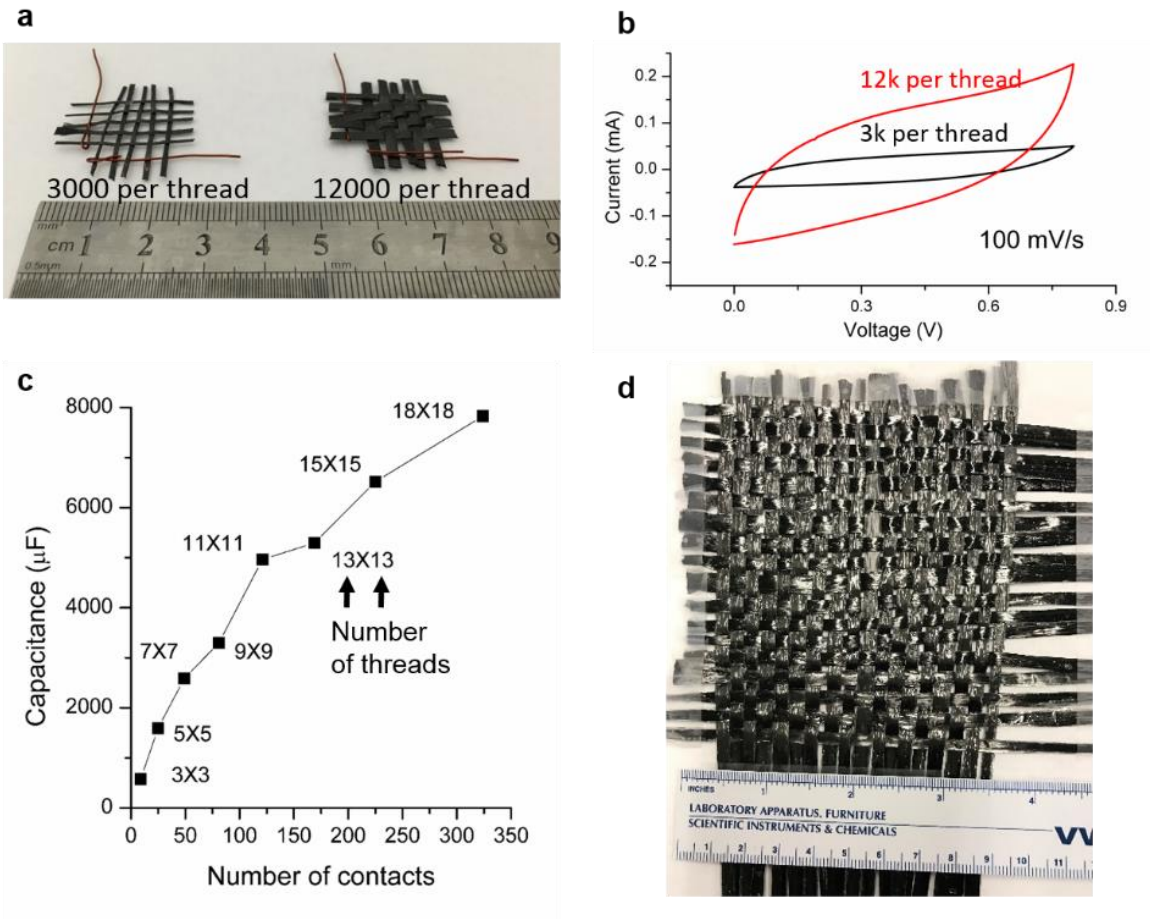

Figure 4-16. (a) A photo of two samples woven by threads of 3000 (3k) filaments and 12000 (12k) filaments, respectively. (b) CV curves of the two samples. (c) The capacitance of SC fabrics as a function of number of contacts (crossing points). All the samples are woven by CF-A0. (d) A photo of a sample woven by 18 × 18 threads with an area of ~100 cm^2.

A handwoven supercapacitor fabric sample using CF-A2 is shown in Figure 4-17a. Cyclic voltammetry (CV) curves of the sample in Figure 4-17b and 4-17c display a quasi-rectangular shape at lower scan rates from 2 mV s^{-1} to 20 mV s^{-1}, with current increasing almost linearly with scan rate, which indicates excellent EDL capacitance behavior. Deviation from a rectangular shape happens at higher scan rates of 50 mV s^{-1} and 100 mV s^{-1} due to low ionic conductivity of the solid electrolyte that limits the speed of charge/discharge.

Galvanostatic charge–discharge (GCD) curves in Figure 4-17d exhibit a nearly triangular shape for various current densities. Slight deviation of charge and discharge curves from straight lines is also caused by relatively slow ion transport. Equivalent series resistance estimated from the IR drop is ~0.81 Ω g, which is mostly contributed from the ionic resistance because the electrical resistance of carbon fiber threads is measured to be less than 0.02 Ω g. Another evidence is that the ionic conductivity of the solid electrolyte is measured to be ~0.081 S m^{-1}, much smaller than the electronic conductivity of the CF electrode (~5.8×10^4 S m^{-1}).

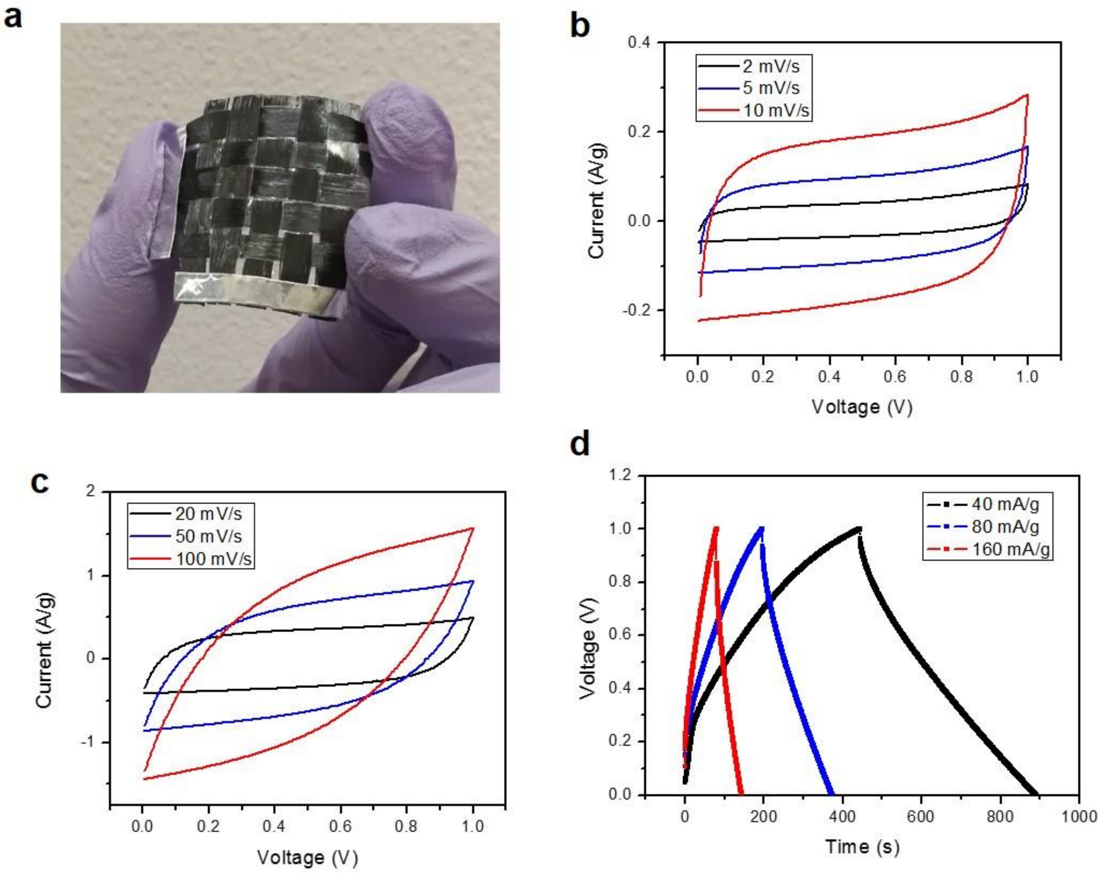

Figure 4-17. (a) A photo of a load bearing supercapacitor fabric with the size of 2.5 cm × 2.5 cm. Cyclic voltammetry (CV) curves of the supercapacitor fabric at (b) lower scan rates and (c) higher scan rates with current normalized to the total weight of all carbon fiber threads (~25 mg). (d) Galvanostatic charge–discharge curves of the device under various current densities (normalized to the total weight of all carbon fiber threads).

Specific capacitances of 18.6 F g^{-1} and 17.8 F g^{-1}, corresponding to energy densities of 2.58 mWh g^{-1} and 2.47 mWh g^{-1}, are calculated from the CV curve at 2 mV s^{-1} and the GCD curve at 40 mA g^{-1}, respectively (normalized to the total weight of the fabric). The energy density as a function of power density is also calculated and plotted in Figure 4-18.

Such energy densities are comparable to those of rigid commercial supercapacitors which are usually 1 to 10 mWh g^{-1} [13], [21]. If the total area of the fabric (2.5 cm × 2.5 cm) and the density of the electrolyte-coated thread electrode (~1.4 g cm^{-3}) are calculated, the SC fabric provides areal capacitance of ~300 mF cm^{-2} and energy density of ~42 μWh cm^{-2}, or volumetric capacitance of ~26 F cm^{-3} and energy density of ~3.6 mWh cm^{-3} (all the metrics are normalized to the total volume/areal of the fabric).

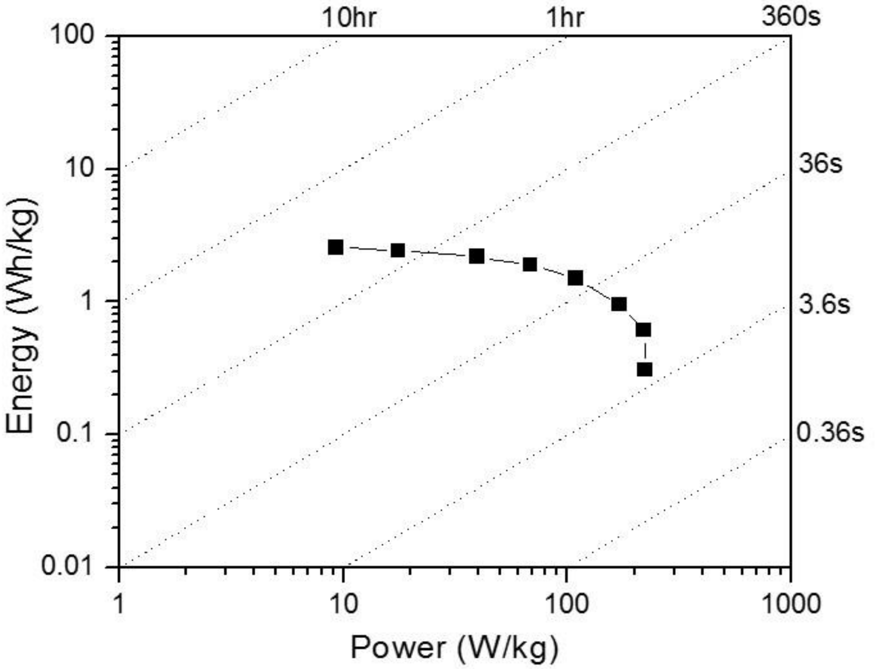

Figure 4-18. Ragone plot of the woven supercapacitor fabric shown in Figure 4-17a..

More information on the impedance of the device is shown in the Nyquist plot in Figure 4-19a. For comparison, the impedance of a fabric device woven by CF-A0 is also plotted in the same graph. Capacitive behavior is dominating at low frequencies for both devices as indicated by the rapid change of the imaginary part. The curve is more inclined at middle frequency range because of the diffusion impedance (Warburg impedance) associated with slow ion diffusion in the solid electrolyte. A semicircle at higher frequency range, which is attributed to the transport processes of both electrons and ions in nanoporous electrodes [134], is presented for the device using CF-A2, but is not seen for the one using CF-A0 with no nanoporous structures.

Electrochemical stability of the sample device is tested and over 80% of the capacitance is retained after 10000 cycling tests at a scan rate of 20 mV s^{-1} (Figure 4-19b). The test is done without any encapsulation, and the drop of capacitance can be resulted from the loss of water in the electrolyte [135].

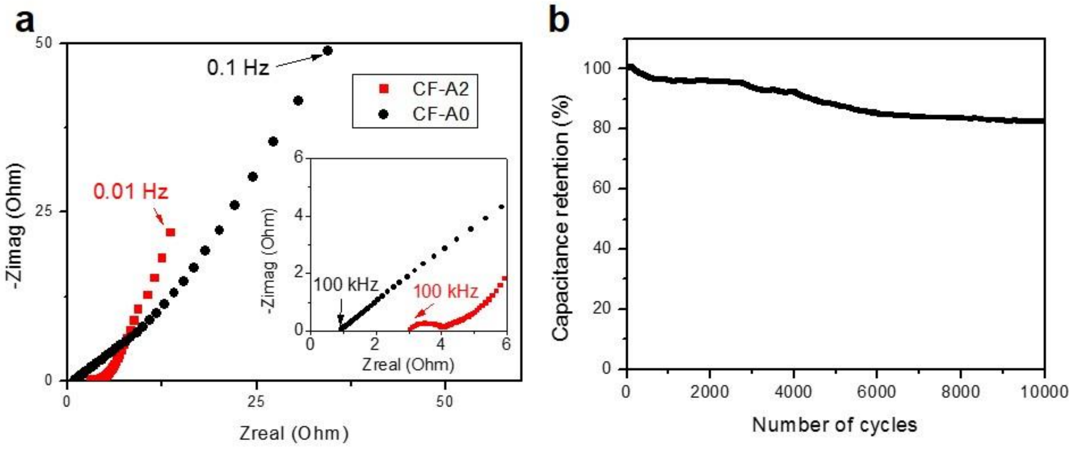

Figure 4-19. (a) Nyquist plots of the impedances of the woven devices using CF-A0 and CF-A2 with the frequency range from 0.01 to 100k Hz. (b) Capacitance retention of the device using CF-A2 during 10,000 charge/discharge cycling tests.

For practical applications, simple treatment can be used to make such SC fabrics waterproof without losing performance. For example, a very thin and conformal coating of parylene (~800 nm) through chemical vapor deposition can serve as a protection layer, and the sample device retains its energy storage property after dipped in water for 1 hour (Figure 4-20).

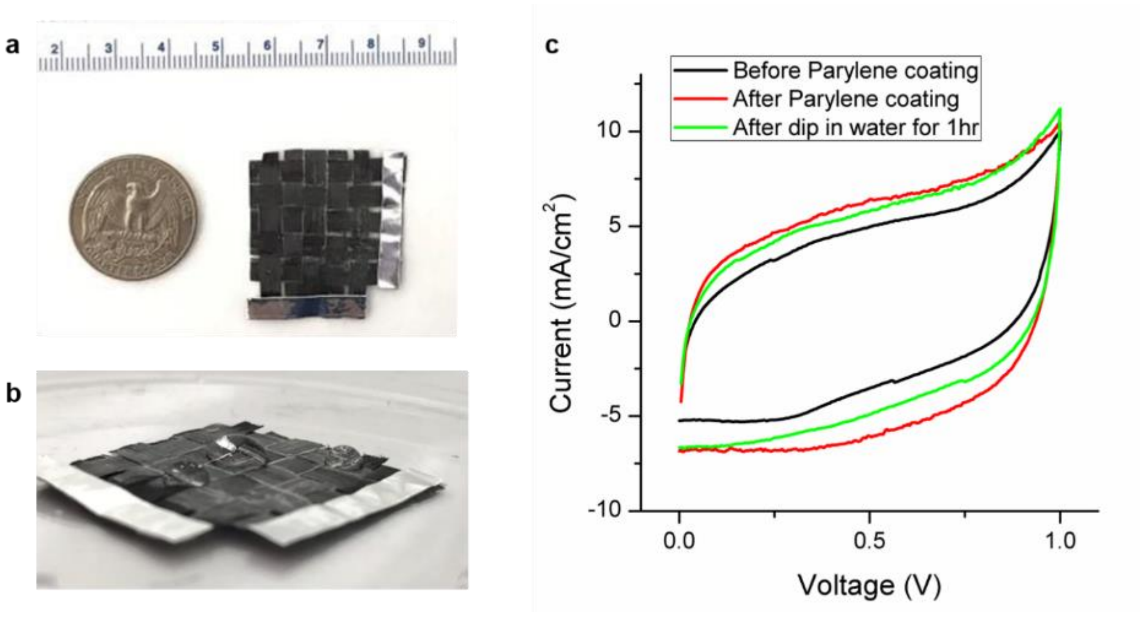

Figure 4-20. (a), (b): Photos of a waterproof SC fabric coated with an 800 nm-thick Parylene layer. (c) CV curves of the sample before and after the Parylene coating process, and after dipping into water for 1 hour, at a scan rate of 20 mV/s.

4.4.2 Tensile and compressive strength of the device

Wearable devices are constantly under tensile and compressive forces in practical uses such that most flexible energy storage devices require support and protection with substrates and packages, which occupy a large portion of the overall volume/weight. Furthermore, their electrochemical performances under high tensile and compressive loads, however, are seldom reported. In this work, the electrodes and electrolyte alone can serve as the load-bearing substrate without extra package. Figure 4-21a shows the CV curves of a SC fabric when it is stretched at a high tensile stress of 1000 MPa with almost no change in electrochemical performance. The tensile stress of 1000 MPa, however, will break most of the wearable fibers [133] and functional fibers with energy storage properties made of CNT, Graphene, etc. [80], [89], [92]. Furthermore, the tensile strength of the woven supercapacitor fabrics qualifies the most stringent requirements in the automobile industry as the “GigaPascal steel” for Advanced High-Strength Steels (AHSS) with tensile strength of at least 1000 MPa [136]. The SC fabric also shows unchanged performance under a high pressure of 100 MPa (Figure 4-21b). For example, a man of ~70 kg standing on an area of ~7 cm^2 would generate a pressure of ~1 MPa and a failure pressure over 100 MPa would have a high built-in safety factor of 100.

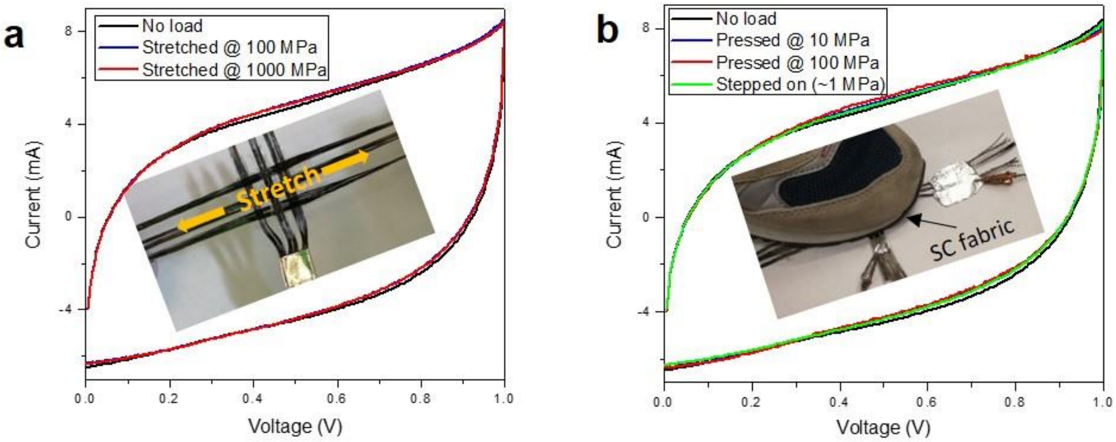

Figure 4-21. (a) CV curves of a supercapacitor fabric (as shown in the inset photo) when stretched at different stresses at the scan rate of 20 mV s^{-1}. (b) CV curves of the sample when pressed with different pressures at the scan rate of 20 mV s^{-1}. The inset photo shows how it is tested when the sample is stepped on.

4.4.3 Configuration design of high-voltage device

In addition to high mechanical strength and stability, a variety of form-factor designs can be constructed for such woven supercapacitor fabrics. While a single supercapacitor cell usually has limited voltage range, multiple cells need to be connected in series to provide higher voltage for practical applications. Figure 4-22a and b show schematics of how to fabricate 4 supercapacitor cells connected in series in a single piece of fabric. The CF threads are partially coated with electrolyte. The uncoated parts are used as electrical connection between cells. Such design connects 4 cells, each work within 1V, and can work up to 4V. Figure 4-22c shows the photo of the 4-cell-connect-in-series fabric lighting up a 2V LED. Moreover, the size of threads may not necessarily be the same in different directions. For example, a strap consisting of 4 cells connected in series can be designed as shown in Figure 4-22d.

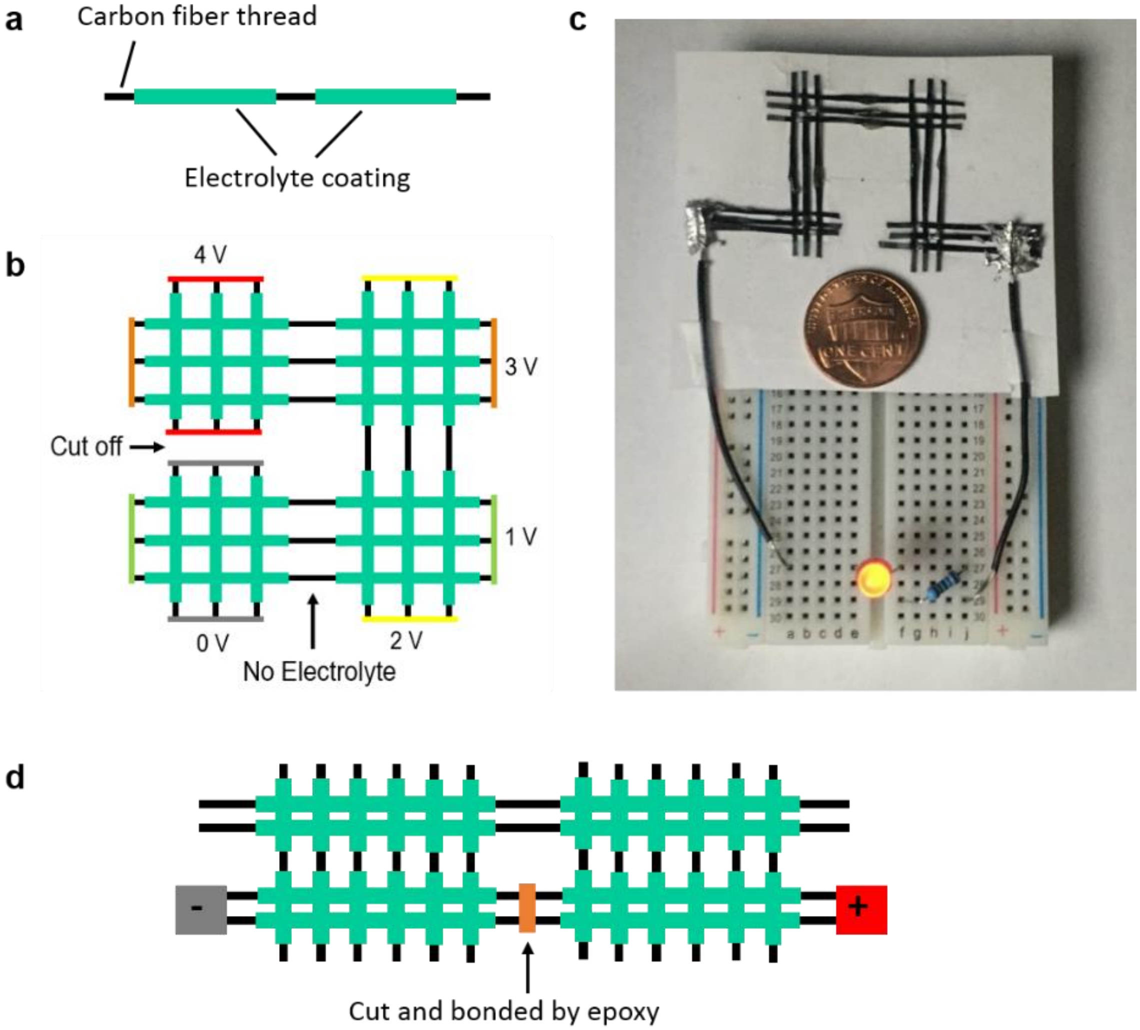

Figure 4-22. Schematics of (a) a carbon fiber thread that is partially coated with electrolyte; (b) a 4-cell-connect-in-series fabric woven by CF threads. (c) A photo showing an LED powered by a 4-cell-connect-in-series fabric. (d) Schematic showing the design of a SC strap with 4 cells connected in series.

Based on the design in Figure 4-22d, a SC strap with high flexibility is woven as shown in Figure 4-23a. The strap can be charged to 4V as indicated by the galvanostatic charge–discharge curve in Figure 4-23b. The electrochemical performance is also tested when the strap was bent at different states, including coiled on a pen or a plastic bottle without showing significant changes under various bending radii (Figure 4-23c). A possible application of such SC straps is a power watchstrap (Figure 4-23d). The capacitance retention of the SC strap is tested for 1000 put-on/take-off cycles on a human wrist, corresponding to a bending radius of ~2.5 cm without losing its performances in Figure 4-23d.

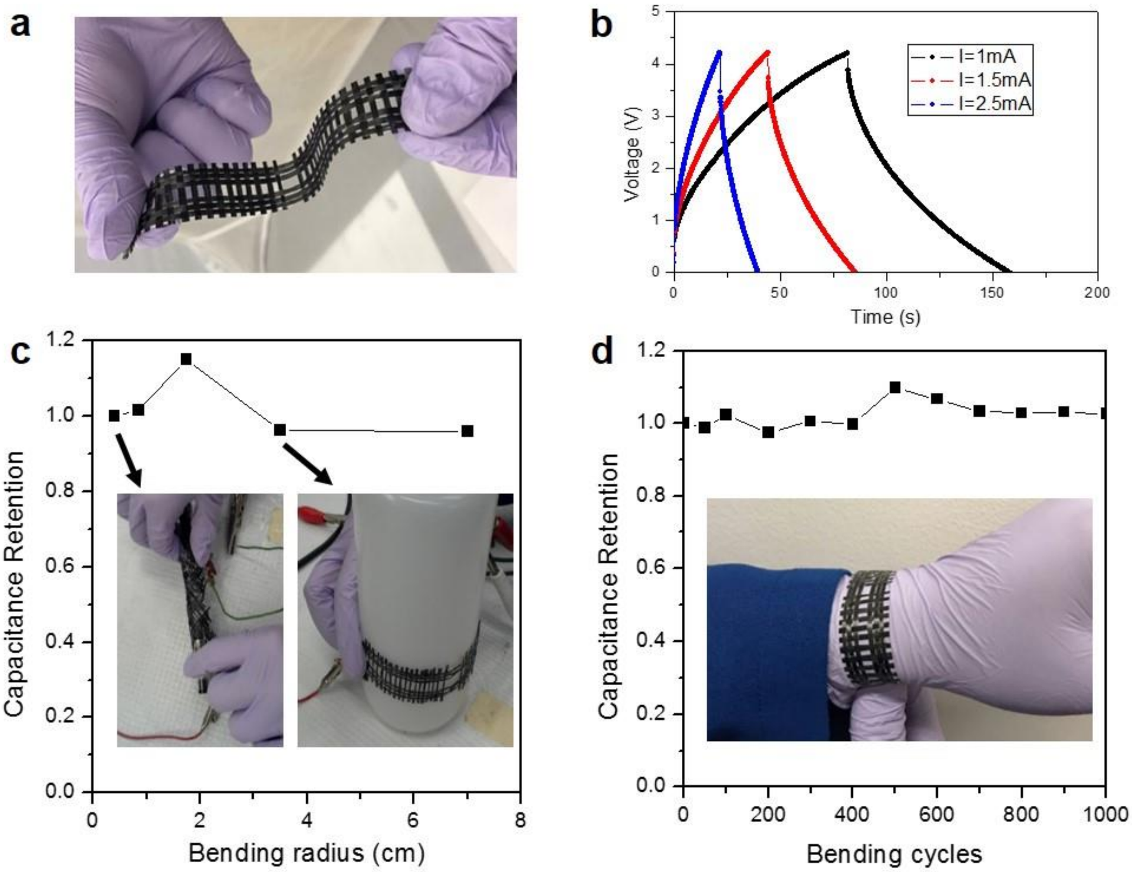

Figure 4-23. (a) A photo of a load bearing supercapacitor strap with the 4-cell connect-in-series design. (b) Galvanostatic charge–discharge tests of the strap working at 4 V. (c) Capacitance retention of the strap under different bending radii. (d) Capacitance retention of the strap during 1000 bending cycles around a human wrist.

4.5 Summary

In summary, this chapter demonstrates flexible woven SC fabrics with both high energy density and load-bearing properties by using multifunctional nanoporous CF threads that work as mechanical support, current collector, and capacitive material simultaneously. The thread electrodes are prepared by KOH activation of commercial carbon fibers with three orders of magnitude increase in the specific surface area and 86% retention of tensile strength. Combined with the directly woven electrode configurations, the SC fabrics feature scalable fabrication, arbitrary form-factor designs, excellent flexibility, and good mechanical stability. As a result, the woven SC fabrics are promising flexible power sources for wearable electronics.

Future research on woven SC fabrics can be continued in the following directions to further improve the performance and facilitate their practical application:

First, the electrochemical performance including energy and power densities can be improved. To improve energy density: (a) new approaches to uniformly deposit functional nanomaterials on CF threads can further increase the capacitance of the electrodes; (b) the use of non-aqueous electrolyte system can enlarge the working voltage range of the SC. The combination of both can result in much higher energy density. To improve power density: (a) thinner thread and electrolyte coating can be used to reduce the ion transport path; (b) the design of solid electrolyte with higher ionic conductivity can reduce the overall ionic resistance. The reduction in ionic resistance will result in higher power density.

Second, the mechanical property should be adjustable based on specific applications. For most of the wearable applications, lower stiffness of threads is preferred. The using of softer solid electrolyte and thinner thread electrode can lower the overall stiffness of the woven SC fabrics. The balance between strength and stiffness should be found, and the process to control the CF thread thickness need to be developed.

Third, biocompatible, mechanically stable, and waterproof protection coating for the fabrics should be developed, which will eventually make the woven fabrics practical and commercializeable.

5 Conclusions and future directions

5.1 Conclusions

Three types of flexible supercapacitors (FSCs) based on micro/nanofibers with various features and target applications have been successfully demonstrated in this report.

Micro FSCs prepared using direct-write nanofibers for the potential integration with flexible microelectronics is demonstrated in Chapter 2. A new solution of conducting polymer compatible with the near-field electrospinning, which is also a direct-write approach, is developed. The micro FSCs are highly flexible with excellent electrochemical performance and cycling stability. The approach is simple, versatile, and compatible with different substrates for the direct integration of energy storage devices in flexible microsystems.

An ultra-thin micro coaxial fiber supercapacitor (μCFSC) with high energy and power densities, as well as excellent mechanical properties is proven to be promising building blocks for future wearable energy storage fabrics in Chapter 3. The successive coating of functional layers onto a single micro carbon fiber via a scalable process is developed. A simplified electrochemical model for the 1D CFSC structure is proposed and supported by the experimental data. Both simulation and experimental results have verified the improved energy and power densities for fiber-shaped FSC through rational design.

Free-standing woven supercapacitor fabrics that store high energy and sustain large mechanical loads for flexible and wearable power sources are proposed and demonstrated in Chapter 4. A novel device configuration woven by solid electrolyte-coated threads is proposed and experimentally proven to be compatible with weaving technology, highly flexible, and mechanically stable. The activation of CF threads to make highly porous and mechanically strong electrodes for capacitive energy storage is studied. The results show that the combination of novel configuration and optimized electrode materials demonstrates high performance energy storage fabrics readily available for large-scale wearable applications.

5.2 Future directions

Possible future directions following each chapter of the dissertation are discussed as follows.

5.2.1 Direct integration of micro supercapacitor with printed electronics

To directly integrate micro FSC with printed electronics for practical applications, advancements in two directions are suggested.

The first direction is to improve the performance and processability of the functional materials. Doping of PPy and other conducting polymers should be studied to improve the conductivity and solubility. This can be achieved by synthesis of designed dopants and control of the polymerization process. The composition of the final ink for near-field electrospinning should also be optimized. Systematic experiments combined with theoretical analysis can be conducted to better understand how to adjust the viscosity and surface tension of the composite ink.

The second direction is to develop direct-write tools and control system that are compatible with printed electronics process. Current inkjet printing technology squeezes out inkjets using micro actuators so that the amount of ink and the position of printed material can be well controlled. The precise writing of nanofibers can also be achieved by controlling the ink flow rate, the electric field applied to the ink, and the position of the ink outlet.

In addition to on-chip energy storage, the development of practical printed conductive nanofibers can be used as other functional components for flexible electrode, such as micro sensors and transparent electrodes, which are other possible future directions to pursuit.

5.2.2 Direct integration of ultrathin coaxial fiber supercapacitors into textiles

A few fundamental problems need to be solved for the practical application of the ultrathin CFSCs, which are all interesting future research directions.

The first problem is how to guarantee the conformal coating of each layer on the micro fiber in a batch fabrication process. The study of the interface between layers can help solve the problem. Chemical treatment before each coating and composition design of the coating solutions to improve the affinity between layers can be studied.

The second problem is how and make precise electrical connections to all fibers during the assembly large number of CFSCs. The development of new outer electrode layer and co-weaving of CFSC with other conductive fibers/wires may offer potential solutions.

The third problem is how to maintain functionality of the CFSC when many of them are assembled and rubbed against each other, which could scratch the outer electrode and electrolyte layers. Stronger outer electrode with smooth surface can be developed, and a protection layer over the outer electrode may be applied.

The study of coaxial functional coatings on micro fibers is not only significant for the practical applications of CFSCs, but also provides technical solutions to multifunctional components in future smart textiles.

5.2.3 Development of multifunctional structural supercapacitor fabrics

As the woven supercapacitor fabrics store energy and bear mechanical load at the same time, the multifunctional device is promising for a wide range of applications. For almost all mobile electrical systems, including cell phones, wearable electronics, electric vehicles, drones, satellites, etc., most of the weight/volume is used for energy storage (batteries) and mechanical structure as support/protection. The combination of the two functions can either provide more stored energy without increasing the overall weight/volume, or reduce the total weight/volume without sacrificing the stored energy of the systems.

While future flexible electronics require more flexible power sources, current electric systems need more rigid structural energy storage. The supercapacitor fabrics are potentially applicable for both applications as long as their stiffness can be better controlled. Future study of the electrolyte materials and the mechanical and electrochemical interaction between the electrolyte and electrode needs to be conducted to develop practical structural supercapacitors for a variety of applications.

References

[1] M. Armand and J.-M. Tarascon, "Building better batteries," *Nature*, vol. 451, no. 7179, pp. 652–657, Feb. 2008.

[2] Q. Huang, D. Wang, and Z. Zheng, "Textile-Based Electrochemical Energy Storage Devices," *Advanced Energy Materials*, vol. 6, no. 22. pp. 1–28, 2016.

[3] X. Wang, X. Lu, B. Liu, D. Chen, Y. Tong, and G. Shen, "Flexible energy-storage devices: Design consideration and recent progress," *Adv. Mater.*, vol. 26, no. 28, pp. 4763–4782, 2014.

[4] L. Li, Z. Wu, S. Yuan, and X.-B. Zhang, "Advances and challenges for flexible energy storage and conversion devices and systems," *Energy Environ. Sci.*, vol. 7, no. 7, p. 2101, 2014.

[5] S. J. Roundy, P. K. Wright, and J. M. Rabaey, *Energy Scavenging for Wireless Sensor Networks*, vol. 49. Boston, MA: Springer US, 2004.

[6] J. A. Paradiso and T. Starner, "Energy scavenging for mobile and wireless electronics," *IEEE Pervasive Comput.*, vol. 4, no. 1, pp. 18–27, 2005.

[7] Z. L. Wang, "Towards self-powered nanosystems: From nanogenerators to nanopiezotronics," *Adv. Funct. Mater.*, vol. 18, no. 22, pp. 3553–3567, 2008.

[8] Z. L. Wang and W. Wu, "Nanotechnology-enabled energy harvesting for self-powered micro-/nanosystems," *Angew. Chemie - Int. Ed.*, vol. 51, no. 47, pp. 11700–11721, 2012.

[9] S. R. Anton and H. a Sodano, "A review of power harvesting using piezoelectric materials," *Smart Mater. Struct.*, vol. 16, no. 3, pp. R1–R21, 2007.

[10] A. Toprak and O. Tigli, "Piezoelectric energy harvesting: State-of-the-art and challenges," *Appl. Phys. Rev.*, vol. 1, no. 3, p. 031104, 2014.

[11] "No Title." [Online]. Available: https://www.apple.com/airpods/.

[12] B. E. Conway, *Electrochemical Supercapacitors*. Boston, MA: Springer US, 1999.

[13] P. Simon and Y. Gogotsi, "Materials for electrochemical capacitors," *Nat. Mater.*, vol. 7, no. 11, pp. 845–854, Nov. 2008.

[14] J. R. Miller and P. Simon, "MATERIALS SCIENCE: Electrochemical Capacitors for Energy Management," *Science (80-.).*, vol. 321, no. 5889, pp. 651–652, Aug. 2008.

[15] X. Lu, M. Yu, G. Wang, Y. Tong, and Y. Li, "Flexible solid-state supercapacitors: design, fabrication and applications," *Energy Environ. Sci.*, vol. 7, no. 7, p. 2160, 2014.

[16] P. Yang and W. Mai, "Flexible solid-state electrochemical supercapacitors," *Nano Energy*, vol. 8, pp. 274–290, 2014.

[17] C. Wang and G. G. Wallace, "Flexible Electrodes and Electrolytes for Energy Storage," *Electrochimica Acta*, vol. 175. Elsevier Ltd, pp. 87–95, 2015.

[18] K. Jost, G. Dion, and Y. Gogotsi, "Textile energy storage in perspective," *J. Mater. Chem. A*, vol. 2, no. 28, p. 10776, 2014.

[19] C. Shen, S. Xu, Y. Xie, M. Sanghadasa, X. Wang, and L. Lin, “A Review of On-Chip Micro Supercapacitors for Integrated Self-Powering Systems,” *J. Microelectromechanical Syst.*, vol. 26, no. 5, 2017.

[20] Y. Zhu, S. Murali, M. D. Stoller, K. J. Ganesh, W. Cai, P. J. Ferreira, A. Pirkle, R. M. Wallace, K. A. Cychosz, M. Thommes, D. Su, E. A. Stach, and R. S. Ruoff, “Carbon-Based Supercapacitors Produced by Activation of Graphene,” *Science (80-.).*, vol. 332, no. 6037, pp. 1537–1541, Jun. 2011.

[21] Y. Gogotsi and P. Simon, “True Performance Metrics in Electrochemical Energy Storage,” *Science (80-.).*, vol. 334, no. 6058, pp. 917–918, Nov. 2011.

[22] N. A. Kyeremateng, T. Brousse, and D. Pech, “Microsupercapacitors as miniaturized energy-storage components for on-chip electronics,” *Nat. Nanotechnol.*, vol. 12, no. 1, pp. 7–15, Nov. 2016.

[23] C. Peng, S. Zhang, D. Jewell, and G. Z. Chen, “Carbon nanotube and conducting polymer composites for supercapacitors,” *Prog. Nat. Sci.*, vol. 18, no. 7, pp. 777–788, 2008.

[24] A. Lewandowski, P. Jakobczyk, M. Galinski, and M. Biegun, “Self-discharge of electrochemical double layer capacitors,” *Phys. Chem. Chem. Phys.*, vol. 15, no. 22, p. 8692, Dec. 2013.

[25] J. Kowal, E. Avaroglu, F. Chamekh, A. Šenfelds, T. Thien, D. Wijaya, and D. U. Sauer, “Detailed analysis of the self-discharge of supercapacitors,” *J. Power Sources*, vol. 196, no. 1, pp. 573–579, 2011.

[26] R. Faranda, “A new parameters identification procedure for simplified double layer capacitor two-branch model,” *Electr. Power Syst. Res.*, vol. 80, no. 4, pp. 363–371, 2010.

[27] V. Sedlakova, J. Sikula, J. Majzner, P. Sedlak, T. Kuparowitz, B. Buergler, and P. Vasina, “Supercapacitor equivalent electrical circuit model based on charges redistribution by diffusion,” *J. Power Sources*, vol. 286, pp. 58–65, 2015.

[28] S. Fletcher, V. J. Black, and I. Kirkpatrick, “A universal equivalent circuit for carbon-based supercapacitors,” *J. Solid State Electrochem.*, vol. 18, no. 5, pp. 1377–1387, 2014.

[29] X. Lang, A. Hirata, T. Fujita, and M. Chen, “Nanoporous metal/oxide hybrid electrodes for electrochemical supercapacitors.,” *Nat. Nanotechnol.*, vol. 6, no. 4, pp. 232–236, 2011.

[30] A. Balducci, “Electrolytes for high voltage electrochemical double layer capacitors: A perspective article,” *J. Power Sources*, vol. 326, pp. 534–540, 2016.

[31] J. Chmiola, C. Largeot, P.-L. Taberna, P. Simon, and Y. Gogotsi, “Monolithic carbide-derived carbon films for micro-supercapacitors.,” *Science*, vol. 328, no. 5977, pp. 480–3, Apr. 2010.

[32] M. Toupin, T. Brousse, and D. Bélanger, “Charge Storage Mechanism of MnO 2 Electrode Used in Aqueous Electrochemical Capacitor,” *Chem. Mater.*, vol. 16, no. 16, pp. 3184–3190, Aug. 2004.

[33] C. Shen, C.-P. Wang, M. Sanghadasa, and L. Lin, “Flexible micro-supercapacitors prepared using direct-write nanofibers,” *RSC Adv.*, vol. 7, no. 19, pp. 11724–11731, 2017.

[34] C. Shen, Y. Xie, M. Sanghadasa, Y. Tang, L. Lu, and L. Lin, “Ultrathin Coaxial Fiber Supercapacitors Achieving High Energy and Power Densities,” *ACS Appl. Mater.*

Interfaces, vol. 9, no. 45, 2017.

[35] D. Yu, Q. Qian, L. Wei, W. Jiang, K. Goh, J. Wei, J. Zhang, and Y. Chen, “Emergence of fiber supercapacitors.,” *Chem. Soc. Rev.*, vol. 44, no. 3, pp. 647–62, 2015.

[36] T. Lv, Y. Yao, N. Li, and T. Chen, “Wearable fiber-shaped energy conversion and storage devices based on aligned carbon nanotubes,” *Nano Today*, vol. 11, no. 5, pp. 644–660, 2016.

[37] C. Shen, C.-P. Wang, M. Sanghadasa, and L. Lin, “Flexible micro-supercapacitors prepared using direct-write nanofibers,” *RSC Adv.*, vol. 7, no. 19, 2017.

[38] C. Shen, G. Luo, A. Kozinda, M. Sanghadasa, and L. Lin, “Solid-state flexible micro supercapacitors by direct-write porous nanofibers,” in *2015 28th IEEE International Conference on Micro Electro Mechanical Systems (MEMS)*, 2015, pp. 1133–1136.

[39] Y. Xie, C. Shen, M. Sanghadasa, Y. Tang, and L. Lin, “A coaxial carbon fiber micro supercapacitor,” in *Proceedings of the IEEE International Conference on Micro Electro Mechanical Systems (MEMS)*, 2016, vol. 2016–Febru.

[40] C. Shen, Y. Xie, B. Zhu, M. Sanghadasa, Y. Tang, and L. Lin, “Wearable woven supercapacitor fabrics with high energy density and load-bearing capability,” *Sci. Rep.*, vol. 7, no. 1, p. 14324, Dec. 2017.

[41] J. Maeng, C. Meng, and P. P. Irazoqui, “Wafer-scale integrated micro-supercapacitors on an ultrathin and highly flexible biomedical platform,” *Biomed. Microdevices*, vol. 17, no. 1, 2015.

[42] Y. Jiang and L. Lin, “A two-stage, self-aligned vertical densification process for as-grown CNT forests in supercapacitor applications,” *Sensors Actuators, A Phys.*, vol. 188, pp. 261–267, 2012.

[43] Y. Jiang, P. Wang, X. Zang, Y. Yang, A. Kozinda, and L. Lin, “Uniformly embedded metal oxide nanoparticles in vertically aligned carbon nanotube forests as pseudocapacitor electrodes for enhanced energy storage,” *Nano Lett.*, vol. 13, no. 8, pp. 3524–3530, 2013.

[44] C.-C. C. Liu, D.-S. S. Tsai, W.-H. H. Chung, K.-W. W. Li, K.-Y. Y. Lee, and Y.-S. S. Huang, “Electrochemical micro-capacitors of patterned electrodes loaded with manganese oxide and carbon nanotubes,” *J. Power Sources*, vol. 196, no. 13, pp. 5761–5768, Jul. 2011.

[45] R. Warren, F. Sammoura, F. Tounsi, M. Sanghadasa, and L. Lin, “Highly active ruthenium oxide coating via ALD and electrochemical activation in supercapacitor applications,” *J. Mater. Chem. A*, vol. 3, no. 30, pp. 15568–15575, 2015.

[46] R. Warren, F. Sammoura, K. S. Teh, A. Kozinda, X. Zang, and L. Lin, “Electrochemically synthesized and vertically aligned carbon nanotube-polypyrrole nanolayers for high energy storage devices,” *Sensors Actuators, A Phys.*, vol. 231, pp. 65–73, 2014.

[47] P. Huang, M. Heon, D. Pech, M. Brunet, P.-L. L. Taberna, Y. Gogotsi, S. Lofland, J. D. Hettinger, and P. Simon, “Micro-supercapacitors from carbide derived carbon (CDC) films on silicon chips,” *J. Power Sources*, vol. 225, pp. 240–244, Mar. 2013.

[48] P. Huang, C. Lethien, S. Pinaud, K. Brousse, R. Laloo, V. Turq, M. Respaud, A. Demortiere, B. Daffos, P. L. Taberna, B. Chaudret, Y. Gogotsi, and P. Simon, “On-chip and freestanding elastic carbon films for micro-supercapacitors,” *Science (80-.).*, vol. 351,

no. 6274, pp. 691–695, Feb. 2016.

[49] D. Gaboriau, D. Aradilla, M. Brachet, J. Le Bideau, T. Brousse, G. Bidan, P. Gentile, and S. Sadki, "Silicon nanowires and nanotrees: elaboration and optimization of new 3D architectures for high performance on-chip supercapacitors," *RSC Adv.*, vol. 6, no. 84, pp. 81017–81027, 2016.

[50] J. P. Alper, M. Vincent, C. Carraro, and R. Maboudian, "Silicon carbide coated silicon nanowires as robust electrode material for aqueous micro-supercapacitor," *Appl. Phys. Lett.*, vol. 100, no. 16, p. 163901, 2012.

[51] L. Gu, Y. Wang, R. Lu, W. Wang, X. Peng, and J. Sha, "Silicon carbide nanowires@Ni(OH)2 core-shell structures on carbon fabric for supercapacitor electrodes with excellent rate capability," *J. Power Sources*, vol. 273, pp. 479–485, 2015.

[52] J. P. Alper, M. S. Kim, M. Vincent, B. Hsia, V. Radmilovic, C. Carraro, and R. Maboudian, "Silicon carbide nanowires as highly robust electrodes for micro-supercapacitors," *J. Power Sources*, vol. 230, pp. 298–302, May 2013.

[53] M. Beidaghi, W. Chen, and C. Wang, "Electrochemically activated carbon micro-electrode arrays for electrochemical micro-capacitors," *J. Power Sources*, vol. 196, no. 4, pp. 2403–2409, Feb. 2011.

[54] C. Shen, X. Wang, W. Zhang, and F. Kang, "Direct prototyping of patterned nanoporous carbon: A route from materials to on-chip devices," *Sci. Rep.*, vol. 3, 2013.

[55] D. Pech, M. Brunet, H. Durou, P. Huang, V. Mochalin, Y. Gogotsi, P. Taberna, and P. Simon, "Ultrahigh-power micrometre-sized supercapacitors based on onion-like carbon.," *Nat. Nanotechnol.*, vol. 5, no. 9, pp. 651–4, Sep. 2010.

[56] W. Si, C. Yan, Y. Chen, S. Oswald, L. Han, and O. G. Schmidt, "On chip, all solid-state and flexible micro-supercapacitors with high performance based on MnOx/Au multilayers," *Energy Environ. Sci.*, vol. 6, no. 11, p. 3218, 2013.

[57] K. Wang, W. Zou, B. Quan, A. Yu, H. Wu, P. Jiang, and Z. Wei, "An all-solid-state flexible micro-supercapacitor on a chip," *Adv. Energy Mater.*, vol. 1, no. 6, pp. 1068–1072, Nov. 2011.

[58] X. Wang, B. D. Myers, J. Yan, G. Shekhawat, V. Dravid, and P. S. Lee, "Manganese oxide micro-supercapacitors with ultra-high areal capacitance.," *Nanoscale*, vol. 5, no. 10, pp. 4119–22, May 2013.

[59] N. Kurra, M. K. Hota, and H. N. Alshareef, "Conducting polymer micro-supercapacitors for flexible energy storage and Ac line-filtering," *Nano Energy*, vol. 13, pp. 500–508, 2015.

[60] D. Pech, M. Brunet, P.-L. L. Taberna, P. Simon, N. Fabre, F. Mesnilgrente, V. Conédéra, and H. Durou, "Elaboration of a microstructured inkjet-printed carbon electrochemical capacitor," *J. Power Sources*, vol. 195, no. 4, pp. 1266–1269, Feb. 2010.

[61] W. Gao, N. Singh, L. Song, Z. Liu, A. L. M. Reddy, L. Ci, R. Vajtai, Q. Zhang, B. Wei, and P. M. Ajayan, "Direct laser writing of micro-supercapacitors on hydrated graphite oxide films.," *Nat. Nanotechnol.*, vol. 6, no. 8, pp. 496–500, Aug. 2011.

[62] M. F. El-Kady, V. Strong, S. Dubin, and R. B. Kaner, "Laser Scribing of High-Performance and Flexible Graphene-Based Electrochemical Capacitors," *Science (80-.).*,

vol. 335, no. 6074, pp. 1326–1330, Mar. 2012.

[63] R. Kumar, R. Savu, E. Joanni, a R. Vaz, M. a Canesqui, R. K. Singh, R. A. Timm, L. T. Kubota, and S. a Moshkalev, “Fabrication of interdigitated micro-supercapacitor devices by direct laser writing onto ultra-thin, flexible and free-standing graphite oxide,” *RSC Adv.*, vol. 6, pp. 84769–84776, 2016.

[64] G. a. Snook, P. Kao, and A. S. Best, “Conducting-polymer-based supercapacitor devices and electrodes,” *J. Power Sources*, vol. 196, no. 1, pp. 1–12, Jan. 2011.

[65] C.-L. Zhang and S.-H. Yu, “Nanoparticles meet electrospinning: recent advances and future prospects.,” *Chem. Soc. Rev.*, vol. 43, no. 13, pp. 4423–48, 2014.

[66] D. Sun, C. Chang, S. Li, and L. Lin, “Near-field electrospinning,” *Nano Lett.*, vol. 6, no. 4, pp. 839–842, 2006.

[67] D. Li and Y. Xia, “Electrospinning of Nanofibers: Reinventing the Wheel?,” *Adv. Mater.*, vol. 16, no. 14, pp. 1151–1170, Jul. 2004.

[68] C. Chang, V. H. Tran, J. Wang, Y. K. Fuh, and L. Lin, “Direct-write piezoelectric polymeric nanogenerator with high energy conversion efficiency,” *Nano Lett.*, vol. 10, no. 2, pp. 726–731, 2010.

[69] E. J. Oh, K. S. Jang, and A. G. MacDiarmid, “High molecular weight soluble polypyrrole,” *Synth. Met.*, vol. 125, no. 3, pp. 267–272, 2002.

[70] C. Shen, C.-P. Wang, M. Sanghadasa, and L. Lin, “Direct-write polymeric strain sensors with arbitary contours on flexible substrates,” in *Proceedings of the IEEE International Conference on Micro Electro Mechanical Systems (MEMS)*, 2016, vol. 2016–Febru.

[71] S. Machida, S. Miyata, and A. Techagumpuch, “Chemical synthesis of highly electrically conductive polypyrrole,” *Synth. Met.*, vol. 31, no. 3, pp. 311–318, Sep. 1989.

[72] C. Shen, X. Wang, W. Zhang, and F. Kang, “A high-performance three-dimensional micro supercapacitor based on self-supporting composite materials,” *J. Power Sources*, vol. 196, no. 23, pp. 10465–10471, Dec. 2011.

[73] D. Pech, M. Brunet, T. M. Dinh, K. Armstrong, J. Gaudet, and D. Guay, “Influence of the configuration in planar interdigitated electrochemical micro-capacitors,” *J. Power Sources*, vol. 230, pp. 230–235, May 2013.

[74] M. Beidaghi, Y. Gogotsi, and Y. G. Majid Beidaghi, “Capacitive energy storage in micro-scale devices: recent advances in design and fabrication of micro- supercapacitors,” *Energy Environ. Sci.*, vol. 7, pp. 867–884, 2014.

[75] Y. Q. Jiang, Q. Zhou, and L. Lin, “Planar MEMS Supercapacitor using Carbon Nanotube Forests,” *2009 IEEE 22nd Int. Conf. Micro Electro Mech. Syst.*, pp. 587–590, Jan. 2009.

[76] M. F. El-Kady and R. B. Kaner, “Scalable fabrication of high-power graphene micro-supercapacitors for flexible and on-chip energy storage,” *Nat. Commun.*, vol. 4, p. 1475, Feb. 2013.

[77] W. Zeng, L. Shu, Q. Li, S. Chen, F. Wang, and X.-M. Tao, “Fiber-Based Wearable Electronics: A Review of Materials, Fabrication, Devices, and Applications,” *Adv. Mater.*, vol. 26, no. 31, pp. 5310–5336, 2014.

[78] F. R. Fan, W. Tang, and Z. L. Wang, “Flexible Nanogenerators for Energy Harvesting and

Self-Powered Electronics," *Adv. Mater.*, vol. 28, no. 22, pp. 4283–4305, 2016.

[79] Y. Qin, X. Wang, and Z. L. Wang, "Microfibre-nanowire hybrid structure for energy scavenging," *Nature*, vol. 451, no. 7180, pp. 809–13, 2008.

[80] L. Kou, T. Huang, B. Zheng, Y. Han, X. Zhao, K. Gopalsamy, H. Sun, and C. Gao, "Coaxial wet-spun yarn supercapacitors for high-energy density and safe wearable electronics.," *Nat. Commun.*, vol. 5, no. May, p. 3754, 2014.

[81] G. Qu, J. Cheng, X. Li, D. Yuan, P. Chen, X. Chen, B. Wang, and H. Peng, "A Fiber Supercapacitor with High Energy Density Based on Hollow Graphene/Conducting Polymer Fiber Electrode," *Adv. Mater.*, vol. 28, no. 19, pp. 3646–3652, May 2016.

[82] X. Xiao, T. Li, P. Yang, Y. Gao, H. Jin, W. Ni, W. Zhan, X. Zhang, Y. Cao, J. Zhong, L. Gong, W.-C. Yen, W. Mai, J. Chen, K. Huo, Y.-L. Chueh, Z. L. Wang, and J. Zhou, "Fiber-Based All-Solid-State Flexible Supercapacitors for Self-Powered Systems," *ACS Nano*, vol. 6, no. 10, pp. 9200–9206, Oct. 2012.

[83] Y. H. Lee, J. S. Kim, J. Noh, I. Lee, H. J. Kim, S. Choi, J. Seo, S. Jeon, T. S. Kim, J. Y. Lee, and J. W. Choi, "Wearable textile battery rechargeable by solar energy," *Nano Lett.*, vol. 13, no. 11, pp. 5753–5761, 2013.

[84] N. Li, Z. Chen, W. Ren, F. Li, and H.-M. Cheng, "Flexible graphene-based lithium ion batteries with ultrafast charge and discharge rates.," *Proc. Natl. Acad. Sci. U. S. A.*, vol. 109, no. 43, pp. 17360–5, 2012.

[85] X. Pu, L. Li, M. Liu, C. Jiang, C. Du, Z. Zhao, W. Hu, and Z. L. Wang, "Wearable Self-Charging Power Textile Based on Flexible Yarn Supercapacitors and Fabric Nanogenerators," *Adv. Mater.*, vol. 28, no. 1, pp. 98–105, 2016.

[86] M. Kaempgen, C. K. Chan, J. Ma, Y. Cui, and G. Gruner, "Printable thin film supercapacitors using single-walled carbon nanotubes," *Nano Lett.*, vol. 9, no. 5, pp. 1872–1876, 2009.

[87] Y. Fu, X. Cai, H. Wu, Z. Lv, S. Hou, M. Peng, X. Yu, and D. Zou, "Fiber supercapacitors utilizing pen ink for flexible/wearable energy storage," *Adv. Mater.*, vol. 24, no. 42, pp. 5713–5718, 2012.

[88] Y. Li, K. Sheng, W. Yuan, and G. Shi, "A high-performance flexible fibre-shaped electrochemical capacitor based on electrochemically reduced graphene oxide," *Chem. Commun.*, vol. 49, no. 3, pp. 291–293, 2013.

[89] D. Yu, K. Goh, H. Wang, L. Wei, W. Jiang, Q. Zhang, L. Dai, and Y. Chen, "Scalable synthesis of hierarchically structured carbon nanotube-graphene fibres for capacitive energy storage.," *Nat. Nanotechnol.*, vol. 9, no. May, pp. 1–8, 2014.

[90] K. Jost, D. P. Durkin, L. M. Haverhals, E. K. Brown, M. Langenstein, H. C. De Long, P. C. Trulove, Y. Gogotsi, and G. Dion, "Natural fiber welded electrode yarns for knittable textile supercapacitors," *Adv. Energy Mater.*, vol. 5, no. 4, pp. 1–8, 2015.

[91] J. Bae, M. K. Song, Y. J. Park, J. M. Kim, M. Liu, and Z. L. Wang, "Fiber supercapacitors made of nanowire-fiber hybrid structures for wearable/flexible energy storage," *Angew. Chemie - Int. Ed.*, vol. 50, no. 7, pp. 1683–1687, 2011.

[92] J. A. Lee, M. K. Shin, S. J. S. H. Kim, H. U. Cho, G. M. Spinks, G. G. Wallace, M. D. Lima, X. Lepró, M. E. Kozlov, R. H. Baughman, and S. J. S. H. Kim, "Ultrafast charge

and discharge biscrolled yarn supercapacitors for textiles and microdevices," *Nat. Commun.*, vol. 4, no. May, p. 1970, 2013.

[93] J. Ren, W. Bai, G. Guan, Y. Zhang, and H. Peng, "Flexible and weaveable capacitor wire based on a carbon nanocomposite fiber," *Adv. Mater.*, vol. 25, no. 41, pp. 5965–5970, 2013.

[94] L. Gao, J. U. Surjadi, K. Cao, H. Zhang, P. Li, S. Xu, C. Jiang, J. Song, D. Sun, and Y. Lu, "Flexible Fiber-Shaped Supercapacitor Based on Nickel–Cobalt Double Hydroxide and Pen Ink Electrodes on Metallized Carbon Fiber," *ACS Appl. Mater. Interfaces*, vol. 9, no. 6, pp. 5409–5418, Feb. 2017.

[95] J. Sun, Y. Huang, C. Fu, Z. Wang, Y. Huang, M. Zhu, C. Zhi, and H. Hu, "High-performance stretchable yarn supercapacitor based on PPy@CNTs@urethane elastic fiber core spun yarn," *Nano Energy*, vol. 27, pp. 230–237, 2016.

[96] L. Liu, Y. Yu, C. Yan, K. Li, and Z. Zheng, "Wearable energy-dense and power-dense supercapacitor yarns enabled by scalable graphene–metallic textile composite electrodes," *Nat. Commun.*, vol. 6, p. 7260, 2015.

[97] H. Jin, L. Zhou, C. L. Mak, H. Huang, W. M. Tang, and H. L. W. Chan, "High-performance fiber-shaped supercapacitors using carbon fiber thread (CFT)@polyanilne and functionalized CFT electrodes for wearable/stretchable electronics," *Nano Energy*, vol. 11, pp. 662–670, 2015.

[98] Z. Yu and J. Thomas, "Energy storing electrical cables: Integrating energy storage and electrical conduction," *Adv. Mater.*, vol. 26, no. 25, pp. 4279–4285, 2014.

[99] X. Chen, L. Qiu, J. Ren, G. Guan, H. Lin, Z. Zhang, P. Chen, Y. Wang, and H. Peng, "Novel electric double-layer capacitor with a coaxial fiber structure," *Adv. Mater.*, vol. 25, no. 44, pp. 6436–6441, 2013.

[100] Q. Zhang, X. Wang, Z. Pan, J. Sun, J. Zhao, J. Zhang, C. Zhang, L. Tang, J. Luo, B. Song, Z. Zhang, W. Lu, Q. Li, Y. Zhang, and Y. Yao, "Wrapping Aligned Carbon Nanotube Composite Sheets around Vanadium Nitride Nanowire Arrays for Asymmetric Coaxial Fiber-Shaped Supercapacitors with Ultrahigh Energy Density," *Nano Lett.*, vol. 17, no. 4, pp. 2719–2726, 2017.

[101] D. Harrison, F. Qiu, J. Fyson, Y. Xu, P. Evans, and D. Southee, "A coaxial single fibre supercapacitor for energy storage," *Phys. Chem. Chem. Phys.*, vol. 15, no. 29, pp. 12215–12219, 2013.

[102] V. T. Le, H. Kim, A. Ghosh, J. Kim, J. Chang, Q. A. Vu, D. T. Pham, J. H. Lee, S. W. Kim, and Y. H. Lee, "Coaxial fiber supercapacitor using all-carbon material electrodes," *ACS Nano*, vol. 7, no. 7, pp. 5940–5947, 2013.

[103] Q. Kang, J. Zhao, X. Li, G. Zhu, X. Feng, Y. Ma, W. Huang, and J. Liu, "A single wire as all-inclusive fully functional supercapacitor," *Nano Energy*, vol. 32, no. December 2016, pp. 201–208, 2017.

[104] J. Wen, S. Li, K. Zhou, Z. Song, B. Li, Z. Chen, T. Chen, Y. Guo, and G. Fang, "Flexible coaxial-type fiber solid-state asymmetrical supercapacitor based on Ni3S2 nanorod array and pen ink electrodes," *J. Power Sources*, vol. 324, pp. 325–333, 2016.

[105] X. Zang, R. Xu, Y. Zhang, X. Li, L. Zhang, J. Wei, K. Wang, and H. Zhu, "All carbon coaxial supercapacitors based on hollow carbon nanotube sleeve structure,"

Nanotechnology, vol. 26, no. 4, p. 45401, 2015.

[106] X. Zhao, B. Zheng, T. Huang, and C. Gao, “Graphene-based single fiber supercapacitor with a coaxial structure,” *Nanoscale*, vol. 7, no. 21, pp. 9399–9404, 2015.

[107] Q. Wang, X. Wang, J. Xu, X. Ouyang, X. Hou, D. Chen, R. Wang, and G. Shen, “Flexible coaxial-type fiber supercapacitor based on NiCo2O4 nanosheets electrodes,” *Nano Energy*, vol. 8, pp. 44–51, 2014.

[108] Q. Zhang, J. Sun, Z. Pan, J. Zhang, J. Zhao, X. Wang, C. Zhang, Y. Yao, W. Lu, Q. Li, Y. Zhang, and Z. Zhang, “Stretchable fiber-shaped asymmetric supercapacitors with ultrahigh energy density,” *Nano Energy*, vol. 39, no. April, pp. 219–228, 2017.

[109] Z. Yang, J. Deng, X. Chen, J. Ren, and H. Peng, “A highly stretchable, fiber-shaped supercapacitor,” *Angew. Chemie - Int. Ed.*, vol. 52, no. 50, pp. 13453–13457, 2013.

[110] R. C. Agrawal and G. P. Pandey, “Solid polymer electrolytes: materials designing and all-solid-state battery applications: an overview,” *J. Phys. D. Appl. Phys.*, vol. 41, no. 22, p. 223001, Nov. 2008.

[111] “Polyacrylonitrile-based Carbon Fibers.” [Online]. Available: http://www.toray.com/products/carbon/car_001.html.

[112] W. Chen, R. B. Rakhi, L. Hu, X. Xie, Y. Cui, and H. N. Alshareef, “High-performance nanostructured supercapacitors on a sponge,” *Nano Lett.*, vol. 11, no. 12, pp. 5165–5172, Dec. 2011.

[113] H. B. Hu, Z. B. Pei, H. J. Fan, and C. H. Ye, “3D Interdigital Au/MnO2/Au Stacked Hybrid Electrodes for On-Chip Microsupercapacitors,” *Small*, vol. 12, no. 22, pp. 3059–3069, 2016.

[114] S. Dong, X. Chen, L. Gu, X. Zhou, L. Li, Z. Liu, P. Han, H. Xu, J. Yao, H. Wang, X. Zhang, C. Shang, G. Cui, and L. Chen, “One dimensional MnO2/titanium nitride nanotube coaxial arrays for high performance electrochemical capacitive energy storage,” *Energy Environ. Sci.*, vol. 4, no. 9, p. 3502, 2011.

[115] W. Jiang, D. Yu, Q. Zhang, K. Goh, L. Wei, Y. Yong, R. Jiang, J. Wei, and Y. Chen, “Ternary Hybrids of Amorphous Nickel Hydroxide-Carbon Nanotube-Conducting Polymer for Supercapacitors with High Energy Density, Excellent Rate Capability, and Long Cycle Life,” *Adv. Funct. Mater.*, vol. 25, no. 7, pp. 1063–1073, Feb. 2015.

[116] J. Tao, N. Liu, W. Ma, L. Ding, L. Li, J. Su, and Y. Gao, “Solid-state high performance flexible supercapacitors based on polypyrrole-MnO2-carbon fiber hybrid structure.,” *Sci. Rep.*, vol. 3, p. 2286, Jul. 2013.

[117] D. Quéré, “FLUID COATING ON A FIBER,” *Annu. Rev. Fluid Mech.*, vol. 31, no. 1, pp. 347–384, Jan. 1999.

[118] D. A. White and J. A. Tallmadge, “Gravity Corrected Theory for Cylinder Withdrawl,” vol. 13, no. 4, pp. 745–750, 1965.

[119] C. Shang, S. Dong, S. Wang, D. Xiao, P. Han, X. Wang, L. Gu, and G. Cui, “Coaxial Ni x Co 2 x (OH) 6 x /TiN Nanotube Arrays as Supercapacitor Electrodes,” *ACS Nano*, vol. 7, no. 6, pp. 5430–5436, Jun. 2013.

[120] Q. Meng, H. Wu, Y. Meng, K. Xie, Z. Wei, and Z. Guo, “High-performance all-carbon

yarn micro-supercapacitor for an integrated energy system," *Adv. Mater.*, vol. 26, no. 24, pp. 4100–4106, 2014.

[121] P. Han, X. Han, J. Yao, L. Zhang, X. Cao, C. Huang, and G. Cui, "High energy density sodium-ion capacitors through co-intercalation mechanism in diglyme-based electrolyte system," *J. Power Sources*, vol. 297, pp. 457–463, Nov. 2015.

[122] U. Gulzar, S. Goriparti, E. Miele, T. Li, G. Maidecchi, A. Toma, F. De Angelis, C. Capiglia, and R. P. Zaccaria, "Next-generation textiles: from embedded supercapacitors to lithium ion batteries," *J. Mater. Chem. A*, vol. 4, no. 43, pp. 16771–16800, 2016.

[123] H. Xu, X. Hu, Y. Sun, H. Yang, X. Liu, and Y. Huang, "Flexible fiber-shaped supercapacitors based on hierarchically nanostructured composite electrodes," *Nano Res.*, vol. 8, no. 4, pp. 1148–1158, 2014.

[124] P. Li, J. Li, Z. Zhao, Z. Fang, M. Yang, Z. Yuan, Y. Zhang, Q. Zhang, W. Hong, X. Chen, and D. Yu, "A General Electrode Design Strategy for Flexible Fiber Micro-Pseudocapacitors Combining Ultrahigh Energy and Power Delivery," *Adv. Sci.*, vol. 4, no. 8, p. 1700003, Aug. 2017.

[125] Q. Zhou, C. Jia, X. Ye, Z. Tang, and Z. Wan, "A knittable fiber-shaped supercapacitor based on natural cotton thread for wearable electronics," *J. Power Sources*, vol. 327, pp. 365–373, 2016.

[126] Y. Huang, H. Hu, Y. Huang, M. Zhu, W. Meng, C. Liu, Z. Pei, C. Hao, Z. Wang, and C. Zhi, "From industrially weavable and knittable highly conductive yarns to large wearable energy storage textiles," *ACS Nano*, vol. 9, no. 5, pp. 4766–4775, 2015.

[127] Y. Meng, Y. Zhao, C. Hu, H. Cheng, Y. Hu, Z. Zhang, G. Shi, and L. Qu, "All-graphene core-sheath microfibers for all-solid-state, stretchable fibriform supercapacitors and wearable electronic textiles," *Adv. Mater.*, vol. 25, no. 16, pp. 2326–2331, 2013.

[128] D. Yu, K. Goh, Q. Zhang, L. Wei, H. Wang, W. Jiang, and Y. Chen, "Controlled functionalization of carbonaceous fibers for asymmetric solid-state micro-supercapacitors with high volumetric energy density," *Adv. Mater.*, vol. 26, no. 39, pp. 6790–6797, 2014.

[129] N. He, Q. Pan, Y. Liu, and W. Gao, "Graphene-Fiber-Based Supercapacitors Favor N -Methyl-2-pyrrolidone/Ethyl Acetate as the Spinning Solvent/Coagulant Combination," *ACS Appl. Mater. Interfaces*, vol. 9, no. 29, pp. 24568–24576, Jul. 2017.

[130] Y. Xie, L. Lu, Y. Tang, F. Zhang, C. Shen, X. Zang, X. Ding, W. Cai, and L. Lin, "Hierarchically nanostructured carbon fiber-nickel-carbon nanotubes for high-performance supercapacitor electrodes," *Mater. Lett.*, vol. 186, 2017.

[131] D. Yu, S. Zhai, W. Jiang, K. Goh, L. Wei, X. Chen, R. Jiang, and Y. Chen, "Transforming Pristine Carbon Fiber Tows into High Performance Solid-State Fiber Supercapacitors," *Adv. Mater.*, vol. 27, no. 33, pp. 4895–4901, 2015.

[132] "T300 DATA SHEET." [Online]. Available: http://www.toraycfa.com/pdfs/T300DataSheet.pdf. [Accessed: 01-Aug-2017].

[133] S. Basu, "Tensile Deformation of Fibers Used in Textile Industry," *Agilent Technologies Application Note*, 2012. [Online]. Available: http://cp.literature.agilent.com/litweb/pdf/5991-0274EN.pdf.

[134] H. D. Yoo, J. H. Jang, J. H. Ryu, Y. Park, and S. M. Oh, "Impedance analysis of porous

carbon electrodes to predict rate capability of electric double-layer capacitors," *J. Power Sources*, vol. 267, pp. 411–420, Dec. 2014.

[135] Y. Yang, Q. Huang, L. Niu, D. Wang, C. Yan, Y. She, and Z. Zheng, "Waterproof, Ultrahigh Areal-Capacitance, Wearable Supercapacitor Fabrics," *Adv. Mater.*, p. 1606679, 2017.

[136] "Automotive Steel Definitions." [Online]. Available: http://www.worldautosteel.org/steel-basics/automotive-steel-definitions/. [Accessed: 01-Aug-2017].